RI | 9327

REPORT OF INVESTIGATIONS/1990

Comparison of Models To Evaluate In Situ Shield Loading

By Thomas M. Barczak and David E. Schwemmer

1910 ★ 80 YEARS ★ 1990

BUREAU OF MINES

UNITED STATES DEPARTMENT OF THE INTERIOR

Mission: As the Nation's principal conservation agency, the Department of the Interior has responsibility for most of our nationally-owned public lands and natural and cultural resources. This includes fostering wise use of our land and water resources, protecting our fish and wildlife, preserving the environmental and cultural values of our national parks and historical places, and providing for the enjoyment of life through outdoor recreation. The Department assesses our energy and mineral resources and works to assure that their development is in the best interests of all our people. The Department also promotes the goals of the Take Pride in America campaign by encouraging stewardship and citizen responsibility for the public lands and promoting citizen participation in their care. The Department also has a major responsibility for American Indian reservation communities and for people who live in Island Territories under U.S. Administration.

Report of Investigations 9327

Comparison of Models To Evaluate In Situ Shield Loading

By Thomas M. Barczak and David E. Schwemmer

UNITED STATES DEPARTMENT OF THE INTERIOR
Manuel Lujan, Jr., Secretary

BUREAU OF MINES
T S Ary, Director

Library of Congress Cataloging in Publication Data:

Barczak, Thomas M.

Comparison of models to evaluate in situ shield loading / by Thomas M. Barczak and David E. Schwemmer.

p. cm. — (Report of investigations; 9327)

Includes bibliographical references.

Supt. of Docs. no.: I 28.23:9327.

1. Mine roof control. 2. Longwall mining. I. Schwemmer, David E. II. Title. III. Series: Report of investigations (United States. Bureau of Mines); 9327.

TN23.U43 [TN288] 622 s—dc20 [622'.28] 90-1917 CIP

CONTENTS

	Page
Abstract	1
Introduction	2
Description of models and parameter considerations	4
Rigid-body models	4
Leg-pin model	4
Leg-link model	5
Elastic stiffness model	6
Finite-element model	9
Parameter considerations	10
Model responses and parameter sensitivity	11
Model sensitivity analysis	12
Force and location prediction analysis	25
Leg-pin (rigid-body) model	25
Leg-link (rigid-body) model	25
Elastic stiffness model	26
Finite-element model	26
Model comparisons	49
Error sources and application limitations	56
Leg-pin (rigid-body) model	56
Leg-link (rigid-body) model	56
Elastic stiffness model	57
Finite-element model	57
Resultant location predictions	58
Conclusions	58
References	59
Appendix A.—Derivation of static equilibrium equations for rigid-body solution of resultant shield loading	60
Appendix B.—Determination of shield stiffness coefficients	61
Appendix C.—Input data for finite-element shield model	62
Appendix D.—Discussion of leg mechanics	67

ILLUSTRATIONS

1.	Bureau research program to optimize mine roof supports	2
2.	Resultant forces acting on shield support	3
3.	Two-dimensional diagram of longwall shield depicting load transfer paths between canopy and base	3
4.	Bureau mine roof simulator	4
5.	Forces acting on shield canopy	5
6.	Instrumented shield loading pin	5
7.	Free-body diagrams for analysis of resultant shield loading	6
8.	Rigid-body models	7
9.	Conceptual illustration of elastic stiffness model	7
10.	Shield stiffness characteristics as a function of canopy contact	8
11.	Shield stiffness characteristics as a function of shield height	9
12.	Two-dimensional finite-element shield model	10
13.	Canopy contact configurations	11
14.	Vertical and face-to-waste displacement loading	11
15.	Data selection from displacement-controlled load profiles	11
16.	Leg-pin model sensitivity to shield height	13
17.	Leg-pin model sensitivity to horizontal constrainment	14
18.	Leg-pin model sensitivity to displacement	15
19.	Leg-pin model sensitivity to canopy contact configuration	16

ILLUSTRATIONS—continued

Page

20. Leg-link model sensitivity to shield height 17
21. Leg-link model sensitivity to horizontal constrainment 18
22. Leg-link model sensitivity to displacement 19
23. Leg-link model sensitivity to canopy contact configuration 20
24. Elastic stiffness model sensitivity to shield height 21
25. Elastic stiffness model sensitivity to horizontal constrainment 22
26. Elastic stiffness model sensitivity to displacement 23
27. Elastic stiffness model sensitivity to canopy contact configuration 24
28. Leg-pin model force predictions for horizontal constrainment parameter considerations 27
29. Leg-pin model force predictions for displacement parameter considerations 29
30. Leg-pin model force predictions for canopy contact parameter considerations 31
31. Leg-link model force predictions for horizontal constrainment parameter considerations 33
32. Leg-link model force predictions for displacement parameter considerations 35
33. Leg-link model force predictions for canopy contact parameter considerations 37
34. Elastic stiffness model force predictions for horizontal constrainment parameter considerations 39
35. Elastic stiffness model force predictions for displacement parameter considerations 41
36. Elastic stiffness model force predictions for canopy contact parameter considerations 43
37. Finite-element model force predictions 45
38. Location predictions for leg-pin (rigid-body) model 46
39. Location predictions for leg-link (rigid-body) model 47
40. Location predictions for elastic stiffness model 48
41. Model comparisons of force predictions for horizontal constrainment parameter considerations 50
42. Model comparisons of force predictions for displacement parameter considerations 52
43. Model comparisons of force predictions for canopy contact parameter considerations 54
44. Effective leg area variations with shield height 56

B-1. Shield stiffness test procedures 61

D-1. Illustration of leg configurations 67
D-2. Analysis of leg forces 68

TABLE

1. Model comparison summary 49

UNIT OF MEASURE ABBREVIATIONS USED IN THIS REPORT

in	inch	min	minute
in^2	square inch	pct	percent
kips/in	kips per inch	psi	pound (force) per square inch

COMPARISON OF MODELS TO EVALUATE IN SITU SHIELD LOADING

By Thomas M. Barczak[1] and David E. Schwemmer[2]

ABSTRACT

The U.S. Bureau of Mines is conducting research to optimize the utilization and design of mine roof support systems. This report describes methods to evaluate resultant loading on longwall shields, defined as external resultant vertical and horizontal force acting on the canopy and base. Four models are considered: two rigid-body models, an elastic model, and a numerical model. The rigid-body models equate measured internal shield forces to unknown external resultant shield forces (loads) through rigid-body analysis of static equilibrium requirements. The elastic model develops a solution to shield mechanics by evaluation of the load-displacement relationship and stiffness characteristics of the support structure. The numerical model is a two-dimensional finite-element representation of a shield structure. Model determination of resultant shield loading is compared to controlled loading of a shield in the Bureau's mine roof simulator. Parameters investigated are shield height, canopy contact configuration, canopy and base horizontal constrainment, and boundary conditions imposed by vertical and horizontal shield displacements. It is concluded that rigid-body models are most applicable to in situ measurement of shield loading. Applications requirements and potential error sources are discussed.

[1]Research physicist, U.S. Bureau of Mines, Pittsburgh Research Center, Pittsburgh, PA.
[2]Structural engineer, Boeing Services International, Pittsburgh, PA (now with Eichleay Engineers, Inc., Pittsburgh, PA).

INTRODUCTION

Longwall supports continue to be designed and selected based upon assumed load conditions that quite often do not accurately represent actual underground loadings. The result is that supports are often oversized and used at only a fraction of their full capacity (*1-2*),[3] or they provide excessive resistance that causes unnecessary stressing of the support structure and surrounding strata. This stressing can be detrimental to strata stability and subsequent ground control. The selection of oversized supports also adds significantly to the cost of the support and required capital for face installation. Likewise, such practices do not promote the design of efficient support systems. Improvements in the basic design of supports will be realized only if the load conditions and interaction between the support and strata can be better defined. As part of a research program to optimize the design and selection of mine roof support systems (fig. 1), the U.S. Bureau of Mines has been evaluating shield mechanics (*3-5*) and developing techniques to use shields as monitors of strata activity by measurement of resultant shield loading (*1, 6-7*).

Figure 2 depicts resultant forces acting on a lemniscate shield support. As illustrated in the figure, these forces consist of a resultant vertical and a resultant horizontal force acting on the shield canopy and base. These forces are imposed on the support as a direct result of strata activity or they are developed indirectly from internal shield component forces and associated shield mechanics. The resultant horizontal force is assumed to act at the canopy tip and rear of the base while the resultant vertical force can act anywhere along the length of the canopy or base. Hence, knowledge of the location of the resultant vertical force is also required in this analysis of resultant shield loading. External forces acting on the caving shield, which may occur from gob loading underground, are not considered in this analysis. Previous analysis has indicated that under worst load conditions gob loading will impact vertical shield load capacity by less than 10 pct and horizontal load capacity by less than 25 pct (*6*).

[3]Italic numbers in parentheses refer to items in the list of references preceding the appendixes at the end of this report.

Efforts to evaluate shield loading previous to these Bureau developments were limited to analysis of leg forces. From the principles of mechanics, externally applied loads (resultant forces acting on canopy and base) must be balanced by internal shield forces. As seen in figure 3, the canopy and base of a shield support are interconnected by not only leg cylinders but also the caving shield-lemniscate assembly. Hence, it is necessary to know the load transfer to both the leg cylinders and caving shield-lemniscate assembly to properly evaluate resultant shield loading.

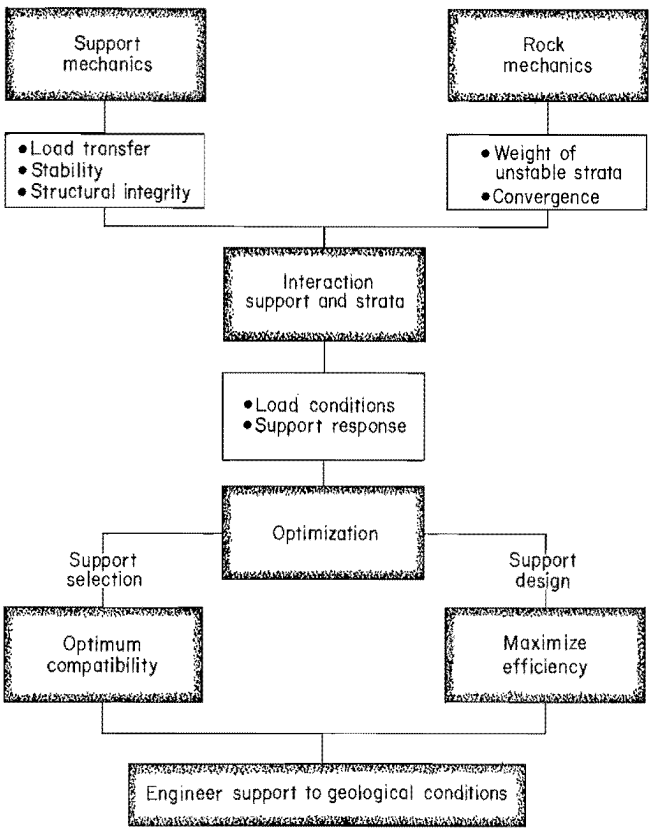

Figure 1.—Bureau research program to optimize mine roof supports.

It is known that the caving shield-lemniscate assembly is not intended to contribute to vertical support resistance, but research conducted by the Bureau has shown that 10 to 20 pct of the total vertical shield resistance can be provided by the caving shield-lemniscate assembly. This resistance is provided when the shield is horizontally constrained and sufficient friction is developed in the numerous pin joints to allow the caving shield-lemniscate assembly to develop some vertical stiffness (*3, 8*). Therefore, assessment of vertical shield loading from the vertical components of the leg forces will produce accurate results only if the shield is unconstrained and there is no moment transferred through the pin joints of the caving shield-lemniscate assembly.

These studies have also shown that the caving shield-lemniscate assembly can provide up to 70 pct of the horizontal shield resistance, depending upon shield configuration and translational freedom in the pin joints as determined by horizontal constrainment of the canopy and base. Horizontal constrainment is defined as horizontal displacement of the canopy relative to the base, which removes freedom in the numerous structural joints. Therefore, it is concluded that horizontal shield loading cannot be determined simply from analysis of leg forces.

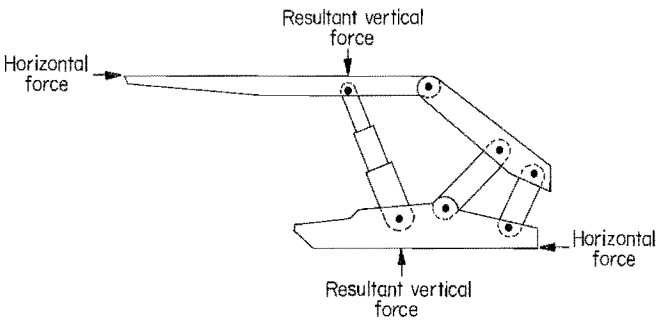

Figure 2.—Resultant forces acting on shield support.

This report describes four models and compares their capabilities to evaluate resultant horizontal and vertical shield loading acting on the shield canopy. (Resultant forces acting on the base can be determined from equilibrium requirements once the canopy forces are known.) The four models include two rigid-body models, an elastic model, and a numerical (finite element) model. Each model was evaluated under known conditions by controlled displacement loading of a representative two-leg longwall shield in the Bureau's mine roof simulator (fig. 4).[4]

Parameters investigated in the model comparison include shield height, canopy contact configuration, canopy and base horizontal constrainment, and boundary conditions imposed by vertical and horizontal shield displacements. The sensitivity of each model to these parameters is analyzed. Based on these analyses, conclusions are drawn regarding the application of these models to in situ measurements of shield loading.

[4]Testing was conducted by David F. Gearheart, test engineer, and Karl M. Chulig, engineering aid, of Boeing Services International (BSI), Pittsburgh, PA, under the direction of Carol L. Tassilo, operations engineer, BSI.

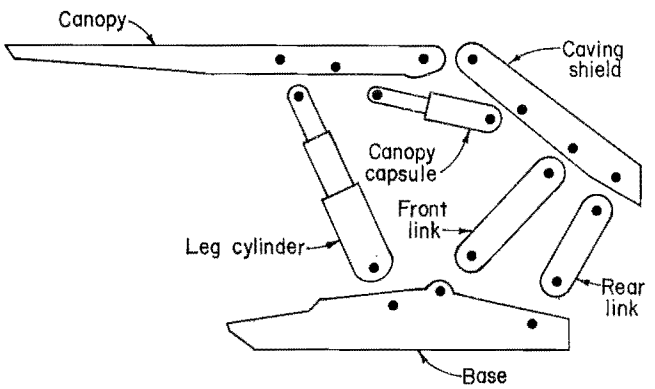

Figure 3.—Two-dimensional diagram of longwall shield depicting load transfer paths between canopy and base.

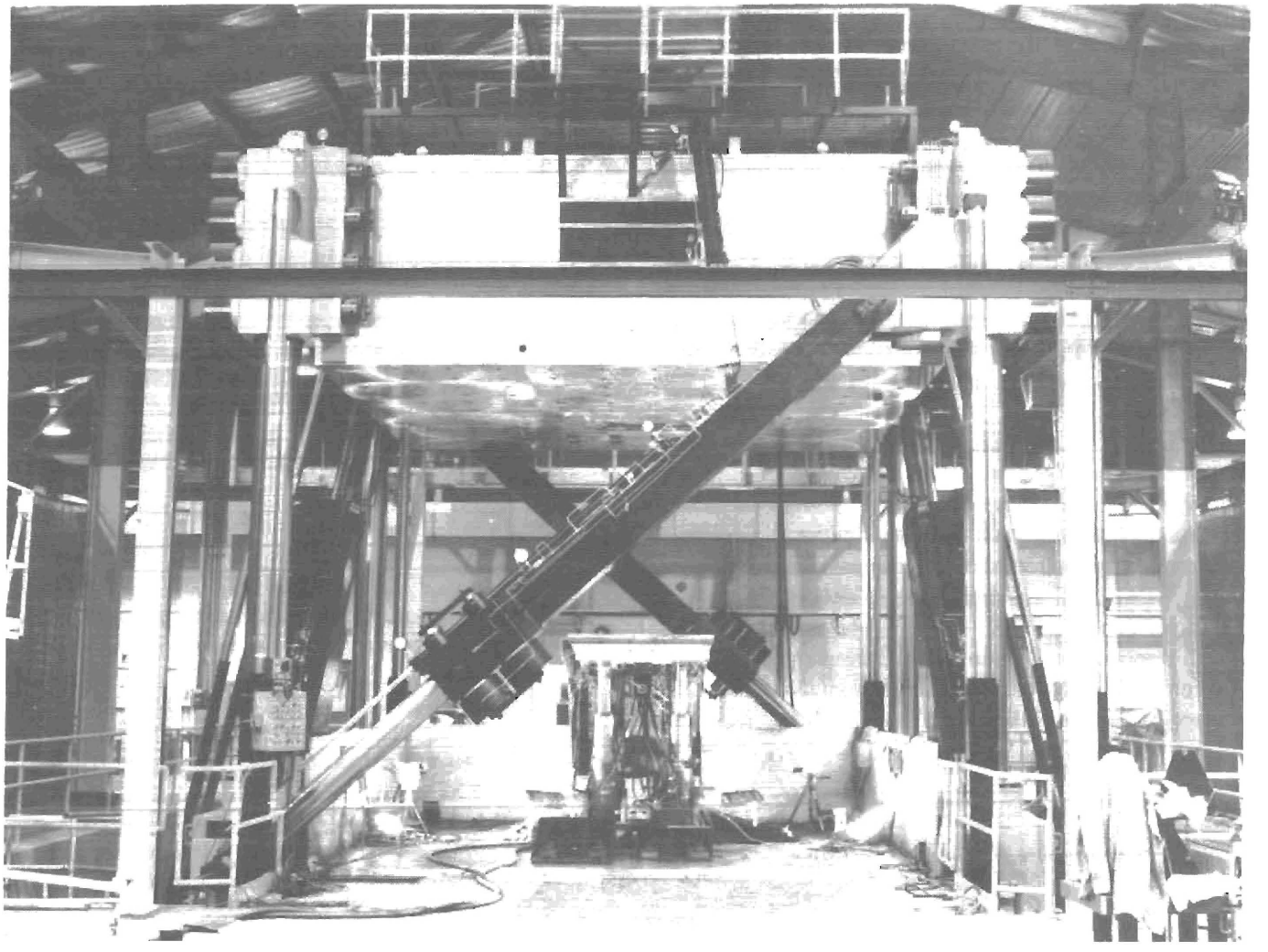

Figure 4.—Bureau mine roof simulator.

DESCRIPTION OF MODELS AND PARAMETER CONSIDERATIONS

Three types of models are evaluated in this study: (1) rigid-body, (2) elastic, and (3) numerical (finite element). Each model type employs a different approach to determine resultant shield loading.

RIGID-BODY MODELS

Rigid-body models equate measured internal shield forces to unknown external resultant shield forces through rigid-body analysis of static equilibrium requirements of the shield components. The underlying assumption is that all components act as rigid bodies without deformation during load application. In reality, structures are never absolutely rigid and they deform under the loads to which they are subjected. However, these deformations are usually small and do not appreciably affect the conditions of equilibrium. Hence, a rigid-body solution to shield mechanics is pursued.

Leg-Pin Model

Forces acting on the shield canopy are depicted in figure 5. Through examination of equilibrium of the canopy, it is seen that if the leg forces and canopy-caving shield pin reactions are known, force and moment equilibrium generate sufficient equations to determine unknown resultant canopy forces (vertical and horizontal) and their locations on the canopy. (Note: The resultant horizontal

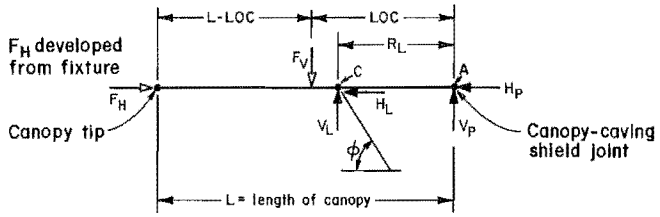

F_V and F_H are resultant canopy force components at LOC (resultant vertical force location)

V_L and H_L are leg force components.

V_P and H_P are canopy-caving shield force components.

R_L is location of leg reaction on canopy.

Figure 5.—Forces acting on shield canopy.

force is assumed to act at the canopy tip so its location is always known.) The governing system of equations are described in matrix notation as follows:

$$\text{and} \quad \begin{Bmatrix} F_V \\ F_H \\ \text{LOC} \end{Bmatrix} = \begin{bmatrix} 1 & 0 & 0 \\ 0 & 1 & 0 \\ 0 & 0 & \dfrac{1}{V_P + V_L} \end{bmatrix} \begin{Bmatrix} V_L + V_P, \\ H_L + H_P, \\ V_L * R_L, \end{Bmatrix} \quad \begin{matrix} (1) \\ (2) \\ (3) \end{matrix}$$

where F_V, F_H = resultant canopy force components,

V_L, H_L = leg force components,

V_P, H_P = canopy-caving shield force components,

LOC = resultant vertical force location,

and R_L = location of leg reaction on canopy.

Figure 6 shows an instrumented pin that was used by the Bureau to monitor pin reactions. The regular pins were replaced by these instrumented pins. These pins are internally instrumented with strain gages and are calibrated to permit determination of force reactions on two orthogonal axes. These pins are commercially available and can be designed to the shield specifications.

Leg forces are determined by multiplication of the effective leg area by the leg pressure as measured with pressure transducers. Effective leg area should be determined from controlled static loading of a leg cylinder at several leg (shield) heights. The effective leg area is computed as the ratio of the applied force acting along the axis of the leg to the measured pressure in the lower chamber of the

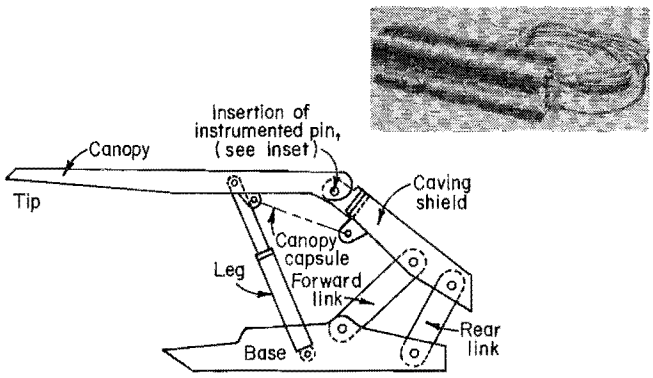

Figure 6.—Instrumented shield loading pin.

leg cylinder. Vertical and horizontal leg force components are then derived from the geometric relationship of leg orientation in the shield.

Leg-Link Model

If the pin reactions are not known, then other information is necessary to provide a determinant system for solution. The second rigid-body model requires determination of leg forces and front link forces by measurement of leg pressures and link strains. The governing system of equations is produced by moment equilibrium requirements of the free-body diagrams depicted in figure 7.

From figure 7*A*, moment equilibrium (M) of the canopy provides

$$\sum M_A = -F_V * \text{LOC} + L * \sin\phi * (X_6 - X_3) = 0. \quad (4)$$

Summation of moments at locus of the link intersection for the canopy-caving shield combination as shown in figure 7*B* provides

$$\sum M_B = -F_v * [\text{LOC} + (X_3 - X_0)] + F_H * (Y_3 - Y_0) + L * \sin\phi * (X_6 - X_0) - L * \cos\phi * (Y_3 - Y_0) = 0. \quad (5)$$

Summation of moments at the tension link-caving shield joint provides (fig. 7*C*):

$$\sum M_C = -F_V * [\text{LOC} + (X_3 - X_1)] + F_H * (Y_3 - Y_1) + L * \sin\phi * (X_6 - X_1) - L * \cos\phi * (Y_3 - Y_1) - F * \cos\beta * (Y_2 - Y_1) - F * \sin\beta * (X_2 - X_1) = 0. \quad (6)$$

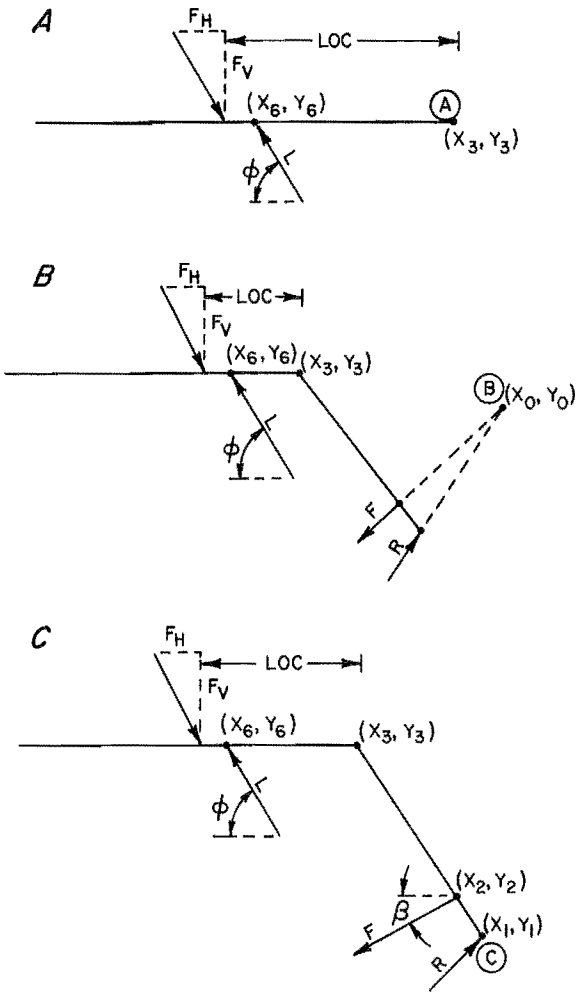

Figure 7.—Free-body diagrams for analysis of resultant shield loading. Moment equilibrium of (*A*) canopy and canopy-caving shield combination [summation of moments at link center (*B*) and summation of moments at tension link pin (*C*)].

Appendix A documents derivation of the following solution to these equations for determination of F_V, F_H, and LOC.

$$F_V = L * V_L + F * V_F, \tag{7}$$

where $V_L = \sin\phi$

$$V_F = \frac{[\cos\beta * (Y_2 - Y_1) + \sin\beta * (X_2 - X_1)] * (Y_3 - Y_0)}{X_1 * (Y_3 - Y_0) - Y_1 * (X_3 - X_0) + ((Y_0 * X_3) - (X_0 * Y_3))},$$

V_F = front link participation factor,

L = leg pressure,

and F = link strain.

$$F_H = L * H_L + F * H_F, \tag{8}$$

where $H_L = \cos\phi$,

$$H_F = \frac{[\cos\beta * (Y_2 - Y_1) + \sin\beta * (X_2 - X_1)] * (X_3 - X_0)}{X_1 * (Y_3 - Y_0) - Y_1 * (X_3 - X_0) + ((Y_0 * X_3) - (X_0 * Y_3))},$$

and H_L, H_F = horizontal leg and front link participation factors, respectively.

$$LOC = \frac{\sin\phi * (X_6 - X_3)}{\sin\phi + (F * V_F)/L}. \tag{9}$$

Leg forces are determined from leg pressure measurements using pressure transducers. Weldable type strain gages are suggested to measure link strain for underground applications. Computation of link force from link strain measurements is determined using elastic strength of materials principles as discussed in detail in other Bureau publications (*1, 5*).

In summary, two rigid-body models are examined. The first requires measurement of leg pressures and canopy-caving shield pin reactions and the second requires measurement of leg forces and front link strains. These models and associated instrumentation are depicted in figure 8.

ELASTIC STIFFNESS MODEL

The elastic stiffness model develops a solution to shield mechanics by evaluation of the load-displacement relationship and stiffness characteristics of the support structure. A conceptual illustration of the elastic stiffness model is shown in figure 9. A two-degree-of-freedom model is used to equate measured vertical and horizontal displacements of the canopy relative to the base and known shield stiffness to vertical and horizontal shield reactions resulting from these displacements (*7-8*). The resulting system of equations is

$$\Delta F_V = K_1^n * \Delta VDSP + K_2^n * \Delta HDSP, \text{ and} \tag{10}$$

$$\Delta F_H = K_3^n * \Delta VDSP + K_4^n * \Delta HDSP, \tag{11}$$

where K_i^n = shield stiffness coefficents that consider effects of vertical and horizontal interaction and is height dependent (tests to determine shield stiffness coefficients are documented in appendix B),

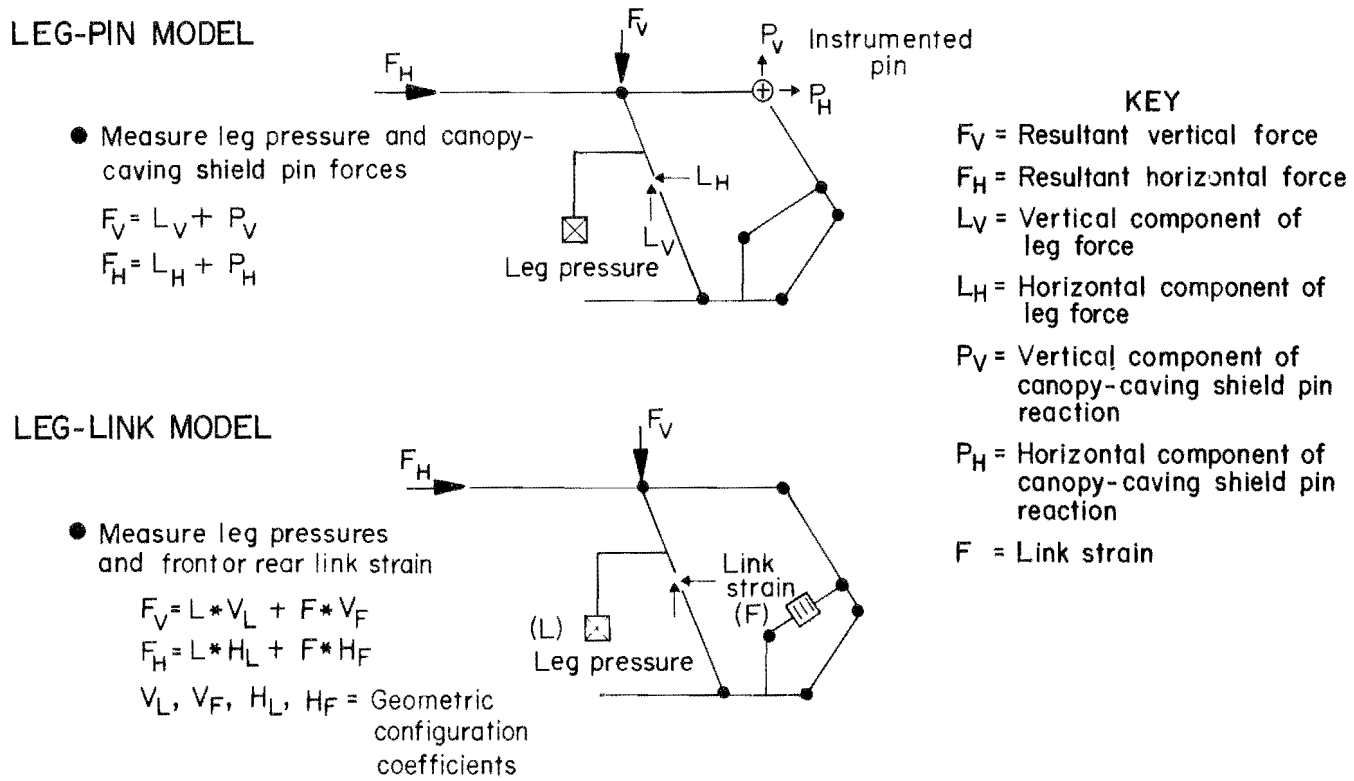

Figure 8.—Rigid-body models.

i = 1,2,3,4,

n = shield height indicator,

ΔF_V = change in resultant vertical force after setting,

ΔF_H = change in resultant horizontal force after setting,

ΔVDSP = change in vertical displacement,

and ΔHDSP = change in horizontal displacement.

As indicated in equations 12 and 13, the elastic stiffness model requires knowledge of initial conditions, vertical and horizontal resultant forces generated at shield setting, to predict total resultant shield loading. Initial readings for the model predictions documented in this report were derived from mine roof simulator readings, but could be determined using one of the rigid-body models. The location of the resultant vertical force is obtained from equilibrium of the canopy.

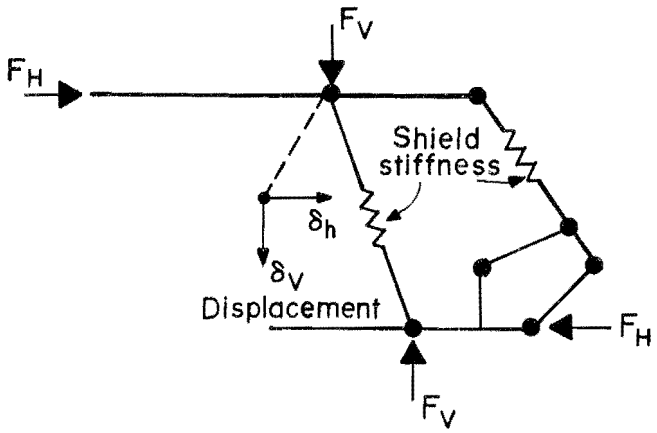

$$F_V = K_1 \delta_V + K_2 \delta_h$$

$$F_H = K_3 \delta_V + K_4 \delta_h$$

Figure 9.—Conceptual illustration of elastic stiffness model.

$$F_V = \delta F_V + F_{Vi}, \quad (12)$$

$$H = \delta F_H + F_{Hi}, \quad (13)$$

and $$LOC = (V_L * R_L)/F_V, \quad (14)$$

where F_{Vi}, F_{Hi} = initial vertical and horizontal resultant forces, respectively.

Previous studies of shield stiffness characteristics have shown shield stiffness to be independent of setting pressure and dependent on shield height (*8*). These studies have also shown shield stiffness, particularly horizontal stiffness, K_4, to be dependent on horizontal constrainment of the canopy and base with increased stiffness for horizontally constrained configurations. Horizontal constraint refers to a shield configuration in which rigid-body translational freedom in the pin joints is removed by horizontal

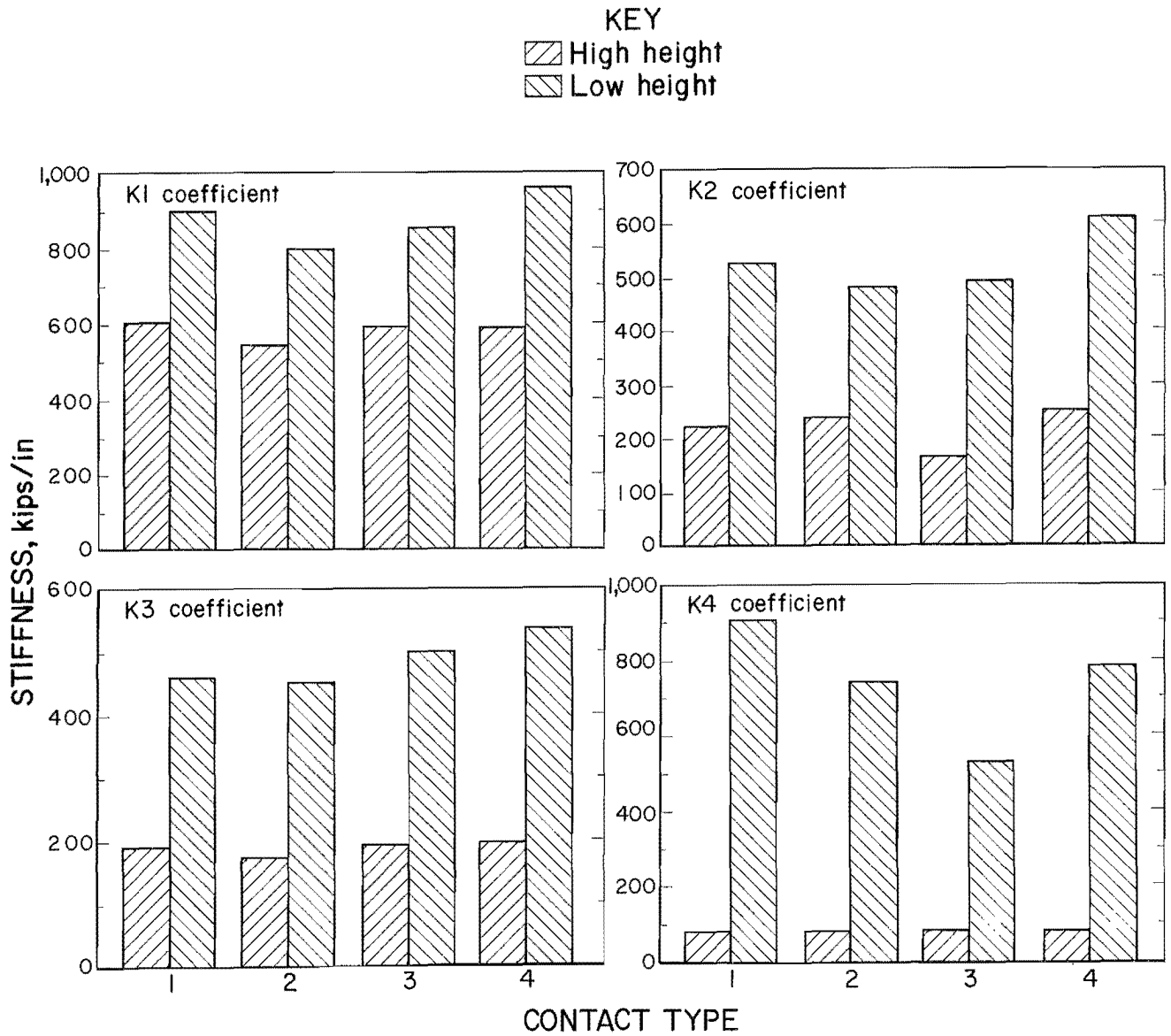

Figure 10.—Shield stiffness characteristics as a function of canopy contact. Type 1—full canopy and base contact, type 2—two-point canopy contact, type 3—one-point canopy contact, type 4—three-point canopy contact.

displacement of the canopy relative to the base. Test results have shown that the caving shield-lemniscate link assembly does not fully participate in the shield load transfer mechanics unless pin freedom is removed, resulting in decreased shield stiffness for unconstrained configurations. Shield stiffness characteristics for the shield used in the model comparisons are illustrated in figure 10 for canopy contact comparison and figure 11 for shield height comparison. Dependency of the shield stiffness on horizontal constrainment is also shown in figure 11.

FINITE-ELEMENT MODEL

A two-dimensional numerical shield model was developed and sectioned into joints and members (fig. 12). Three generic structural shapes characterize the structural members: canopy and base members are sandwiched shapes, the caving shield is a stiffened plate, and both the front and rear links are box sections. These members are modeled as finite-element representations utilizing the tapered beam element for the canopy, base, and caving

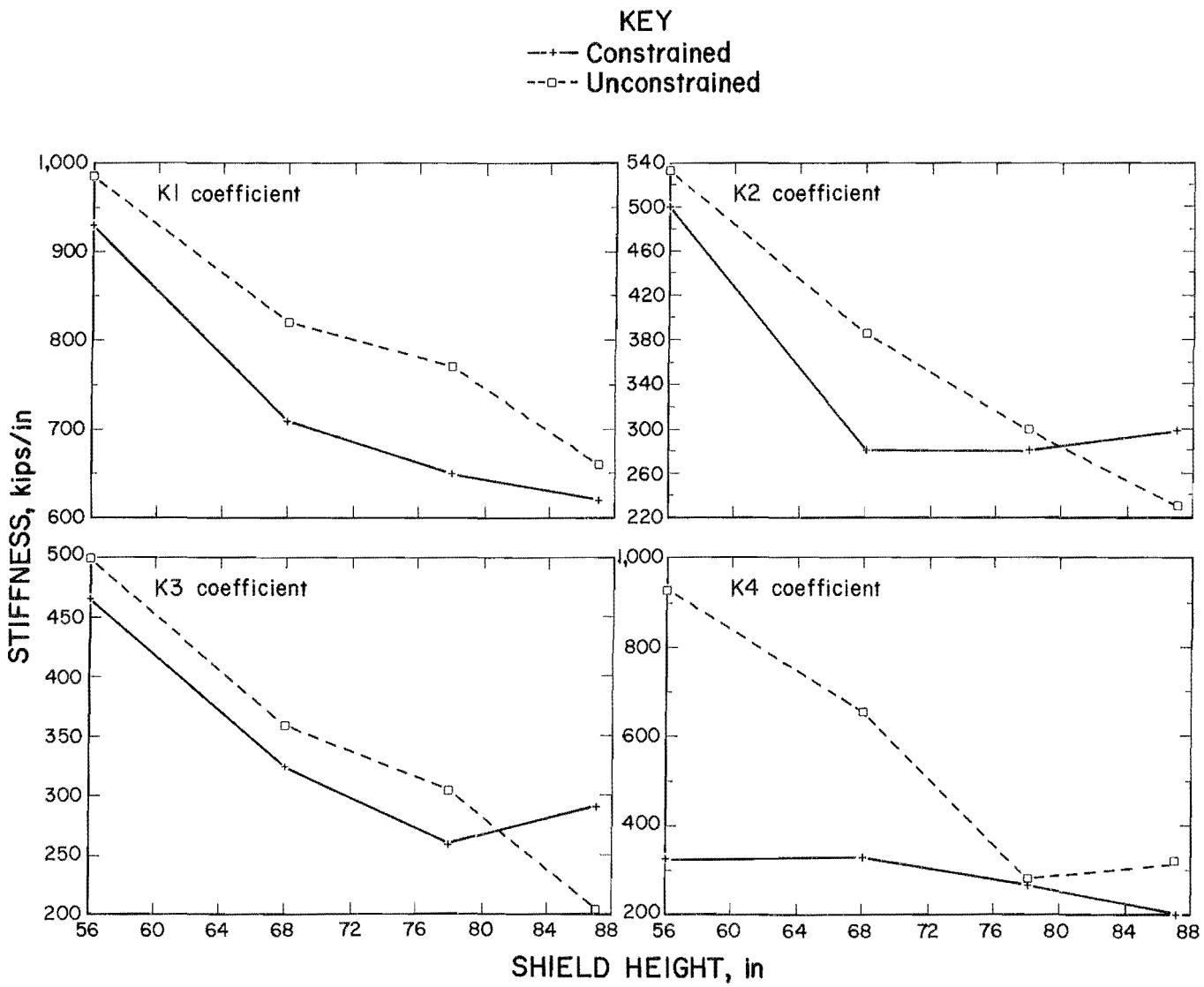

Figure 11.—Shield stiffness characteristics as a function of shield height.

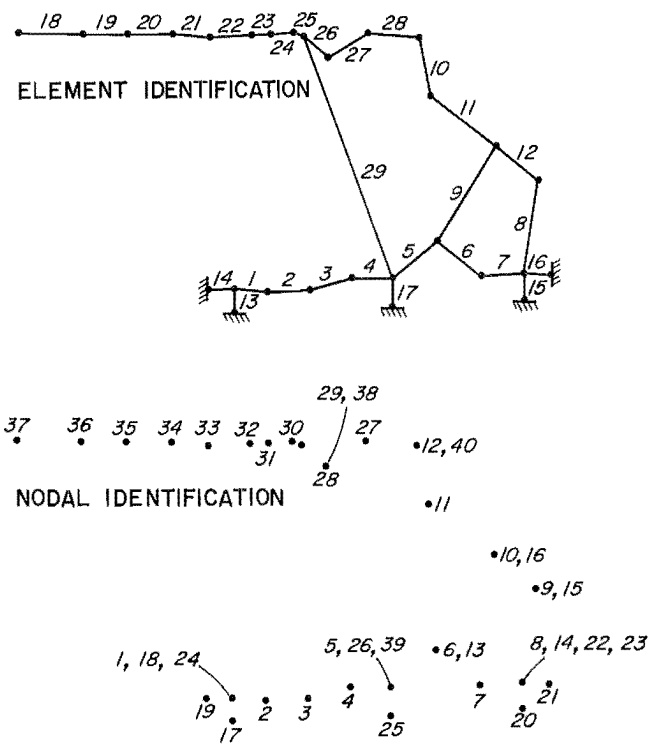

Figure 12.—Two-dimensional finite-element shield model.

shield, and the elastic beam element for the links. In practice, the legs function by hydraulic compression of the fluid in the cylinders. However, the legs are modeled as structural members (spar elements) with a modulus for steel (29,000 psi) in the finite-element representation. The area is computed from the relationship, K = A * E/L, where A = is effective leg area, E = is modulus of elasticity, L = is length of the leg, and K is the leg stiffness, which is determined from testing in the mine roof simulator. The base contact points are also modeled as spar type members with only axial compression capabilities. The canopy capsule is ignored because of its relatively small contribution in shield reactions.

The pin joints are modeled by specifying different nodes at the ends of the individual members (caving shield, links, and base), and coupling the translational displacements for those nodes at the same joint, permitting the rotation to be unrestrained. While frictional restraint at these joints is probable, and is a source of error in the modeling efforts, an efficient scheme to incorporate this effect was not found.

In general, the required input to the finite-element model is the displacement of the canopy, input as selected nodal displacements. The model then computes nodal forces from which resultant shield loading is determined. Because of the method chosen to represent base contact restraints; that is, compression-only springs at the toe and rear of the base and at the leg location for full contact configurations, an iterative static solution technique was necessary. The displacement increment chosen for testing model sensitivity to various step sizes was 1/20 of the total displacement. Only converged solutions are documented in this report.

Appendix C contains the input data necessary for the shield model generation and analysis. These data include element types and material properties, node locations and element connections, element real constants, and coupled nodal degrees of freedom. Because of the variable geometry of the canopy, caving shield, and base members, which are modeled utilizing the tapered beam elements, properties are required at the end of each element. With an averaging technique employed for the area and a fourth-order expression developed to determine element moment of inertia, the finite-element software constructs the stiffness matrix as required to perform an analysis.

PARAMETER CONSIDERATIONS

A study was made of several parameters that are known to influence shield behavior in order to evaluate model responses to these parameter considerations. Parameters investigated in the model comparisons included shield height, canopy contact configuration, canopy and base horizontal constrainment, and boundary conditions imposed by vertical and horizontal shield displacements. Prior to controlled displacement loading, initial load conditions were created by active leg pressurization to 2,500 psi, which was constant for all tests.

Shield height.—Two shield heights were investigated: 56 and 87.5 in. These heights represent a low and high configuration in the overall operating range of the support.

Canopy contact configuration.—Four canopy contact configurations were investigated. All contacts are symmetric about the longitudinal centerline of the canopy and are described in terms of a two-dimensional representation, the actual number of contact points is twice that illustrated. The four canopy contacts (fig. 13) are full contact (type 1), two-point contact (type 2), one-point contact (type 3), and three-point contact (type 4). Full base contact was utilized for all tests.

Canopy and base constrainment.—Both horizontally constrained and unconstrained configurations were evaluated. The intent of constrainment is to remove rigid-body translational freedom from the pin joints to allow the caving shield-lemniscate assembly to fully participate in the shield

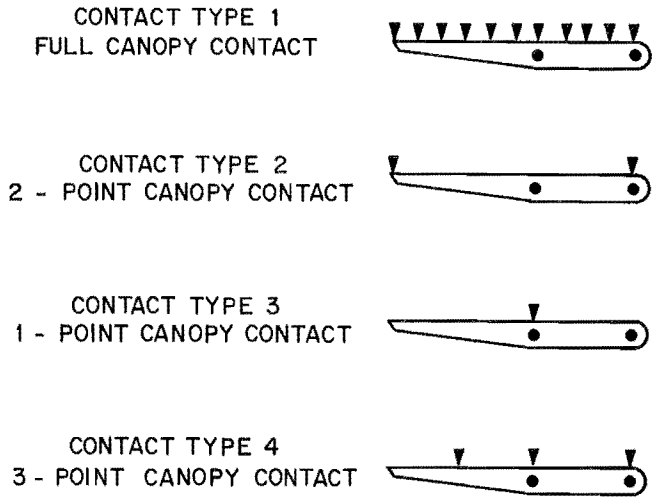

Figure 13.—Canopy contact configurations.

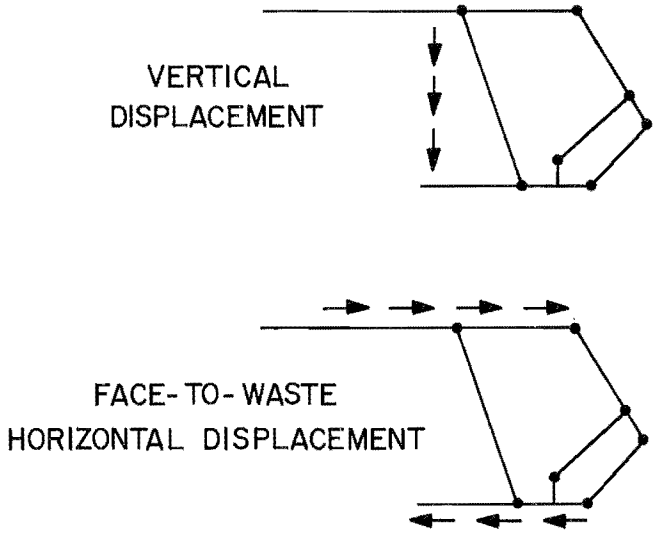

Figure 14.—Vertical and face-to-waste displacement loading.

load transfer mechanics. Constrained configurations are achieved by horizontal displacement of the canopy relative to the base prior to setting the shield.

Displacements.—Both vertical and face-to-waste horizontal displacements are evaluated (fig. 14). Since the internal load-transferring mechanics are different for vertical and horizontal displacement loading, it is essential that both displacements are considered.

MODEL RESPONSES AND PARAMETER SENSITIVITY

Model responses to each parameter consideration are documented in this section. Test data were generated by controlled displacement loading (from time-dependent displacement load ramps) of the shield by the mine roof simulator. Equivalent time-selected data points, which represent varying degrees of shield loading, are selected for each test for analysis to provide a cross section of the model response through the complete displacement load profile (fig. 15). The format and motivation for analysis of model behavior follows.

First, the sensitivity of each model to the four parameter considerations is evaluated. This is necessary to identify application limitations. For example, if a model was shown to be sensitive to contact configuration, then its application to in situ measurements of support loading would be limited since in situ contact configurations are generally not known.

The vertical and horizontal force prediction accuracy of each model is then documented. Predicted vertical and horizontal forces from the models are plotted against actual forces as measured by the simulator. A visual interpretation of model force prediction capability is made by comparing model responses to a 1-to-1 curve that represents a perfect correlation between actual and predicted forces. In addition, average and maximum force prediction errors are computed to quantify force prediction accuracy.

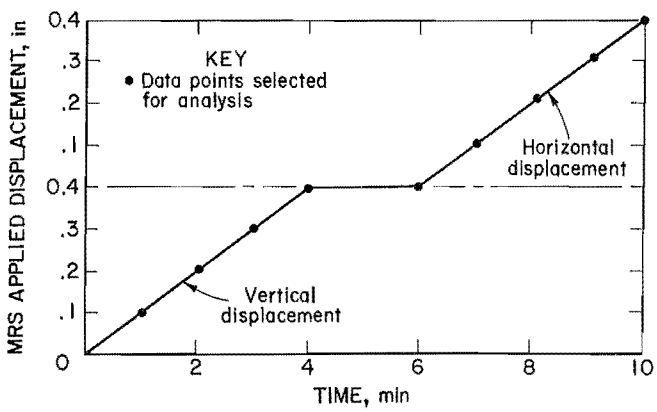

Figure 15.—Data selection from displacement-controlled load profiles.

Also included are resultant vertical force location predictions. Location predictions and actual locations are illustrated in bar chart format. Four location predictions representing increasing shield loading are illustrated for each contact type for the low (56 in) and high (87.5 in) shield height. Since the pressure distribution on the canopy obtained during full contact is not known, the actual resultant location for full canopy contact cannot be computed and is not shown. Computation of actual location for partial contact configuration is described in the "Description of Models and Parameter Considerations" section.

Finally, a comparison of model responses among each of the four models is provided. Bar charts depicting average and maximum force prediction errors for appropriately grouped data are used to compare behavior of the four models.

MODEL SENSITIVITY ANALYSIS

A general sensitivity analysis is shown in figures 16 through 27 by isolating changes in each of the parameter considerations (shield height, constrainment, contact configuration, or displacement). This allows the influence of a particular parameter to be evaluated. For example, test data showing model responses are grouped together for all tests conducted at the low height and all tests conducted at the high height. These data are then depicted in separate graphs to show the effects of shield height for a particular model. Since variances in other parameters (constrainment, contact configuration, and displacement) are common to both graphs, the sensitivity of the model to height can be determined by comparison of the model responses for the low and high shield height.

The model sensitivity is judged by comparing model responses to the 1-to-1 curve for changes in the particular parameter investigated in the figure. The 1-to-1 curve represents perfect correlation between the predicted and actual forces. Also included is a linear regression curve fit of the data points depicting model responses. The regression line is shown to provide assistance in comparing model responses to the 1-to-1 curve. It is useful in depicting representative model responses, but the dispersion of the data must be considered when using the regression line as a visual aid in comparing model responses. Sensitivity as used in this context does not necessarily imply an accurate model; it simply means the model behavior is consistent among the parameter changes.

Using figure 16 as an example, it is seen that the accuracy of this particular model is decreased for the high height compared to the low height, particularly for horizontal forces. Hence, it is concluded that this particular model shows a sensitivity to height. In contrast, this same model appears to be fairly insensitive to contact configuration as shown in figure 19, since the model responses are fairly consistent for each of the four contact types.

Using this analysis technique, observations of parameter sensitivity are summarized as follows:

1. The rigid-body models (leg-pin and leg-link) are most sensitive to displacement, particularly in regard to vertical force predictions. A study of shield mechanics shows that the shield reacts a vertical force to both vertical and face-to-waste horizontal displacements. As illustrated in figures 18 and 22, the rigid-body models predict vertical force developments from vertical displacements more accurately than they do for horizontal displacements, thus demonstrating a vertical force prediction sensitivity to displacement. Since the vertical force generated from vertical displacements is generally significantly greater than that generated from horizontal displacements, this sensitivity is not considered a major limitation in the application of the rigid-body models.

2. All models show some sensitivity to shield height. The general trend is a reduction in vertical force prediction accuracy at the high shield height. The sensitivity is more pronounced for horizontal force predictions than vertical force predictions. Since shield height can be easily determined, the sensitivity to shield height is not considered a limitation for application of these models to in situ shield load investigations.

3. In general, the rigid-body models appear to be fairly insensitive to constrainment with similar trends observed for unconstrained and constrained load cases. The linear elastic model shows some sensitivity to constrainment. Vertical forces tend to be predicted accurately for constrained load cases and underpredicted for unconstrained load cases, while horizontal forces tend to be underpredicted for unconstrained load cases and overpredicted for constrained load cases.

4. All models appear to be insensitive to canopy contact configuration by demonstrating similar behavior for each of the four configurations investigated. This is a desirable response since contact configurations underground are generally not known.

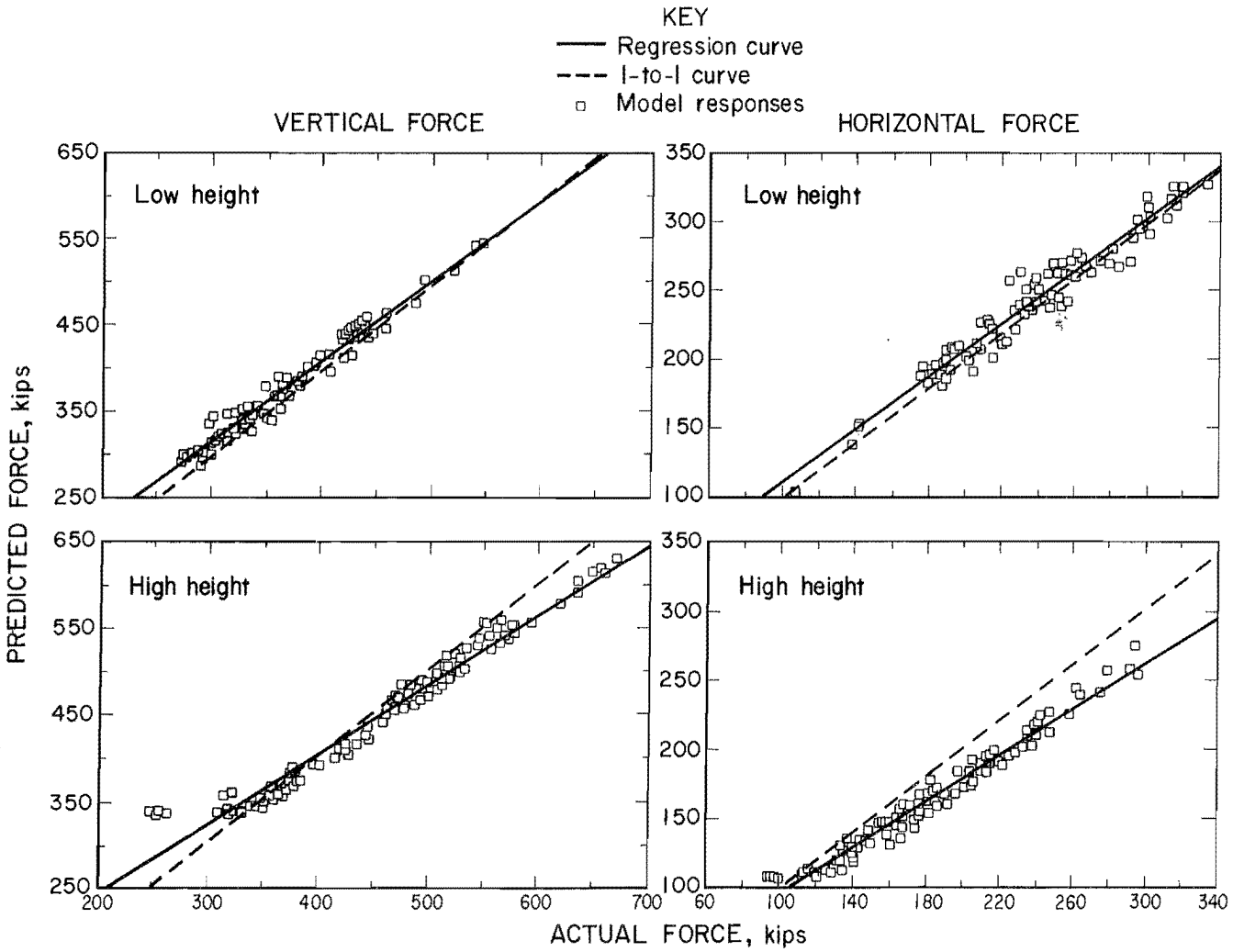

Figure 16.—Leg-pin model sensitivity to shield height.

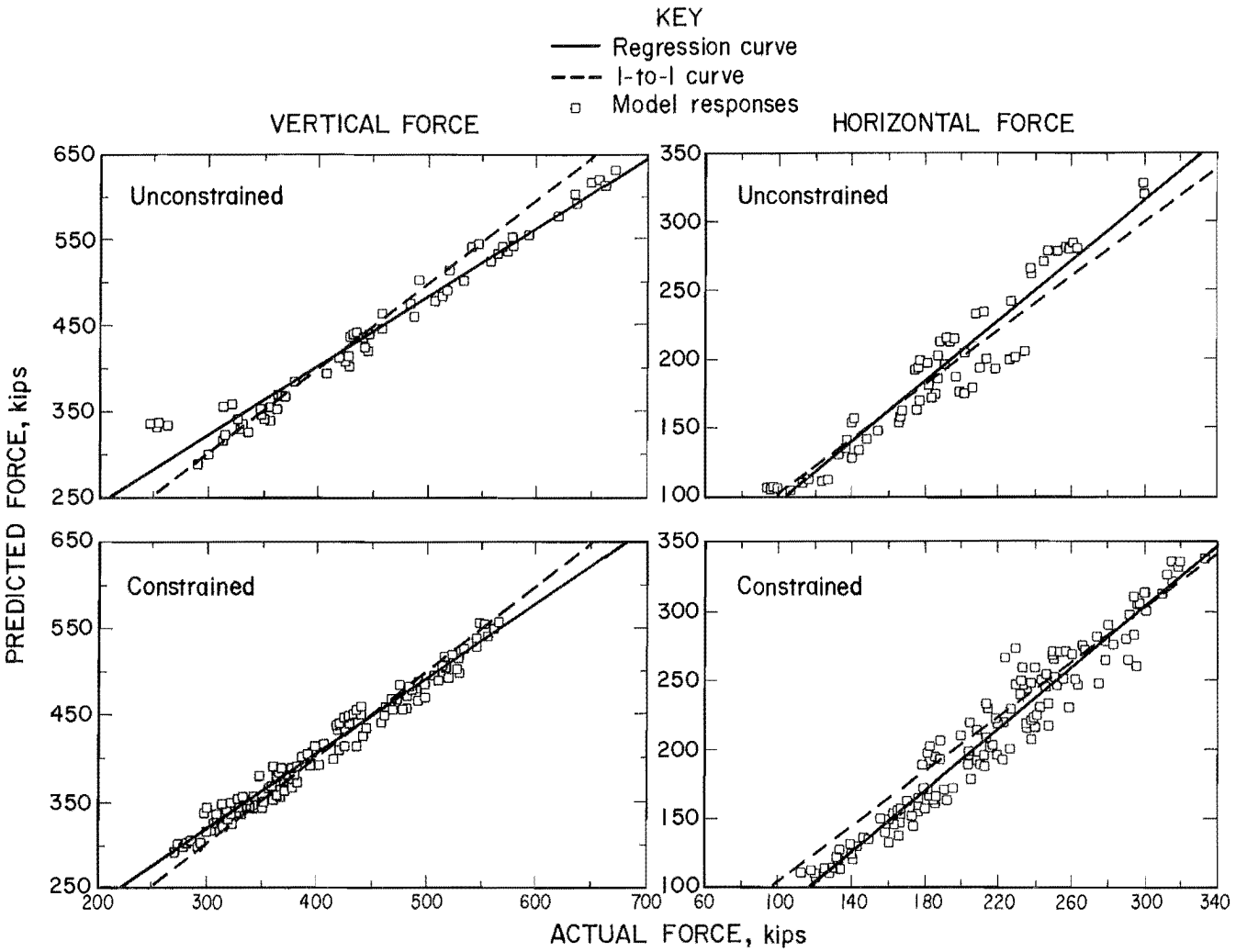

Figure 17.—Leg-pin model sensitivity to horizontal constrainment.

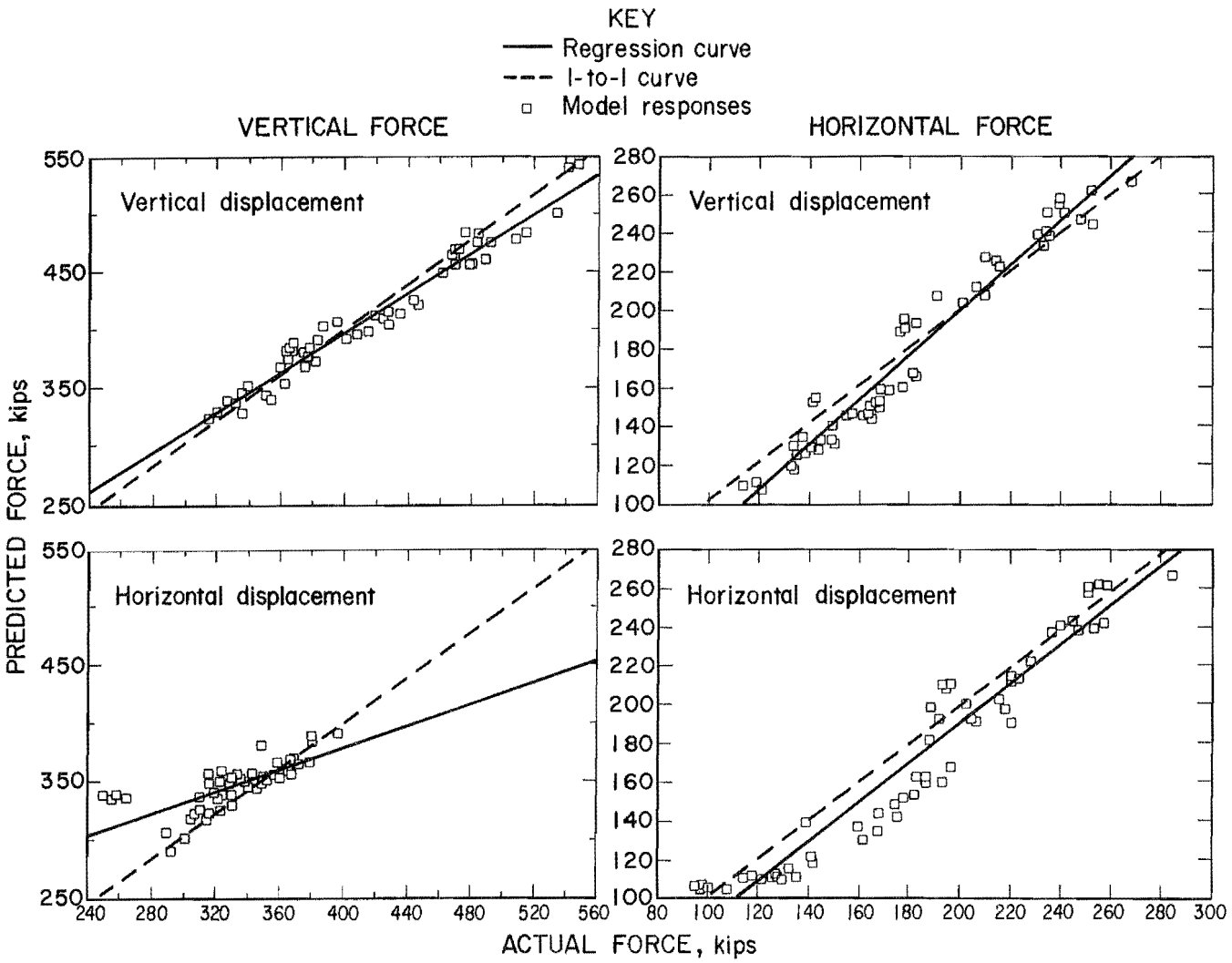

Figure 18.—Leg-pin model sensitivity to displacement.

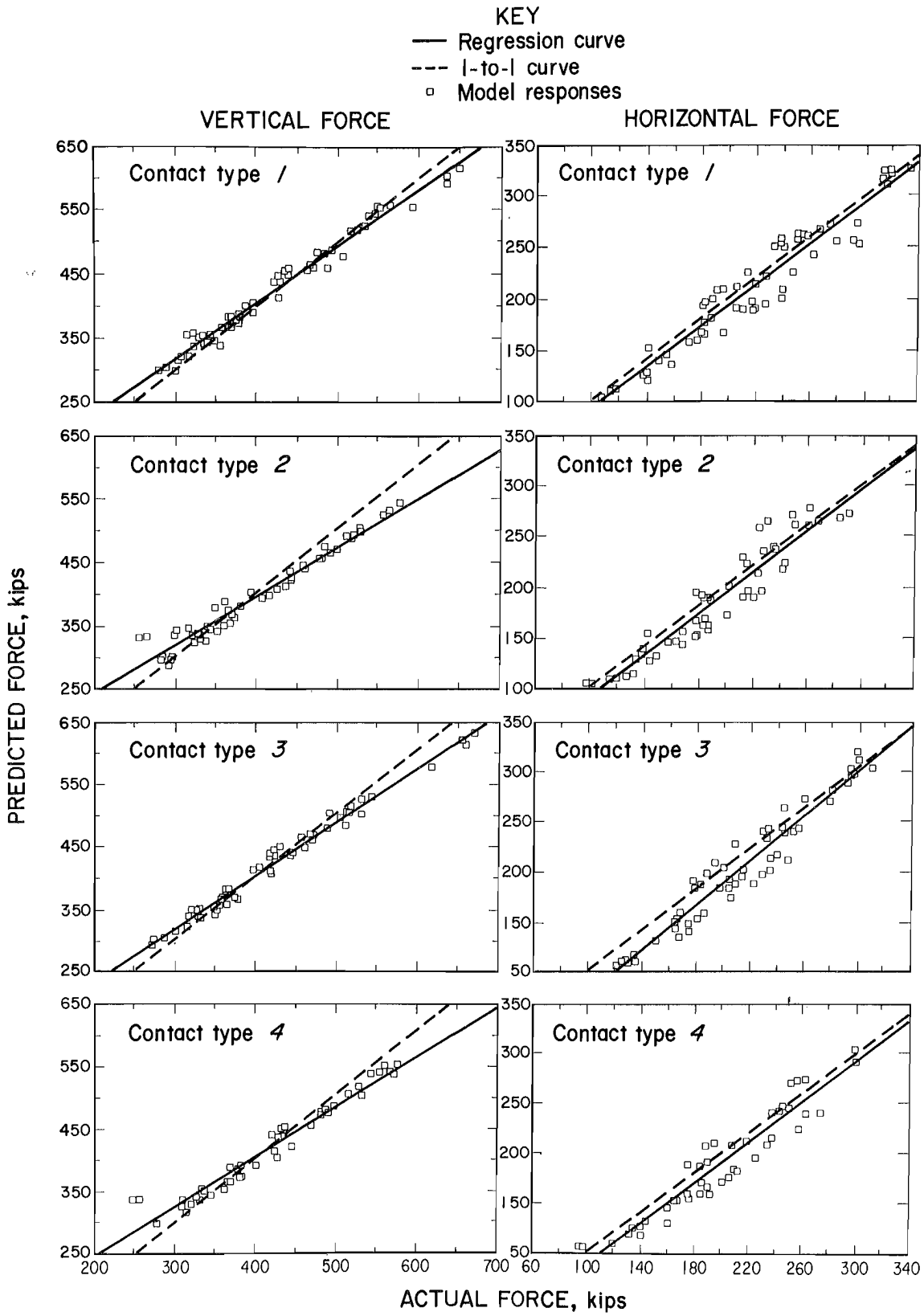

Figure 19.—Leg-pin model sensitivity to canopy contact configuration. Type 1—full canopy and base contact, type 2—two-point canopy contact, type 3—one-point canopy contact, type 4—three-point canopy contact.

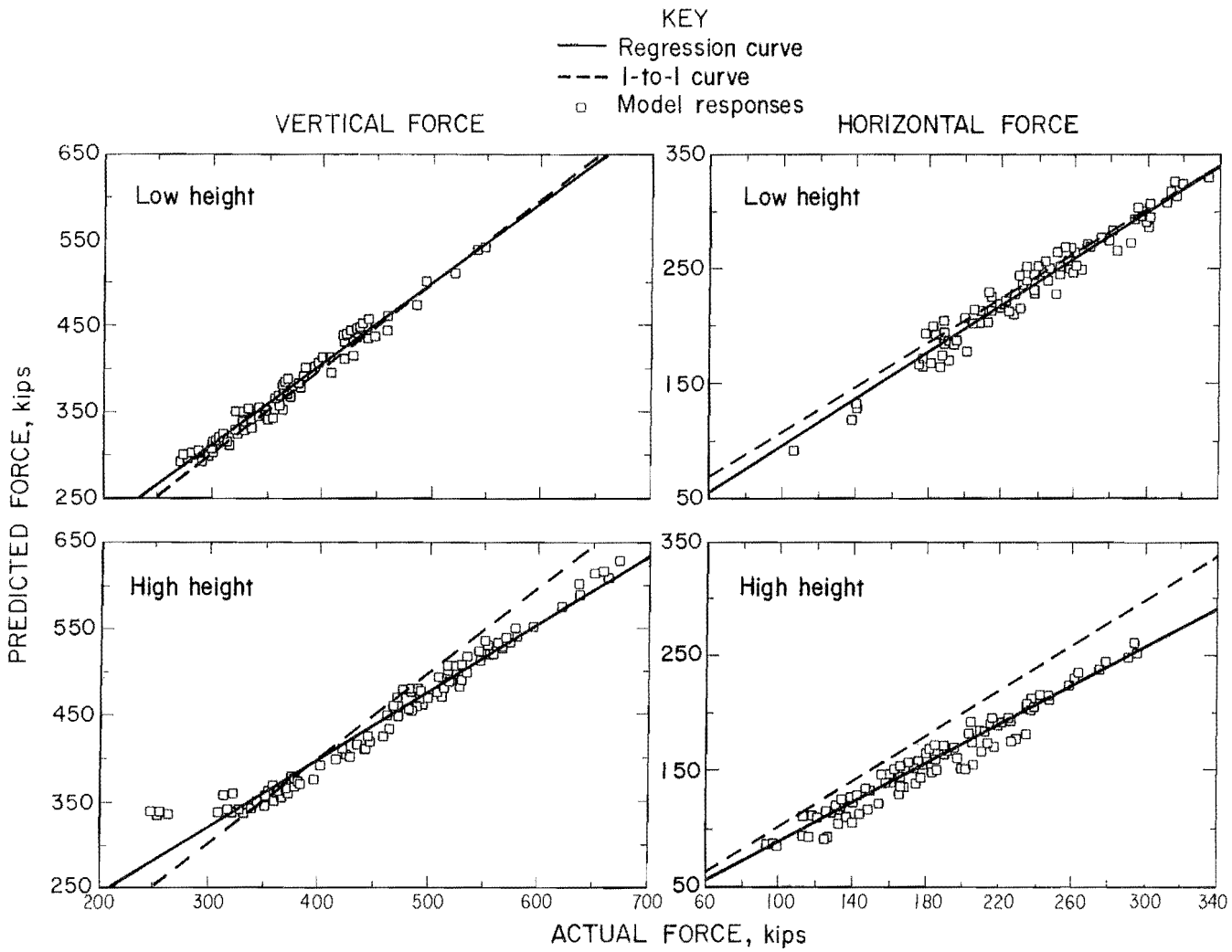

Figure 20.—Leg-link model sensitivity to shield height.

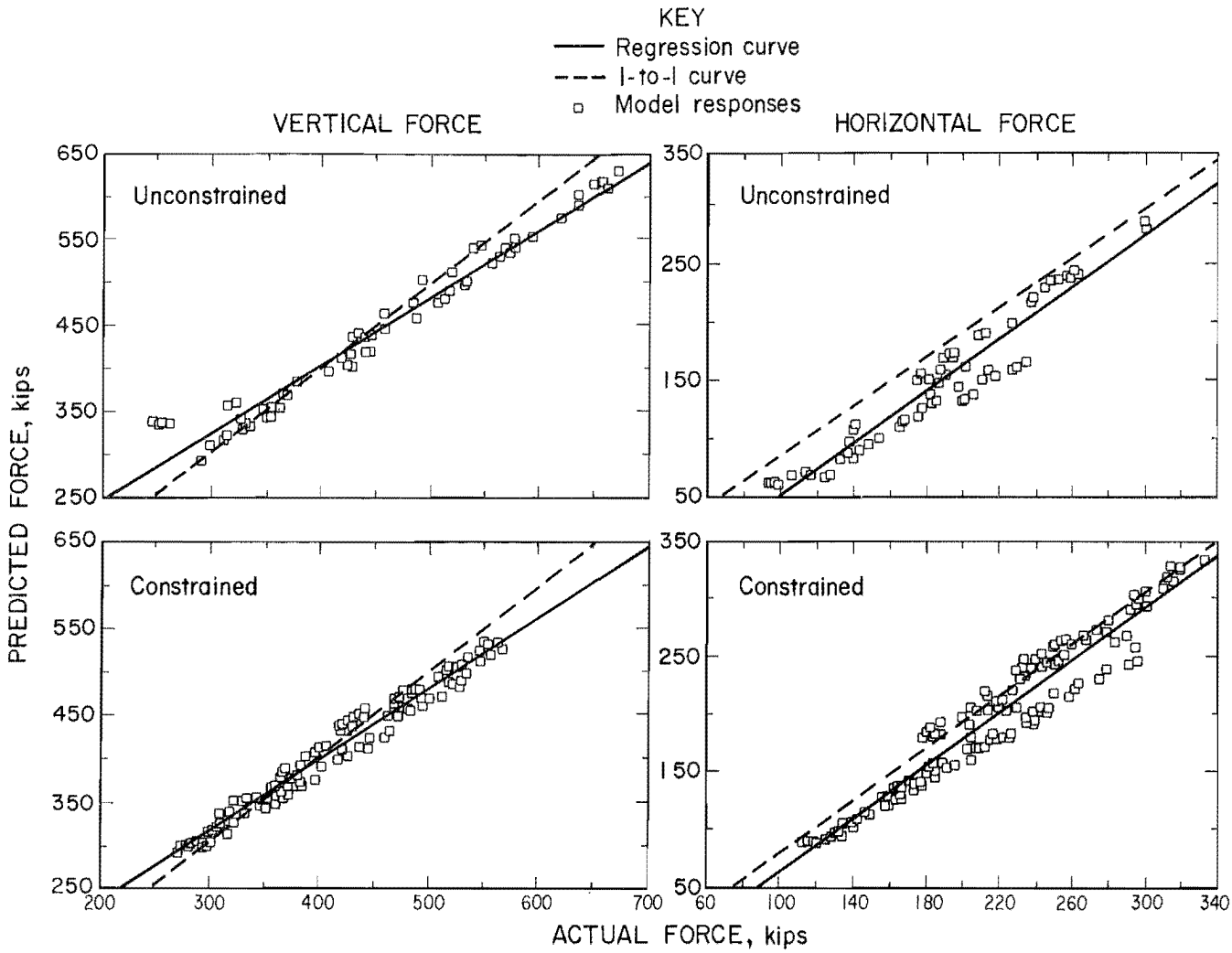

Figure 21.—Leg-link model sensitivity to horizontal constrainment.

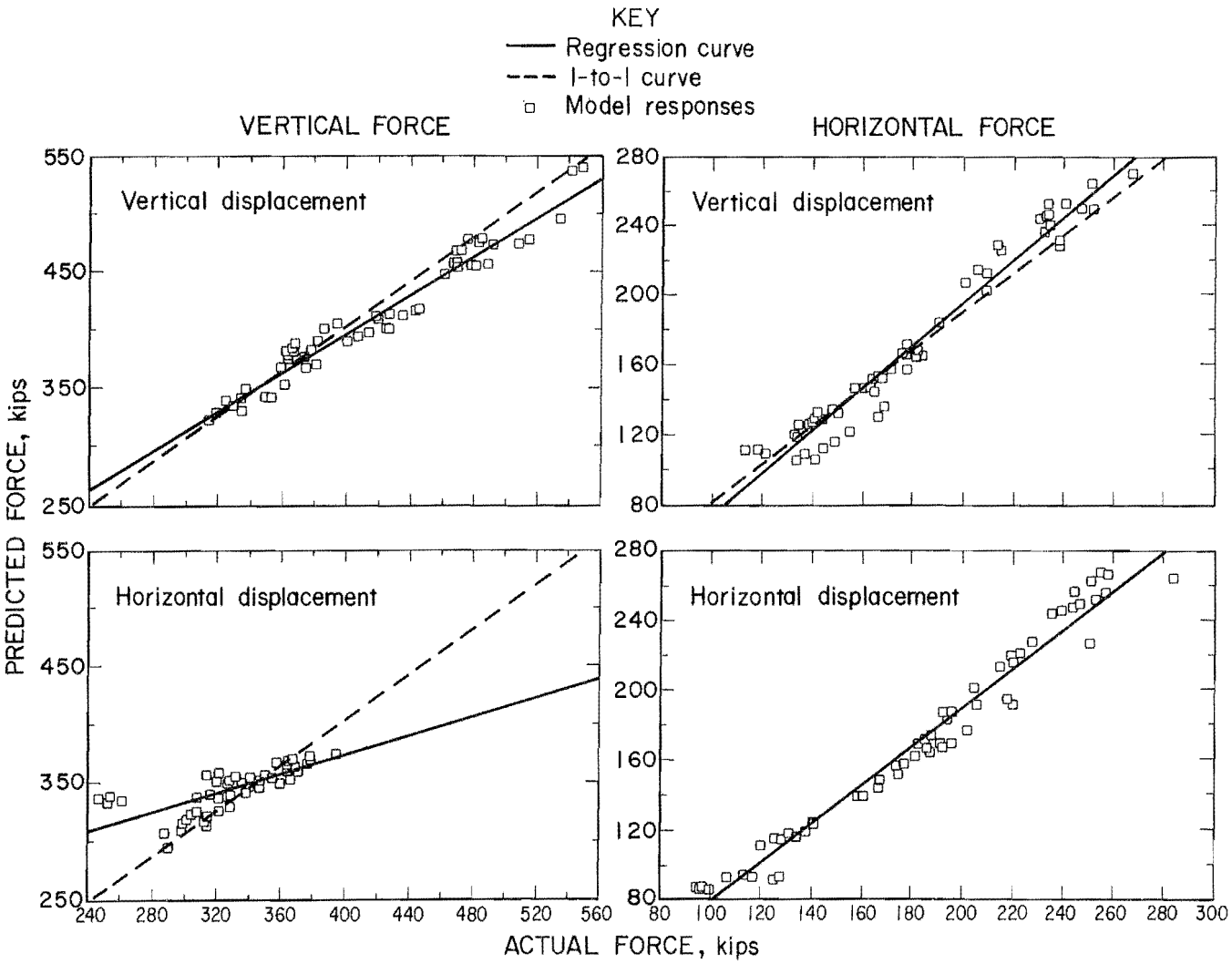

Figure 22.—Leg-link model sensitivity to displacement.

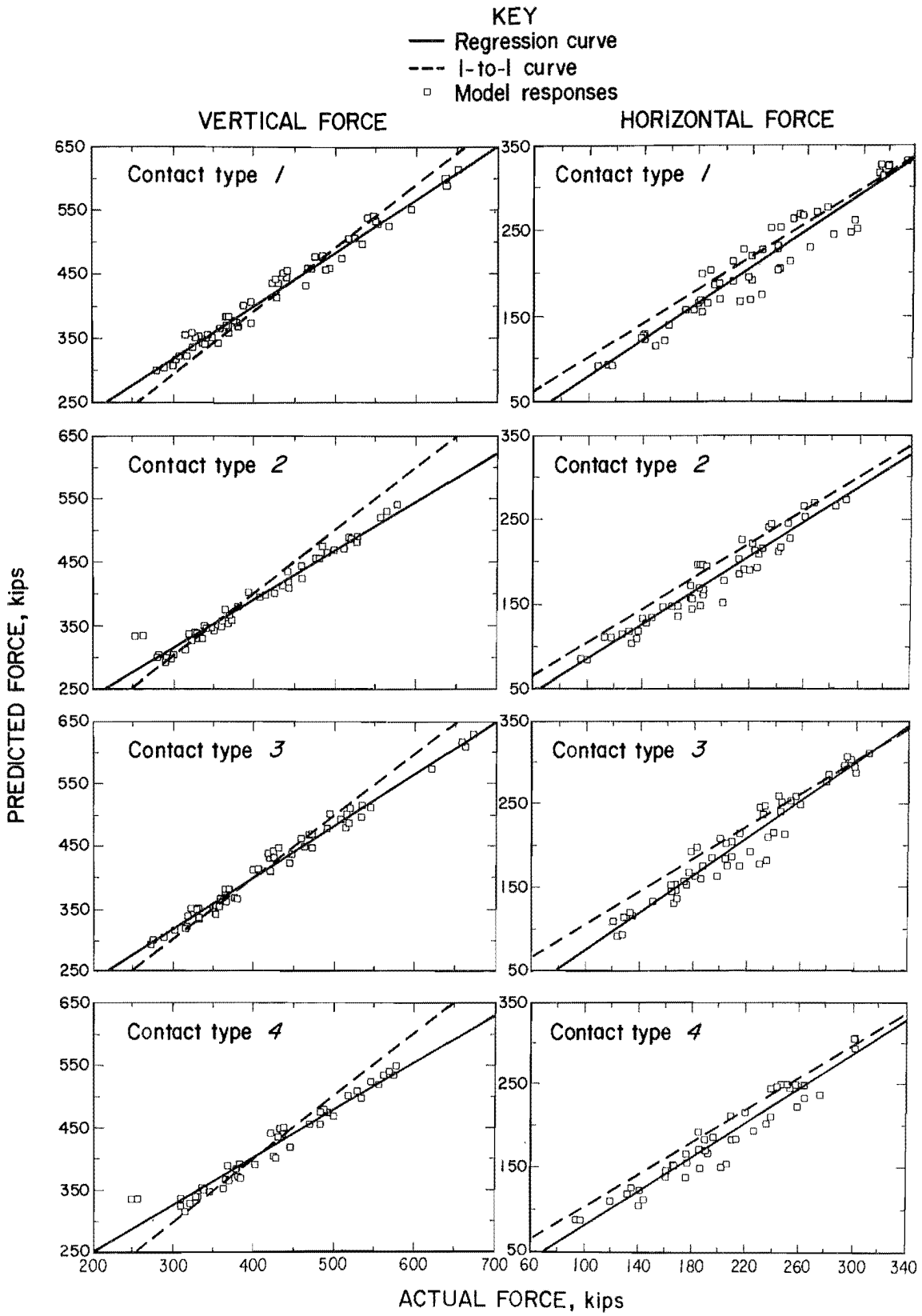

Figure 23.—Leg-link model sensitivity to canopy contact configuration. Type 1—full canopy and base contact, type 2—two-point canopy contact, type 3—one-point canopy contact, type 4—three-point canopy contact.

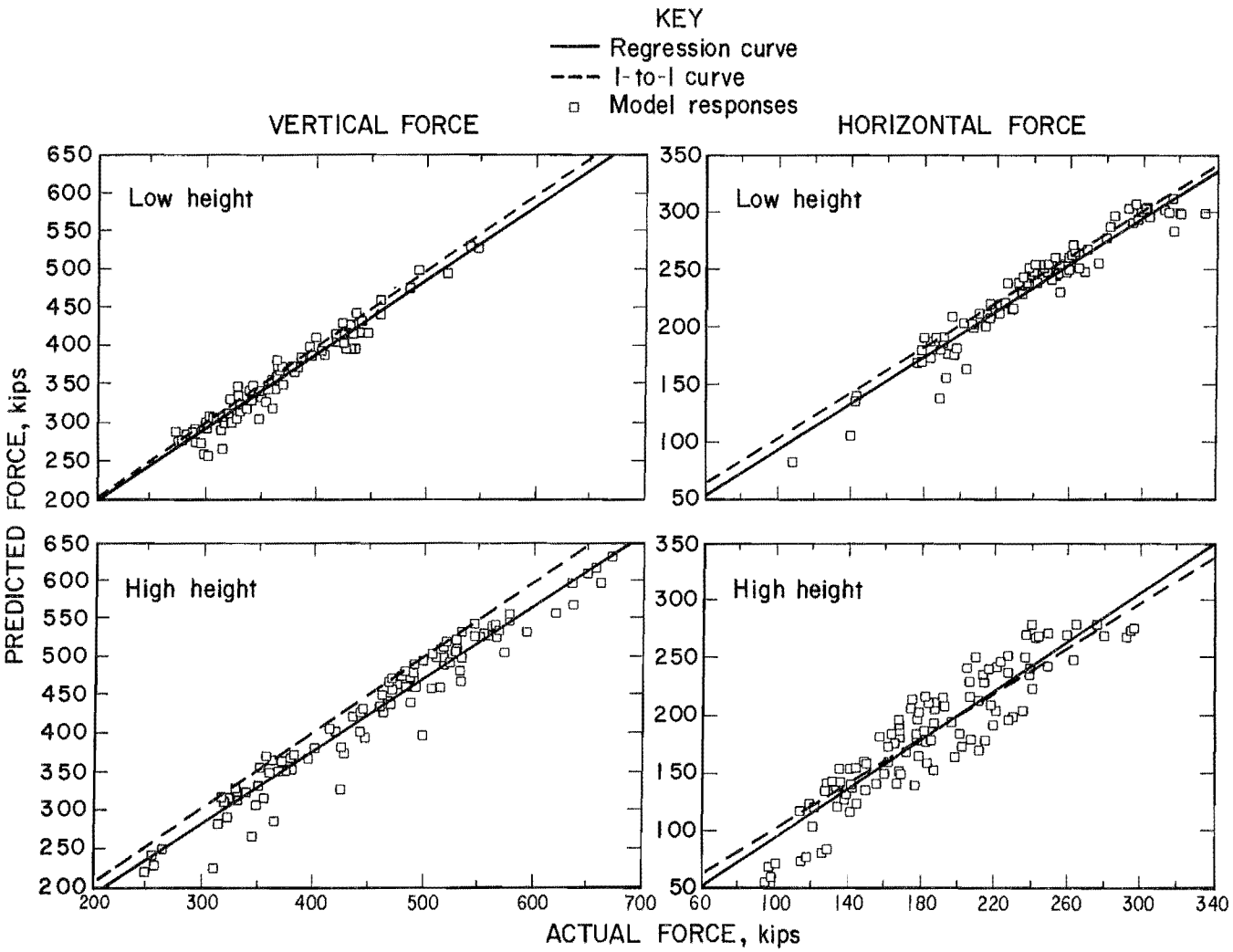

Figure 24.—Elastic stiffness model sensitivity to shield height.

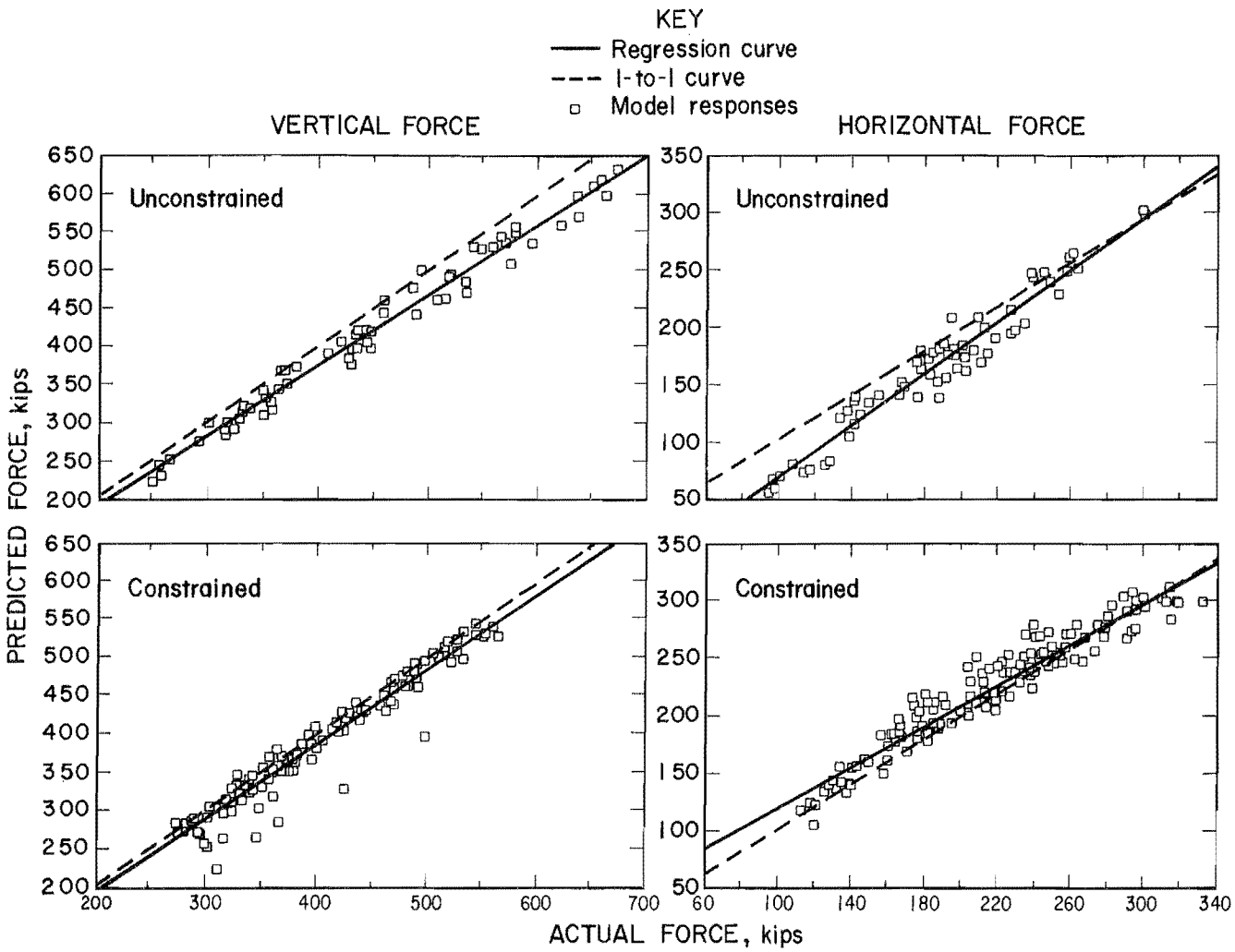

Figure 25.—Elastic stiffness model sensitivity to horizontal constrainment.

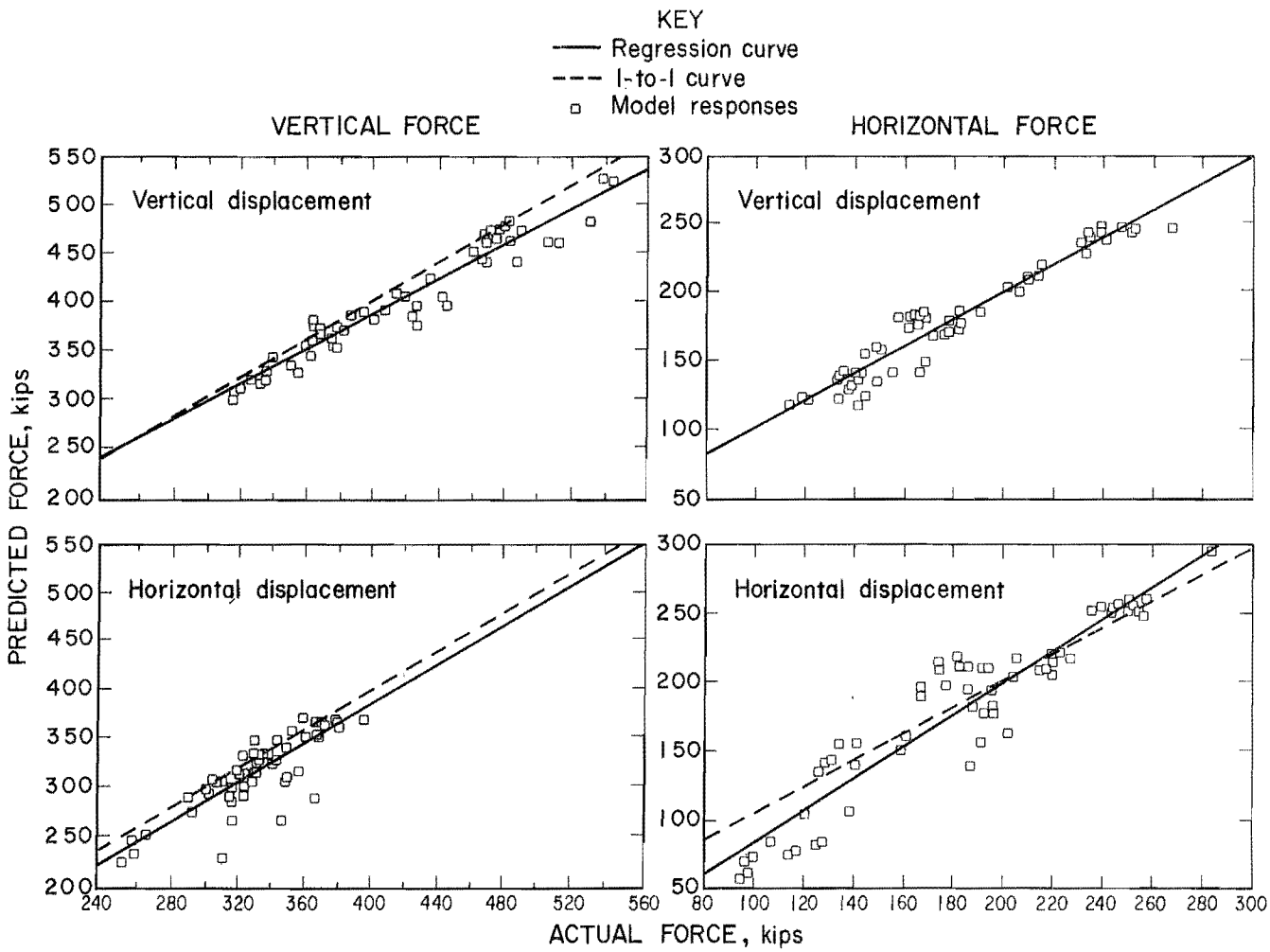

Figure 26.—Elastic stiffness model sensitivity to displacement.

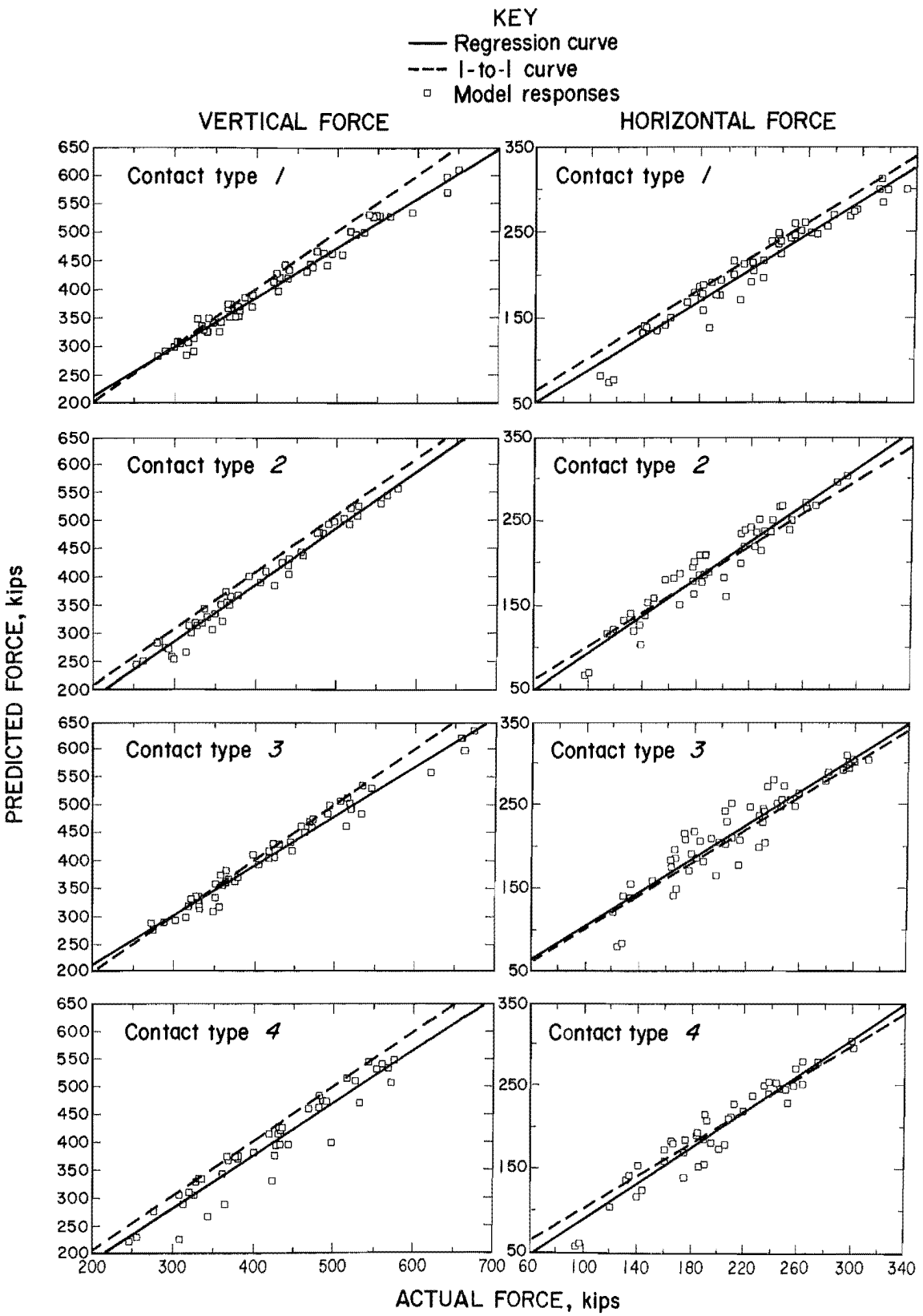

Figure 27.—Elastic stiffness model sensitivity to canopy contact configuration. Type 1—full canopy and base contact, type 2—two-point canopy contact, type 3—one-point canopy contact, type 4—three-point canopy contact.

FORCE AND LOCATION PREDICTION ANALYSIS

Force prediction evaluations are made by comparisons of model responses to the 1-to-1 curve in figures 28 through 37. Force prediction capabilities of the four models are shown for constrainment, displacement, and contact configuration parameter considerations. Since the models demonstrated sensitivity to shield height, force predictions are segregated by shield height in figures 28 through 37. Location predictions are illustrated in figures 38 through 40 for constrained and unconstrained load conditions at the low and high shield heights. Location predictions at four different load magnitudes for each contact type were selected for illustration in these figures.

Leg-Pin (Rigid-Body) Model

Behavior of the leg-pin rigid-body model is illustrated in figures 28 through 30 (force predictions) and figure 38 (location predictions). Observations of resultant force and location prediction capability are summarized as follows:

1. Average force prediction errors ranged from 1.6 to 12.4 pct. Considering average error, the model is least accurate in predicting horizontal forces at the high shield height for horizontal displacements (12.4 pct error) and most accurate in predicting vertical forces at the low shield height (1.6 pct error) for unconstrained initial conditions.
2. Worst case model responses (maximum force prediction error) occurred for the following conditions: (1) vertical force predictions at the high shield height for unconstrained initial conditions, (2) vertical force predictions at the high shield height for horizontal displacements, and (3) vertical force predictions at the high shield height for three-point canopy contact (type 4). Each of these cases exhibited a maximum 36 pct force prediction error. These responses appear to be isolated cases of anomalous shield behavior. These maximum errors always occurred at small displacements (low forces), and therefore probably are related to some mechanically anomalous behavior as the shield "settles in" during initial load application.
3. Forces are generally overpredicted for the low shield height and underpredicted for the high shield height. In general, vertical force predictions are more accurate (average error, 1.6-9.1 pct) than horizontal force predictions (average error, 3.1-12.4 pct).
4. Force predictions for each of the parameter considerations produce fairly linear responses throughout the displacement range. A few parameter considerations, mostly in the high-shield-height configuration, show some nonlinear behavior in the lower force ranges. The nonlinear behavior is most prevalent for unconstrained load cases and horizontal displacements. This suggests a correlation of this behavior to pin freedom in the shield joints.
5. Resultant vertical force location predictions were very consistent, predicting a location very close to the leg connection. The general response was for the model to overpredict (predict location further from the canopy hinge than it actually was) the location by 2 to 4 in.

Overall, the rigid-body model using leg pressures converted to leg forces and canopy-caving shield pin forces acquired from instrumented pins is a fairly accurate and versatile model. The model does not demonstrate a preferred loading condition. It is not critically sensitive to changes in horizontal constrainment or canopy contact configuration.

Leg-Link (Rigid-Body) Model

Behavior of the leg-link model is illustrated in figures 31 through 33 (force predictions) and figure 39 (location predictions). Observations of resultant force and location prediction capability are described as follows:

1. Average force prediction errors ranged from 1.6 to 20.3 pct. The model is least accurate in predicting horizontal forces at high shield heights for unconstrained initial conditions and most accurate in predicting vertical forces at low shield heights for unconstrained load cases.
2. Worst case model responses occurred for vertical force predictions for the same conditions that produced maximum error responses with the leg-pin model. These conditions are (1) high shield height for unconstrained initial conditions, (2) high shield height for horizontal displacements, and (3) high shield height for three-point canopy contact (type 4). Maximum errors ranged from 3.4 to 35.7 pct. As with the link-pin model, maximum errors occurred at relatively low forces.
3. Consistent with the leg-pin model, the leg-link model also tended to underpredict forces for the high shield height and slightly overpredict forces for the low shield height. Vertical force predictions also tended to be more accurate (average error, 1.6-9.6 pct) than horizontal force predictions (average error, 3.2-20.3 pct).
4. The leg-link model also produced fairly linear responses throughout most of the displacement loading range. As with the link-pin model, some nonlinear behavior was observed in the lower force ranges, suggesting this behavior is a reflection of actual shield mechanics.

5. Resultant vertical force predictions were also very consistent for the leg-link model. An overprediction trend of 2 to 4 in was also observed.

From this analysis, it is concluded that the leg-link model is also a versatile model similar in behavior to the leg-pin model. Like the leg-pin model, the leg-link model does not demonstrate a preferred loading condition and is not critically sensitive to changes in horizontal constrainment or canopy contact configuration.

Elastic Stiffness Model

Results of the elastic stiffness model are illustrated in figures 34 through 36 (force predictions) and figure 40 (location prediction). Observations of the model's force and location prediction capability are summarized as follows:

1. Average force prediction error ranged from 2.2 to 18.0 pct. The elastic stiffness model was most accurate in making vertical force predictions for full canopy contact (type 1) at the low shield height and least accurate in horizontal force predictions at the high shield height for unconstrained initial conditions.
2. Worst case force predictions (maximum force prediction error) occurred for horizontal forces produced from horizontal displacements at the high shield height and horizontal force predictions for canopy contact type 4 (three-point contact) at the high shield height. Maximum error for these conditions was 40.5 pct, while the average error was only 16.2 pct at the high shield height and 10.4 pct at the type 4 contact.
3. Vertical forces were predicted more consistently and considerably more accurately than the horizontal forces. Average errors in vertical force predictions ranged from 2.2 to 8.3 pct, while average errors in horizontal force predictions ranged from 2.4 to 18.0 pct for the various parameter considerations.
4. Force predictions, both vertical and horizontal force, were consistently more accurate for the low shield height than the high shield height.
5. The elastic stiffness model performs better for constrained load cases than it does for unconstrained load cases.
6. Resultant vertical force predictions were generally in good agreement with the actual locations, often being within 2 in of the actual locations. There does not appear to be a general trend of overprediction or underprediction except for unconstrained load cases at the low shield height where the vertical resultant location was consistently overpredicted.

Finite-Element Model

The finite-element model responses are shown in figure 37. Only constrained contact configurations subject to vertical displacements were analyzed since the model does not have the capability to incorporate a slip capability in the links to account for pin freedom, a feature necessary to evaluate horizontally unconstrained load cases. Hence, only shield height and vertical canopy contact were varied in the finite-element model investigation. Model responses for a specific amount of vertical displacement (0.2 in) are shown in figure 37. Unlike physical models, which depend on physical measurements of structural behavior, the numerical model is consistent throughout the displacement range, hence one displacement is sufficient to demonstrate its capabilities.

Observations of the finite-element model performance are described as follows:

1. The model underestimates vertical forces by 5 to 11 pct at the low shield height and overestimates horizontal forces by 13 to 42 pct at the high shield height. This implies that the model is too stiff horizontally and not stiff enough vertically.
2. In general, the finite-element model is not adversely affected by canopy contact configuration except for horizontal force predictions at the high shield height. The accuracy of horizontal force predictions was considerably less for full canopy contact (type 1) and two-point canopy contact (type 2) than it was for one-point and three-point canopy contact (types 3 and 4, respectively). Without further analysis, there is no apparent explanation for this behavior.

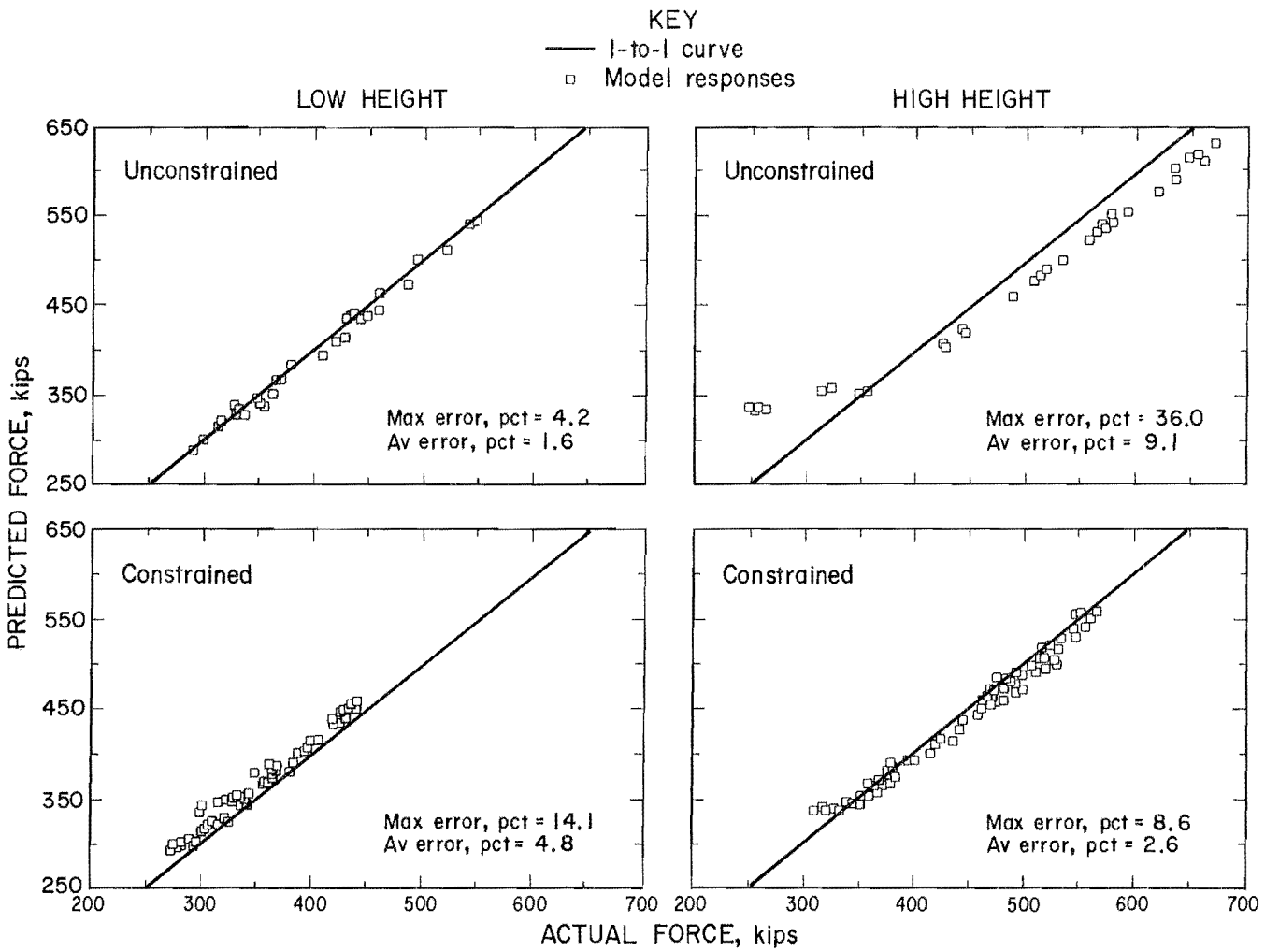

Figure 28.—Leg-pin model force predictions for horizontal constrainment parameter considerations. Vertical force predictions.

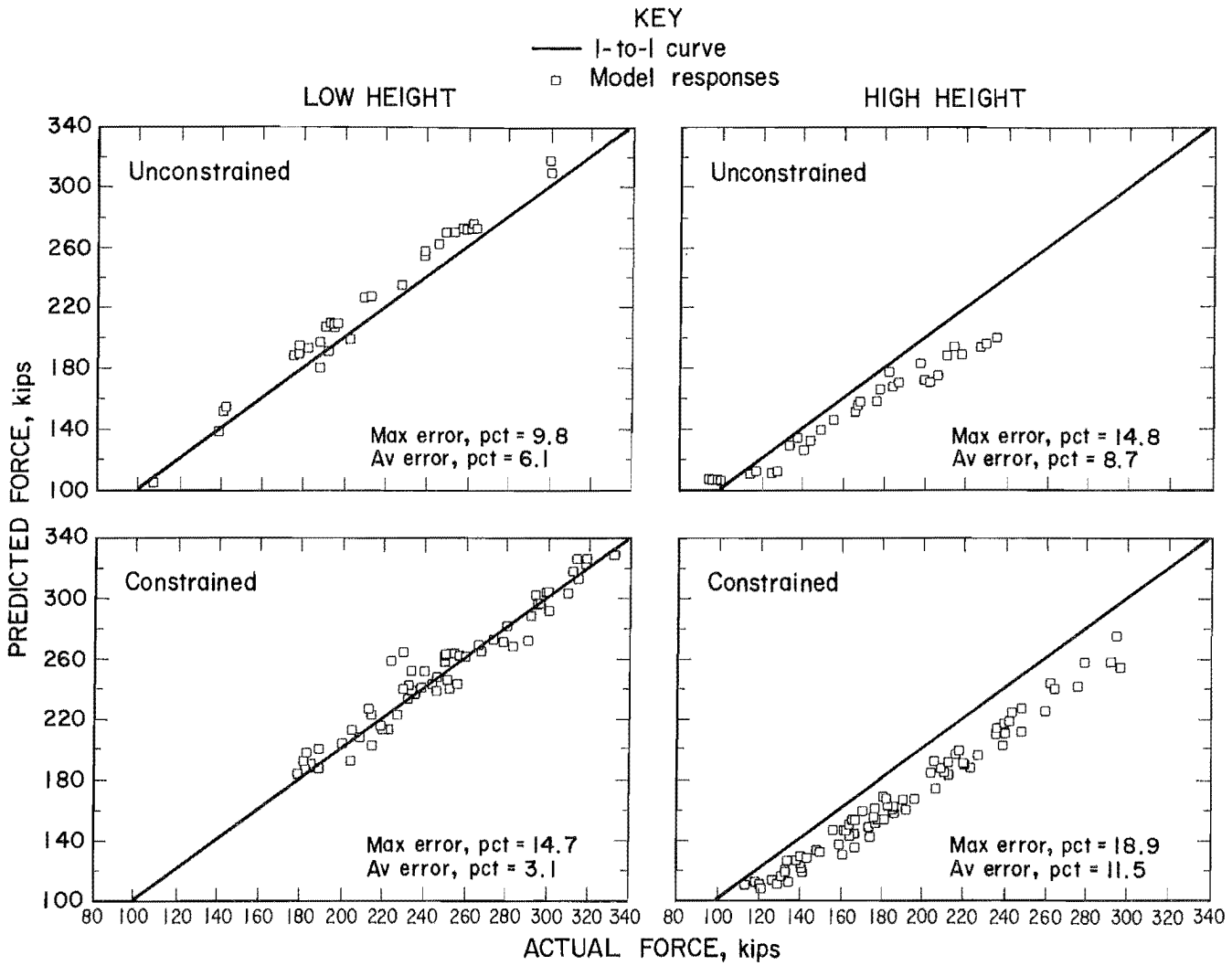

Figure 28.—Leg-pin model force predictions for horizontal constrainment parameter considerations—Continued. Horizontal force predictions.

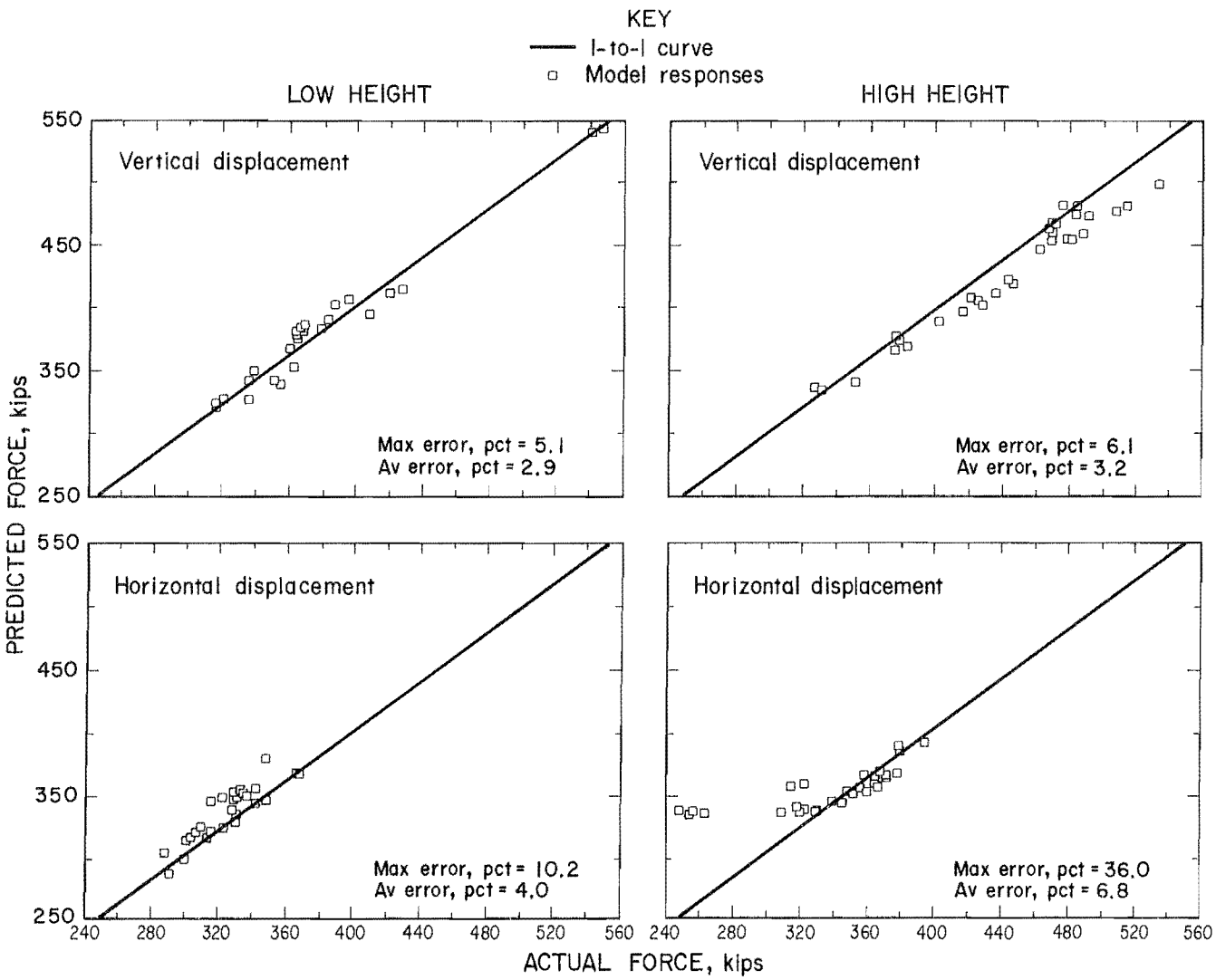

Figure 29.—Leg-pin model force predictions for displacement parameter considerations. Vertical force predictions.

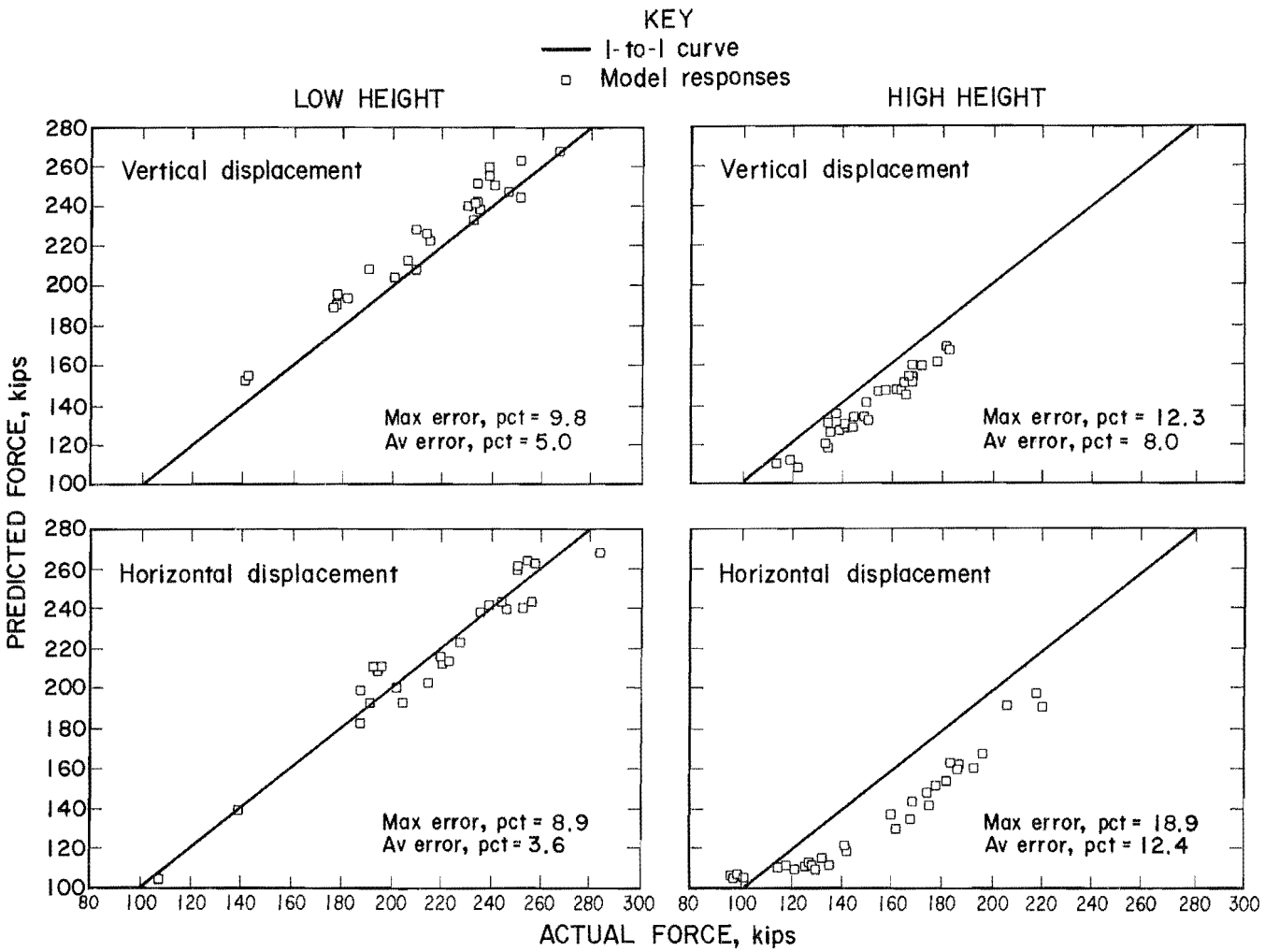

Figure 29.—Leg-pin model force predictions for displacement parameter considerations—Continued. Horizontal force predictions.

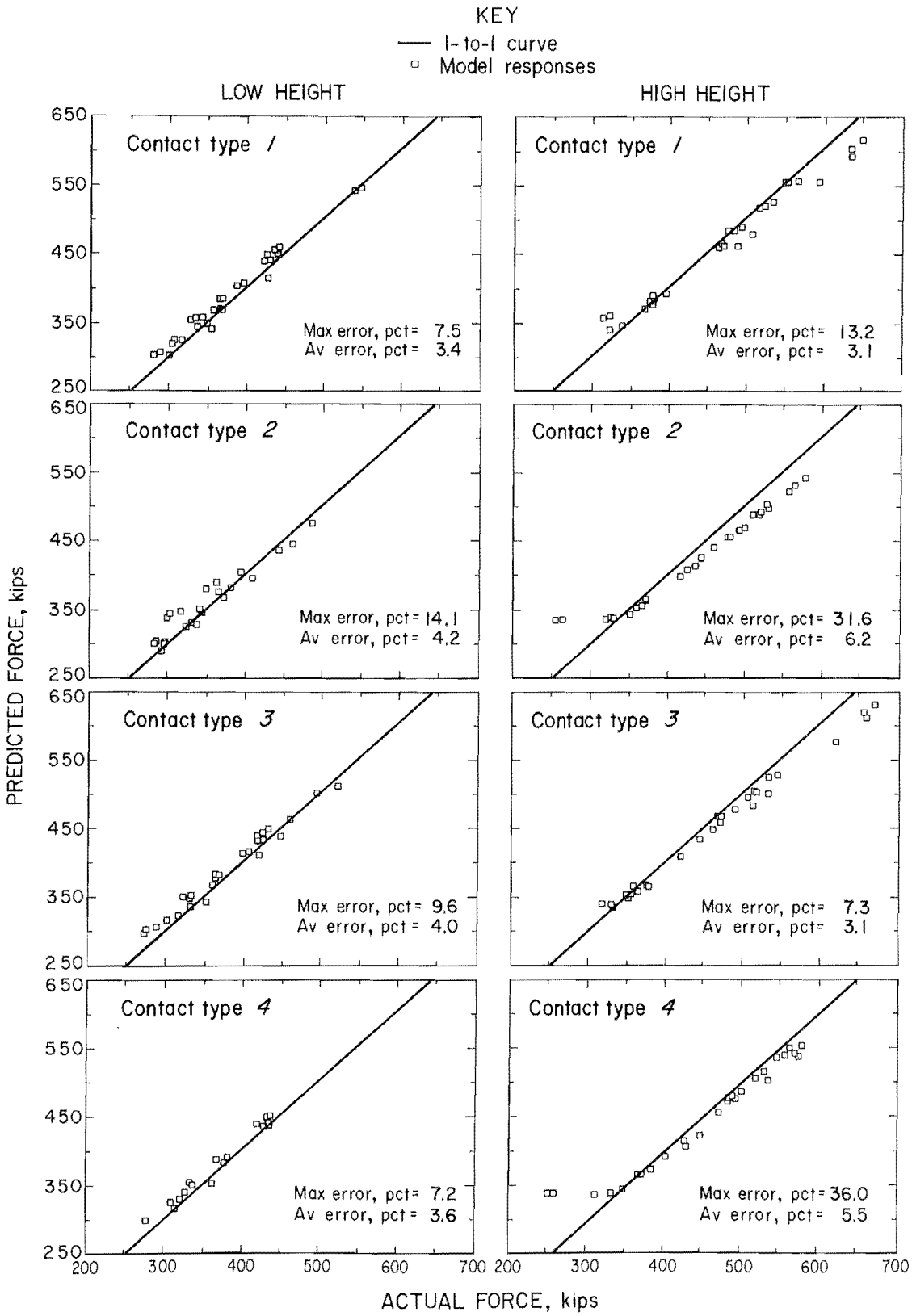

Figure 30.—Leg-pin model force predictions for canopy contact parameter considerations. Vertical force predictions. Type 1—full canopy and base contact, type 2—two-point canopy contact, type 3—one-point canopy contact, type 4—three-point canopy contact.

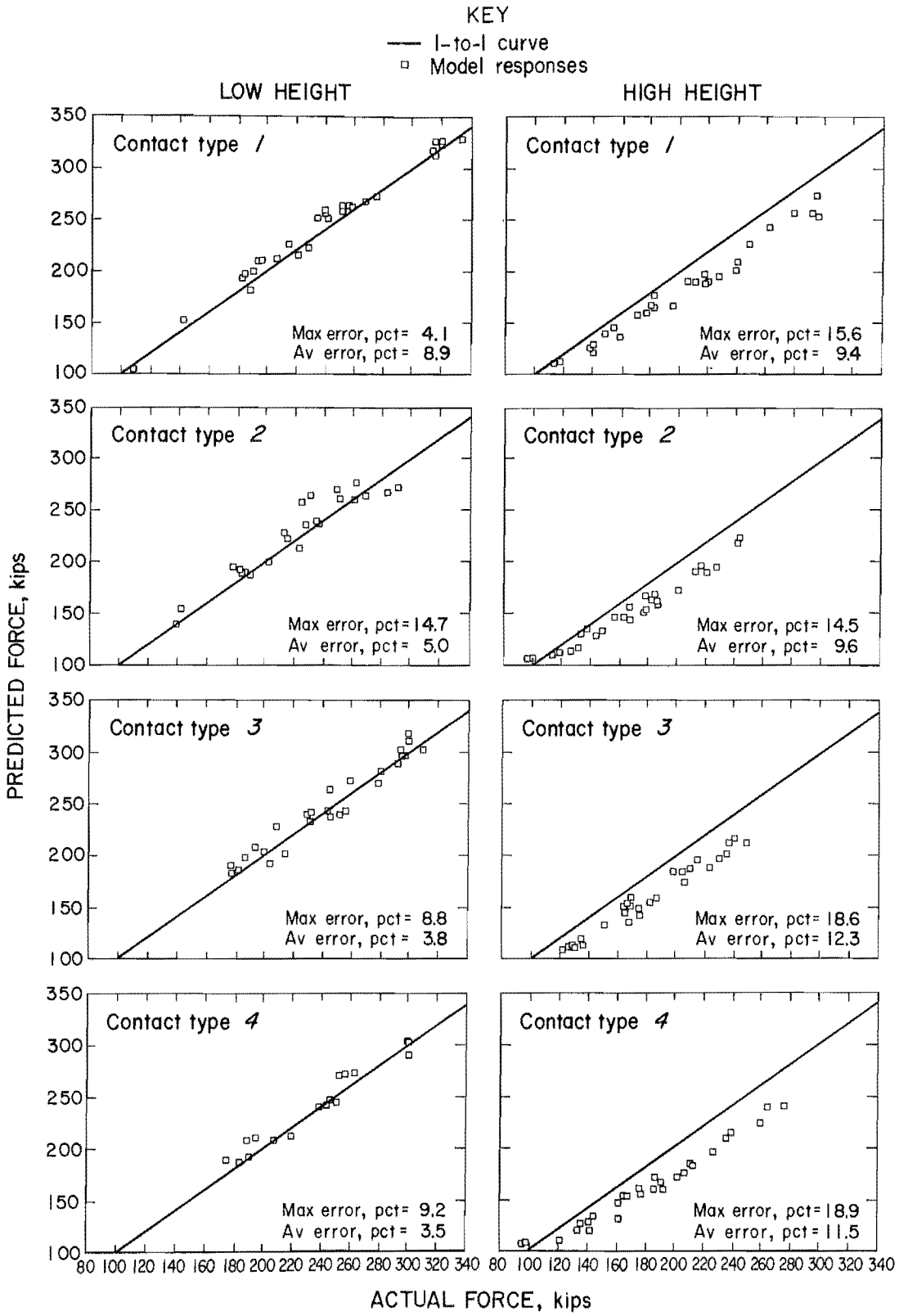

Figure 30.—Leg-pin model force predictions for canopy contact parameter considerations—Continued. Horizontal force predictions.

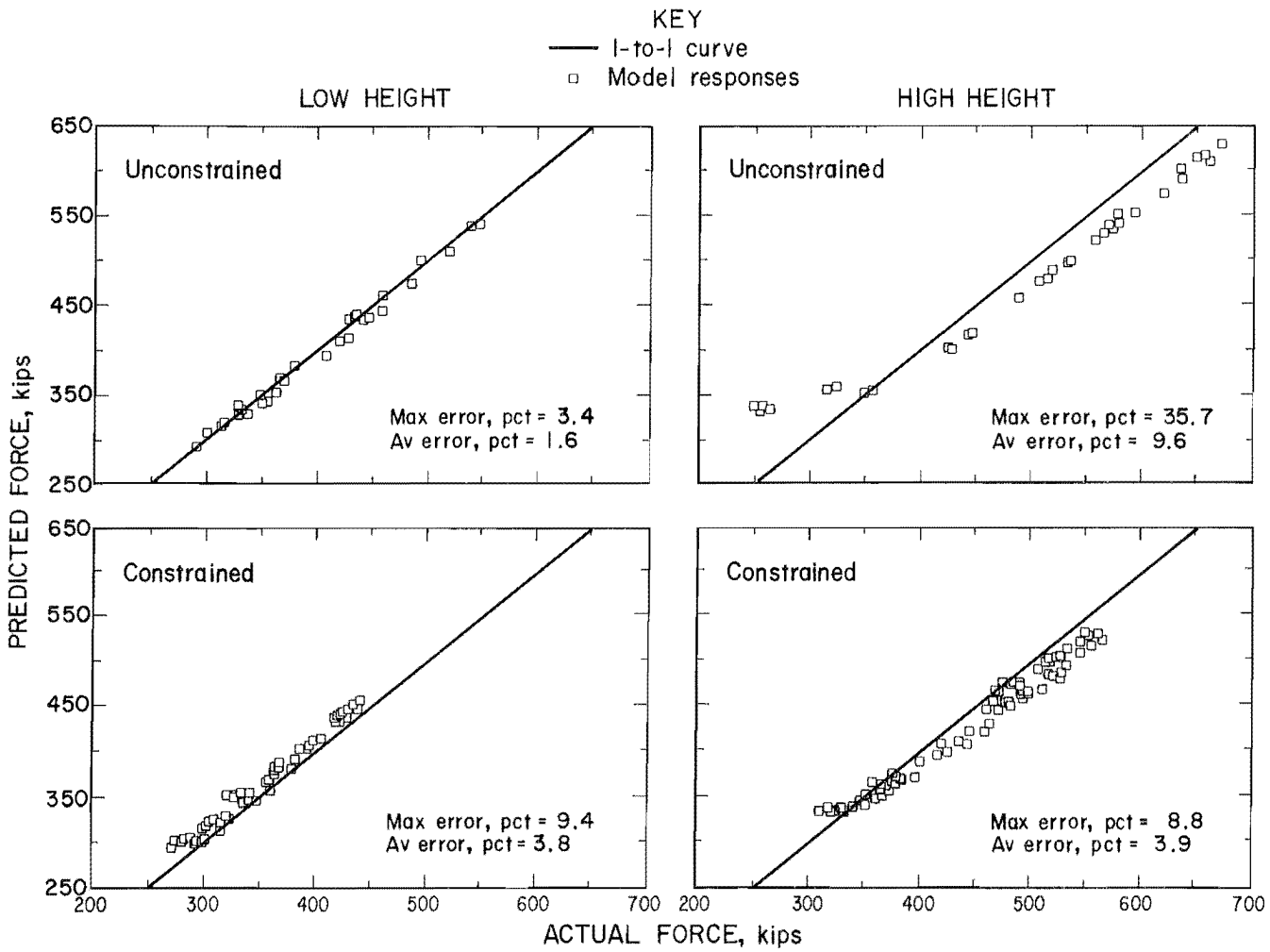

Figure 31.—Leg-link model force predictions for horizontal constrainment parameter considerations. Vertical force predictions.

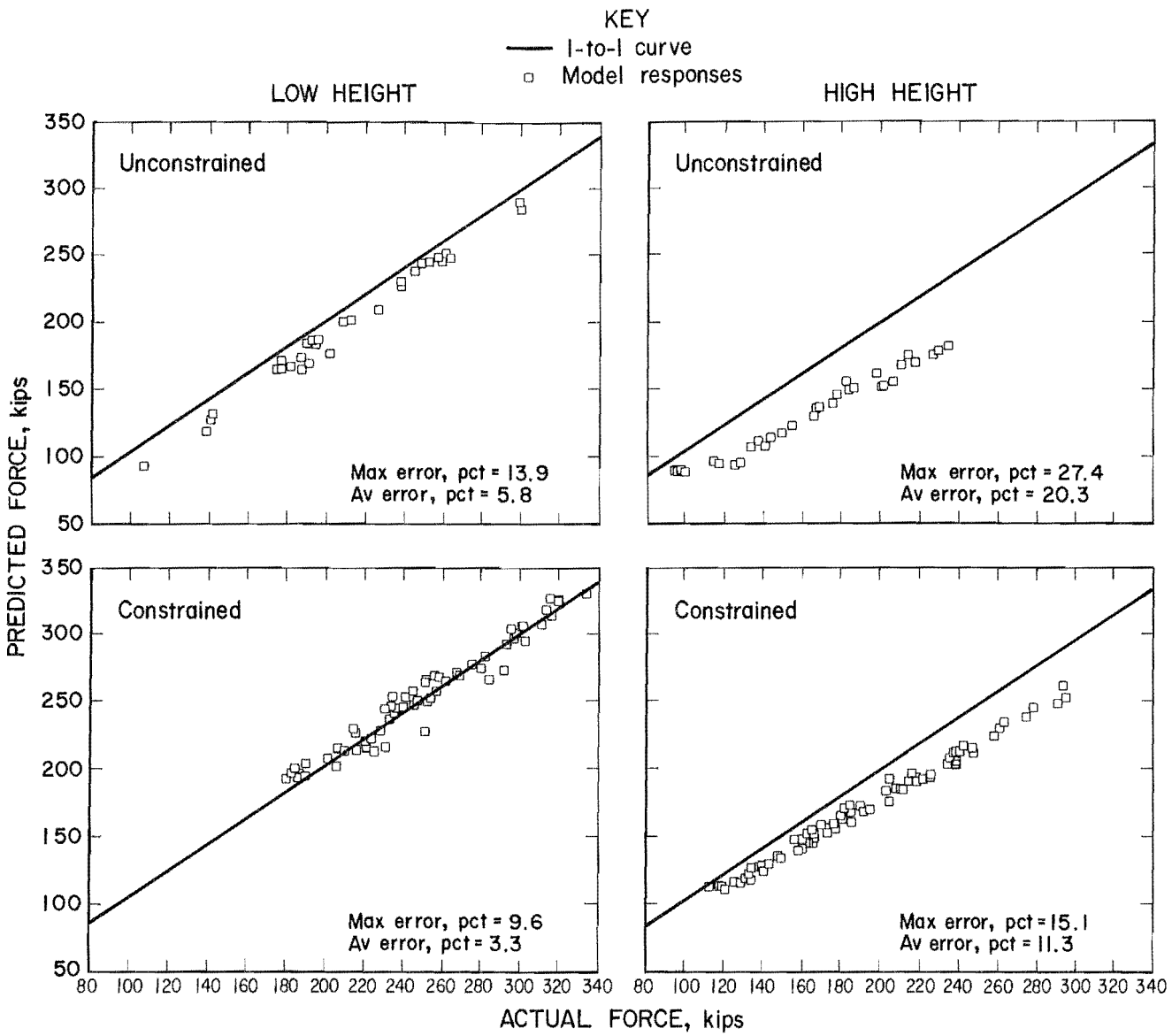

Figure 31.—Leg-link model force predictions for horizontal constrainment parameter considerations—Continued. Horizontal force predictions.

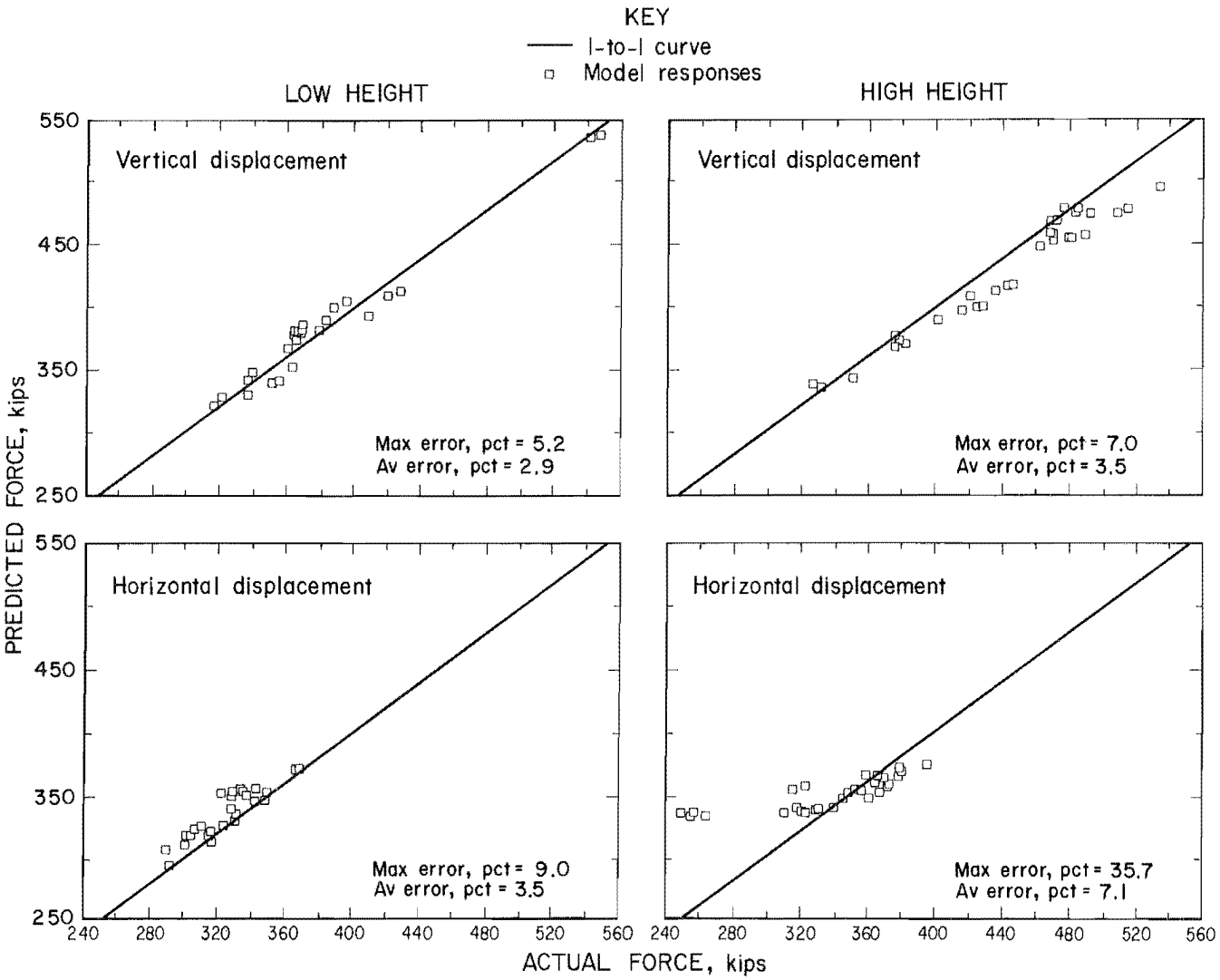

Figure 32.—Leg-link model force predictions for displacement parameter considerations. Vertical force predictions.

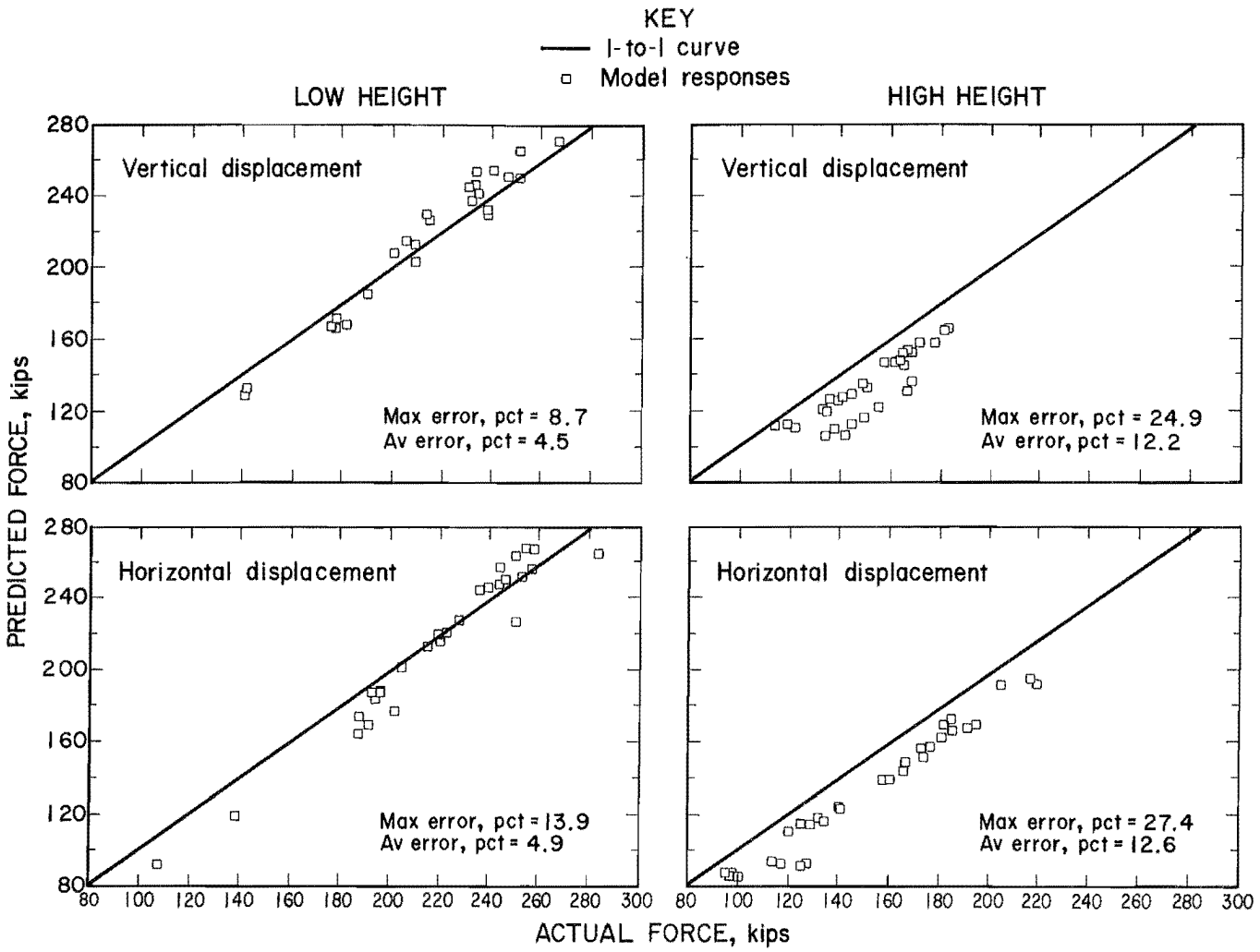

Figure 32.—Leg-link model force predictions for displacement parameter considerations—Continued. Horizontal force predictions.

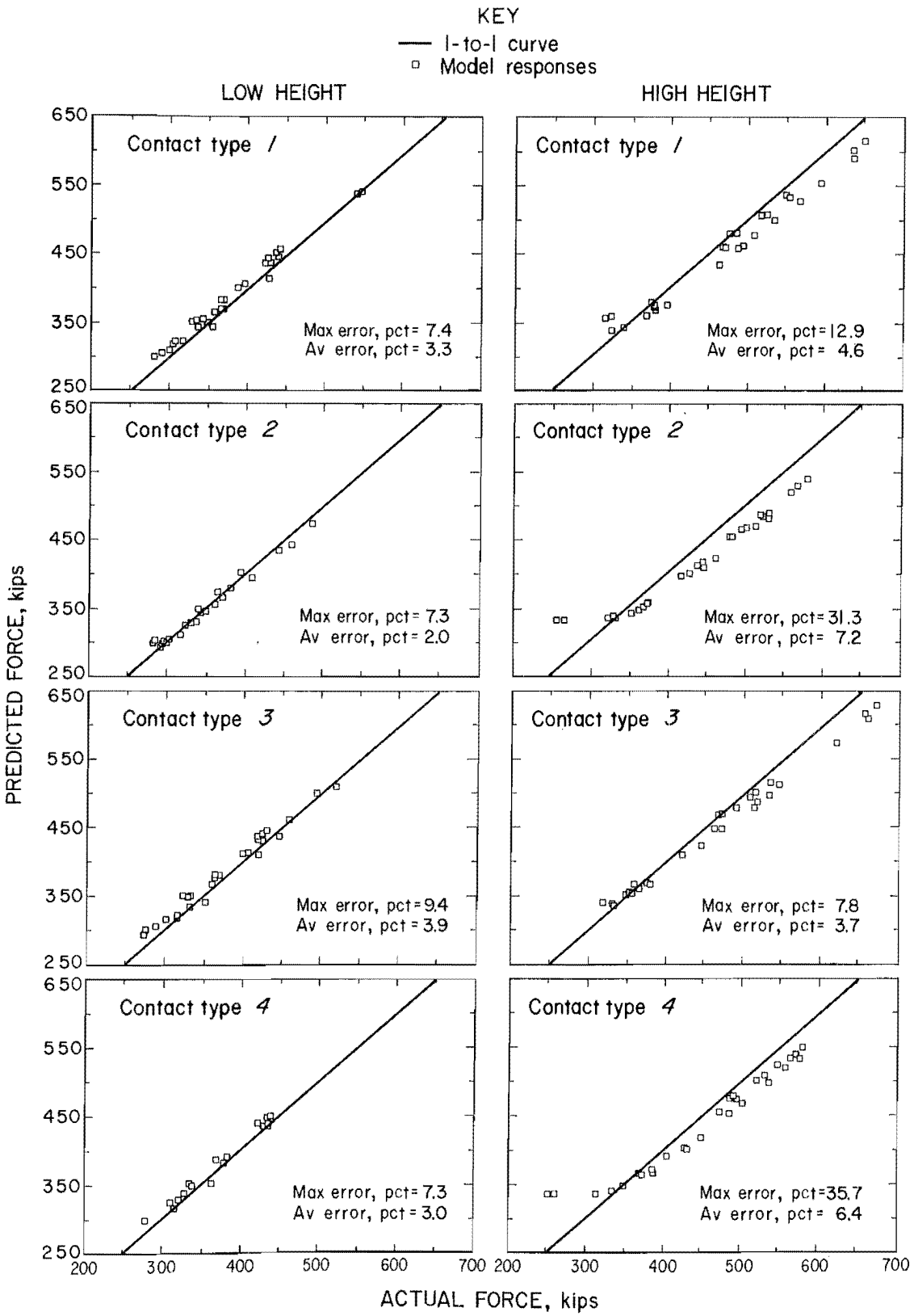

Figure 33.—Leg-link model force predictions for canopy contact parameter considerations. Vertical force predictions. Type 1—full canopy and base contact, type 2—two-point canopy contact, type 3—one-point canopy contact, type 4—three-point canopy contact.

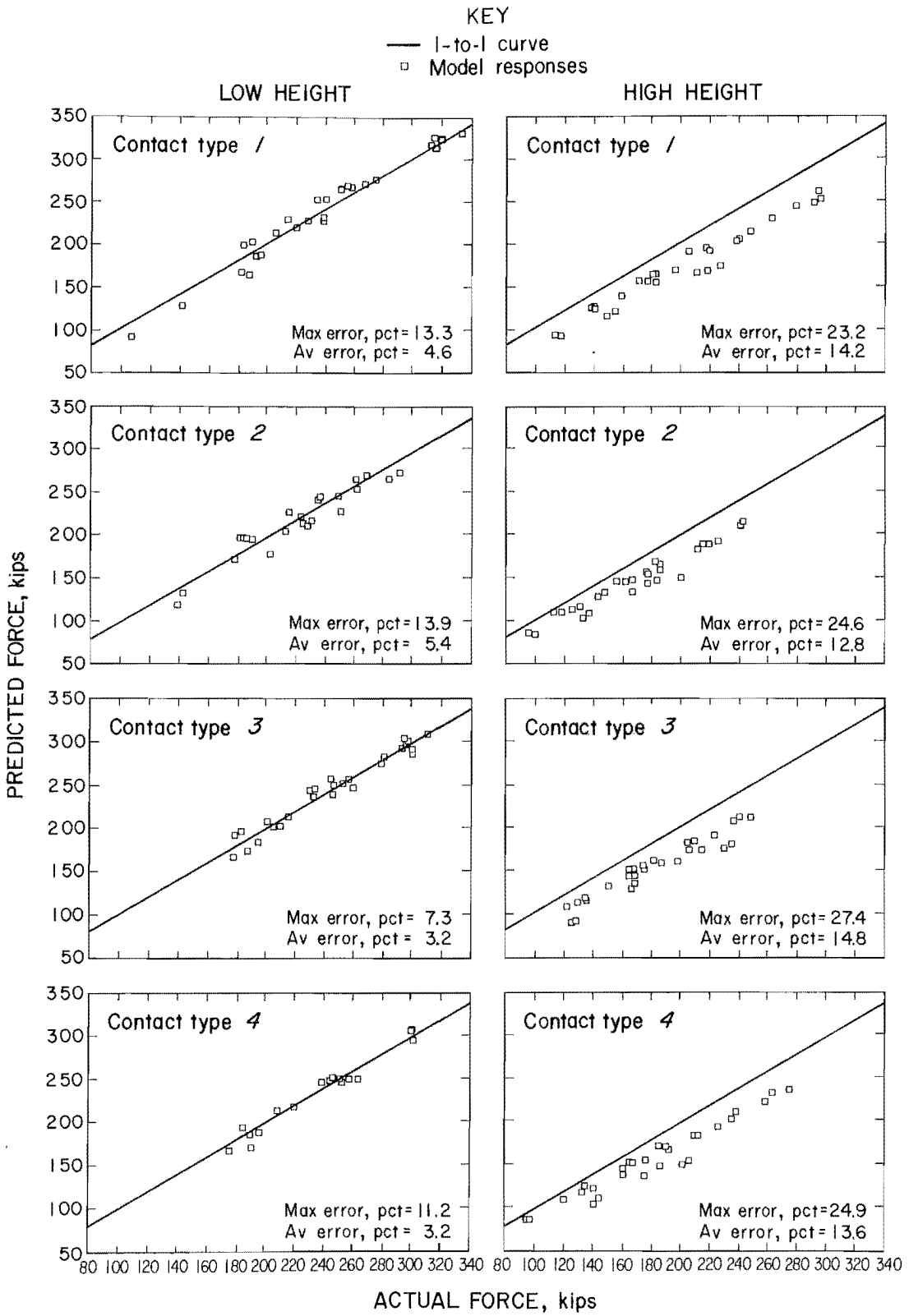

Figure 33.—Leg-link model force predictions for canopy contact parameter considerations—Continued. Horizontal force predictions.

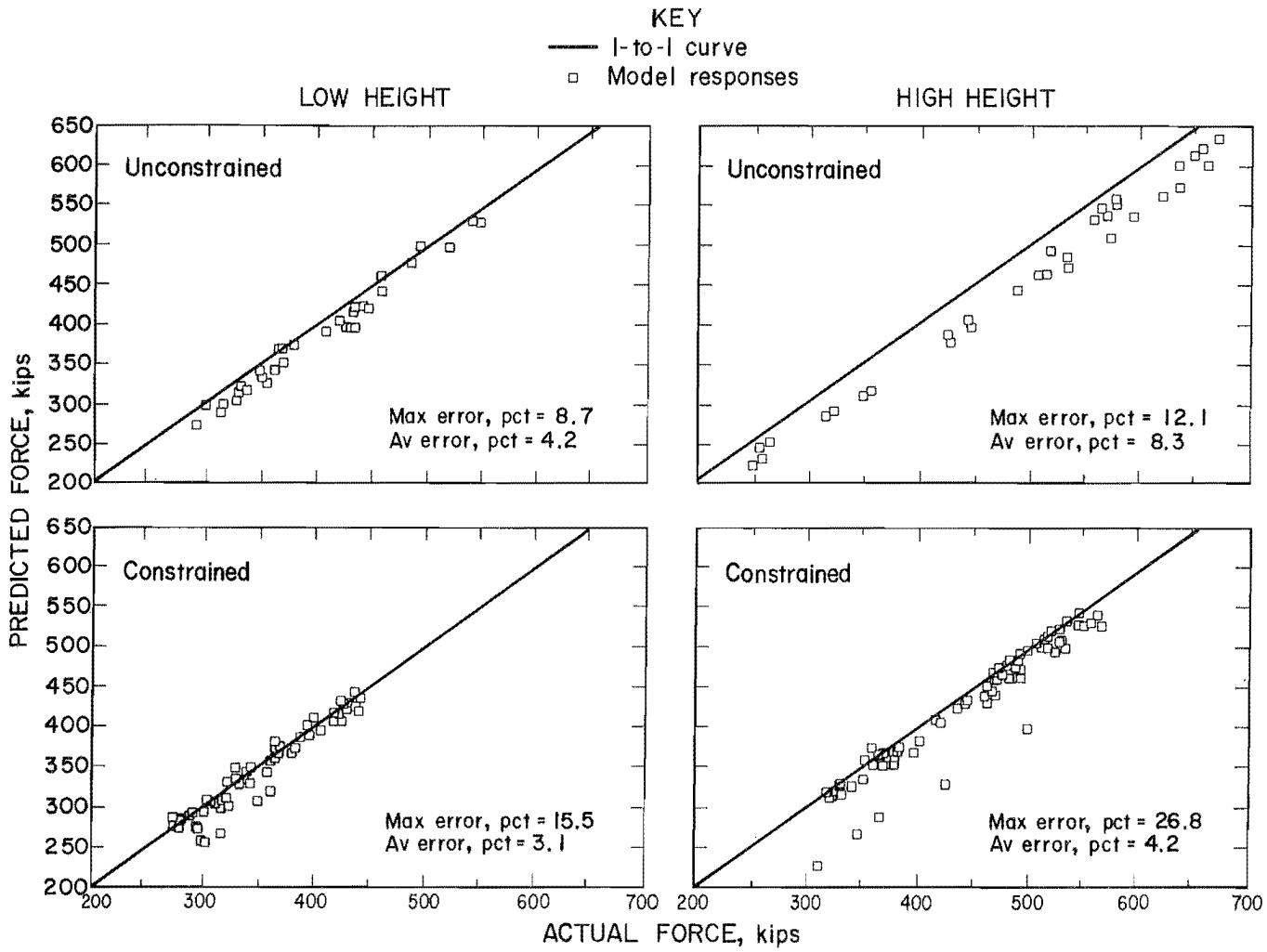

Figure 34.—Elastic stiffness model force predictions for horizontal constrainment parameter considerations. Vertical force predictions.

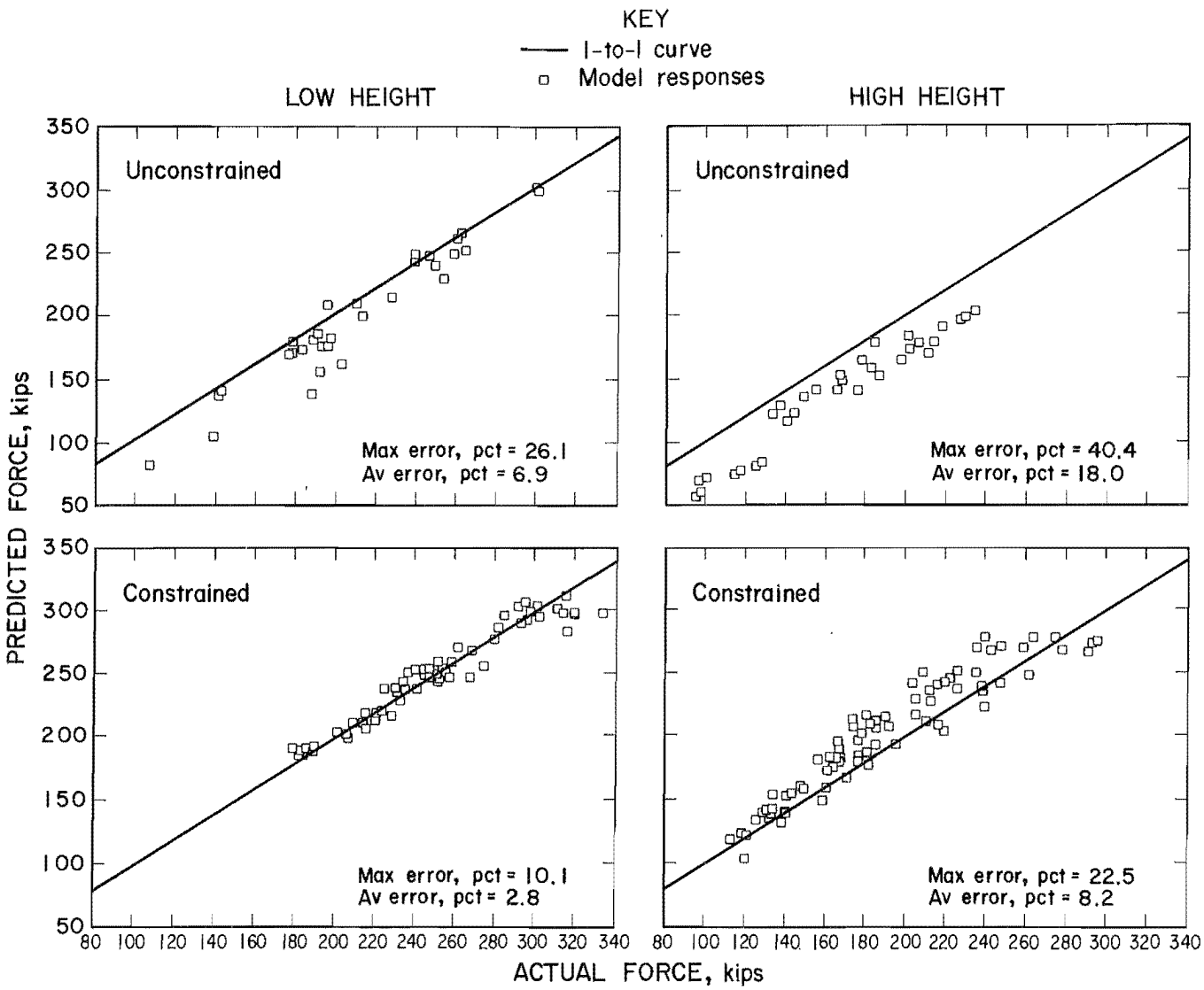

Figure 34.—Elastic stiffness model force predictions for horizontal constrainment parameter considerations—Continued. Horizontal force predictions.

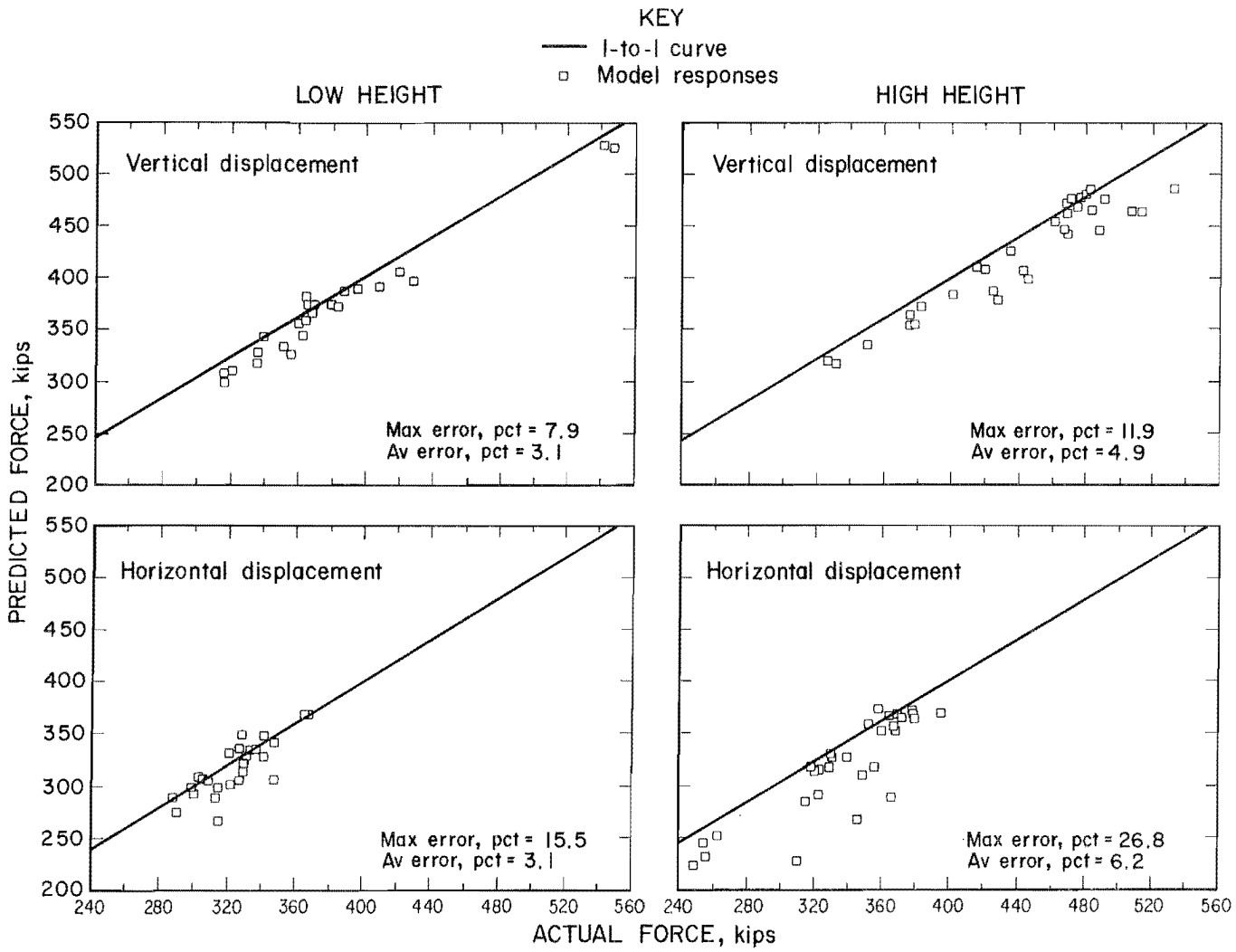

Figure 35.—Elastic stiffness model force predictions for displacement parameter considerations. Vertical force predictions.

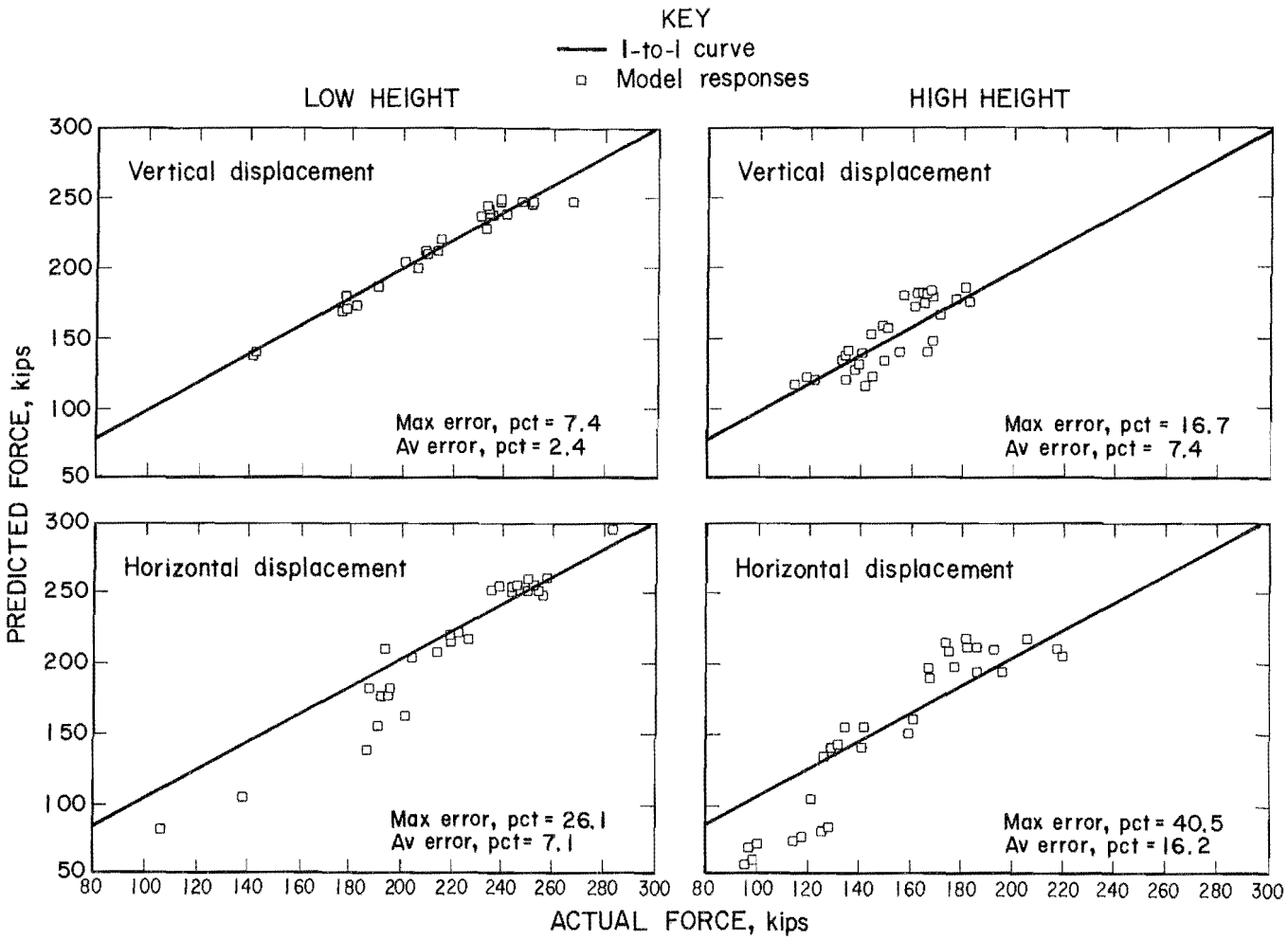

Figure 35.—Elastic stiffness model force predictions for displacement parameter considerations—Continued. Horizontal force predictions.

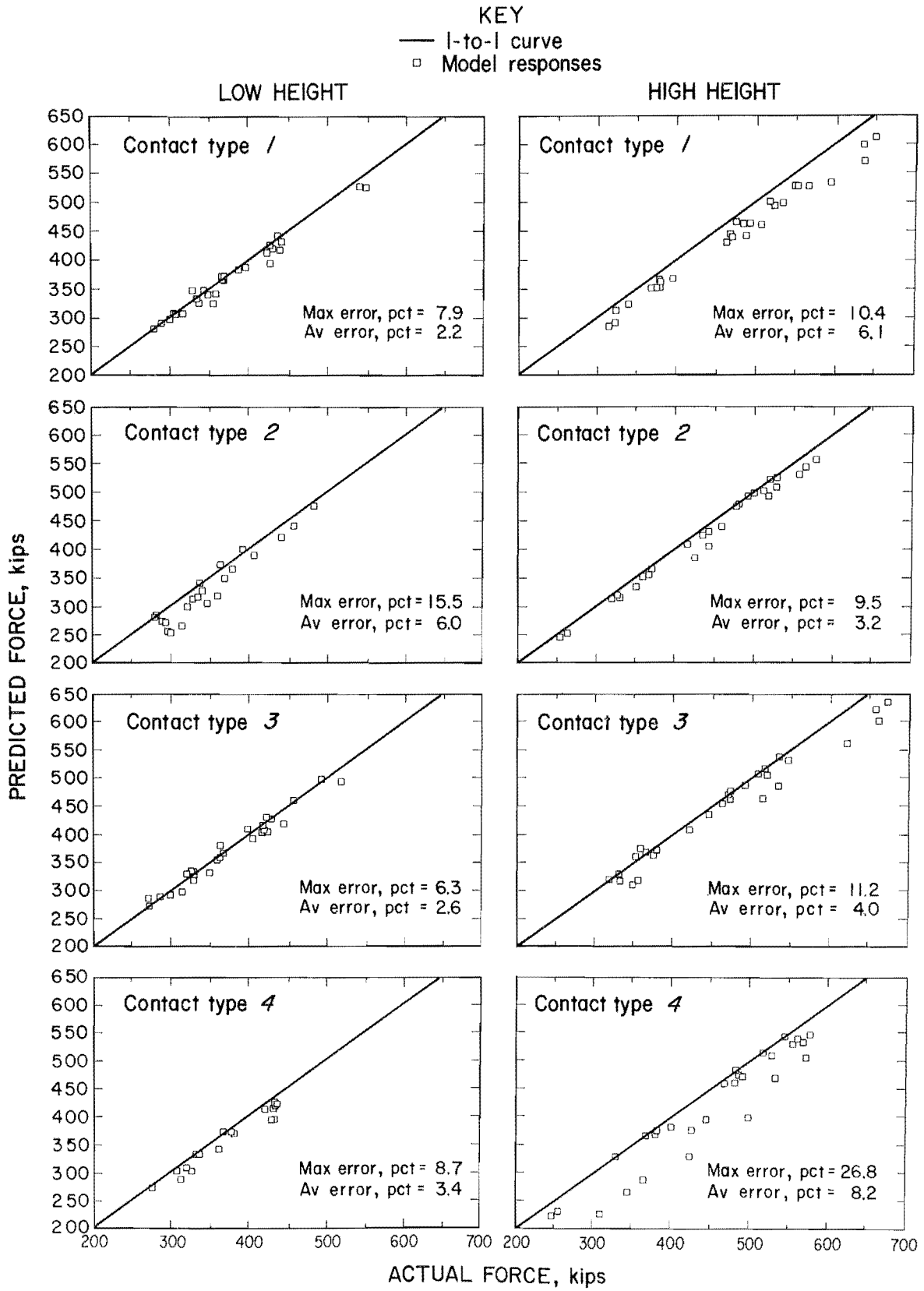

Figure 36.—Elastic stiffness model force predictions for canopy contact parameter considerations. Vertical force predictions. Type 1—full canopy and base contact, type 2—two-point canopy contact, type 3—one-point canopy contact, type 4—three-point canopy contact.

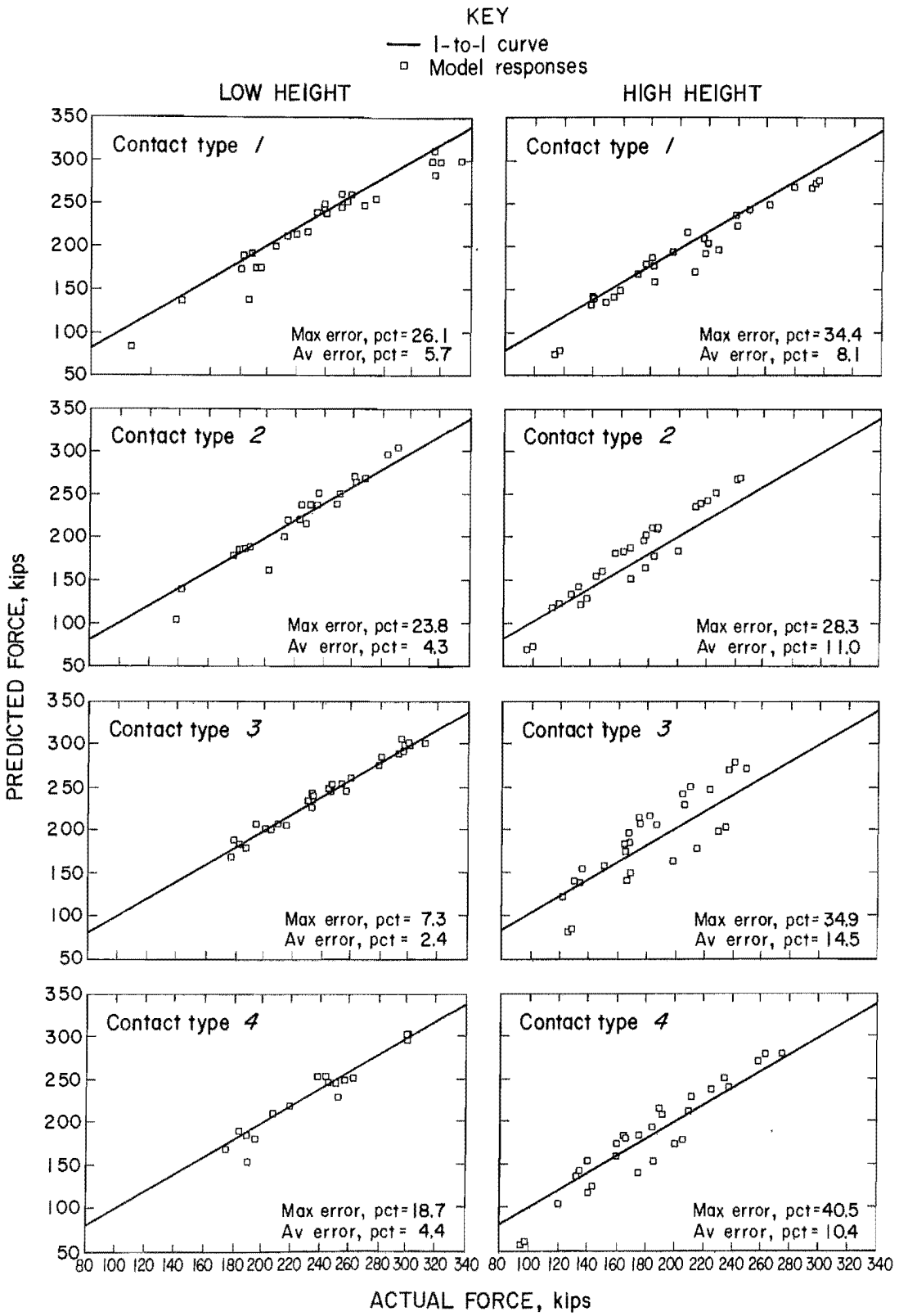

Figure 36.—Elastic stiffness model force predictions for canopy contact parameter considerations—Continued. Horizontal force predictions.

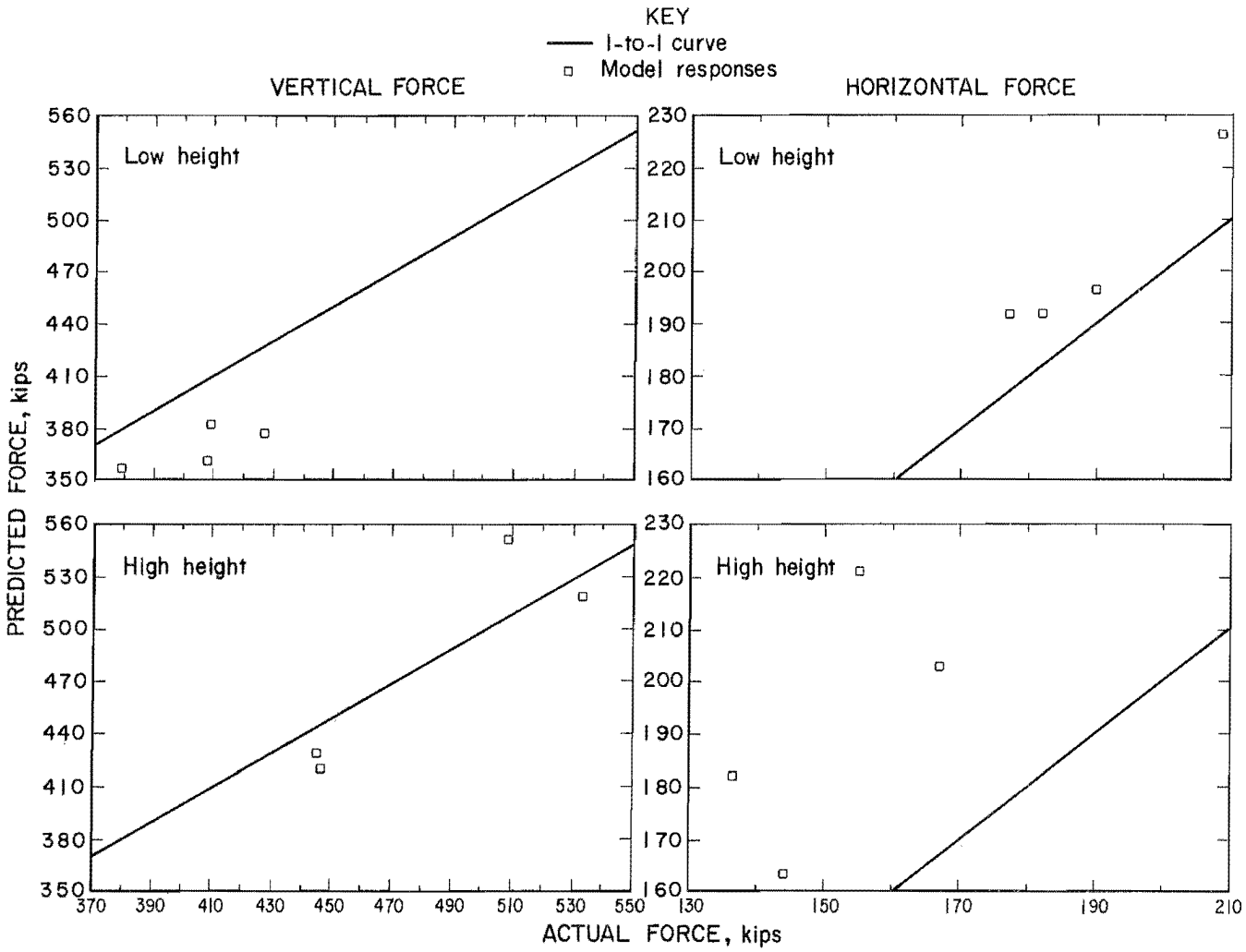

Figure 37.—Finite-element model force predictions.

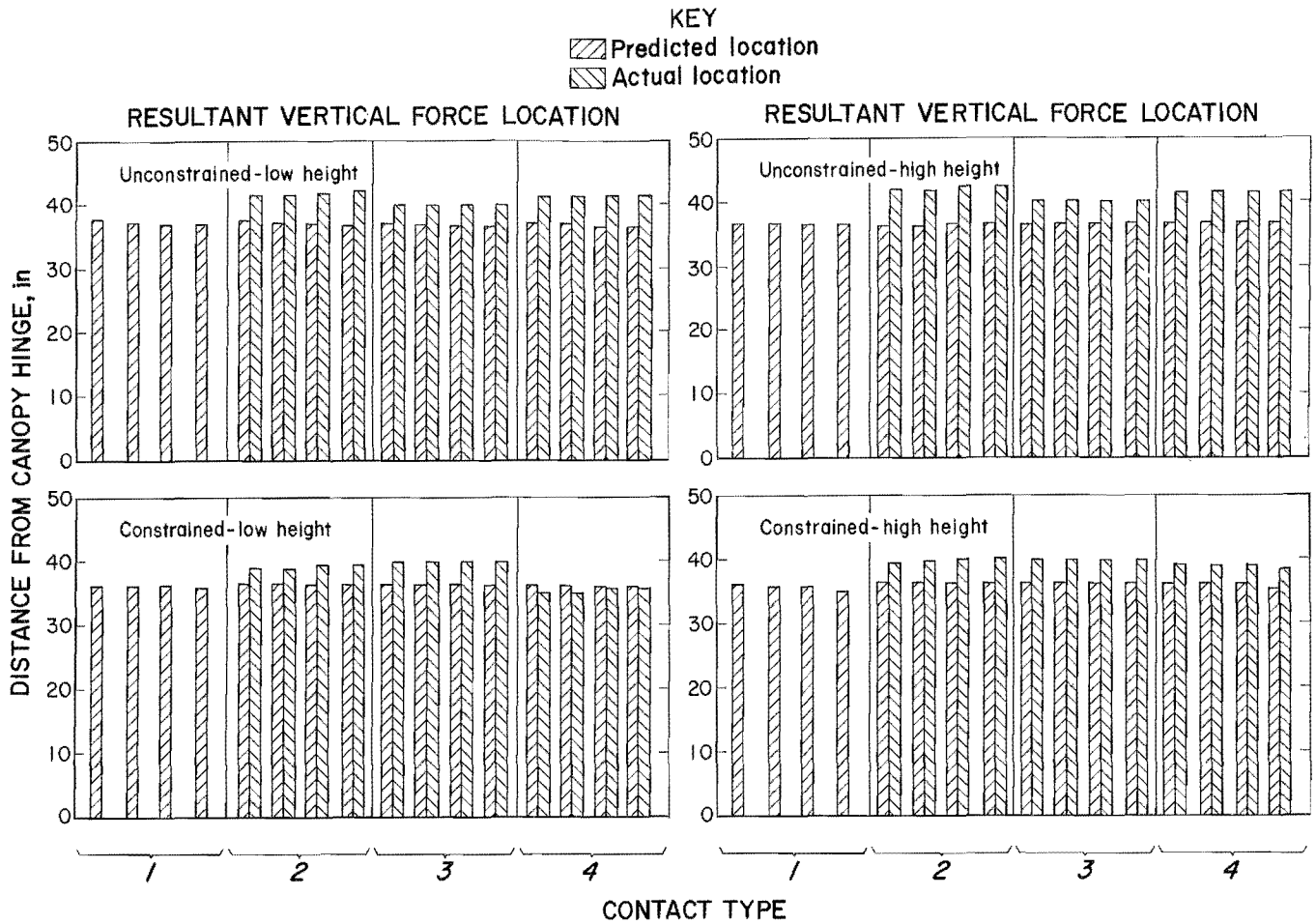

Figure 38.—Location predictions for leg-pin (rigid-body) model. Type 1—full canopy and base contact, type 2—two-point canopy contact, type 3—one-point canopy contact, type 4—three-point canopy contact.

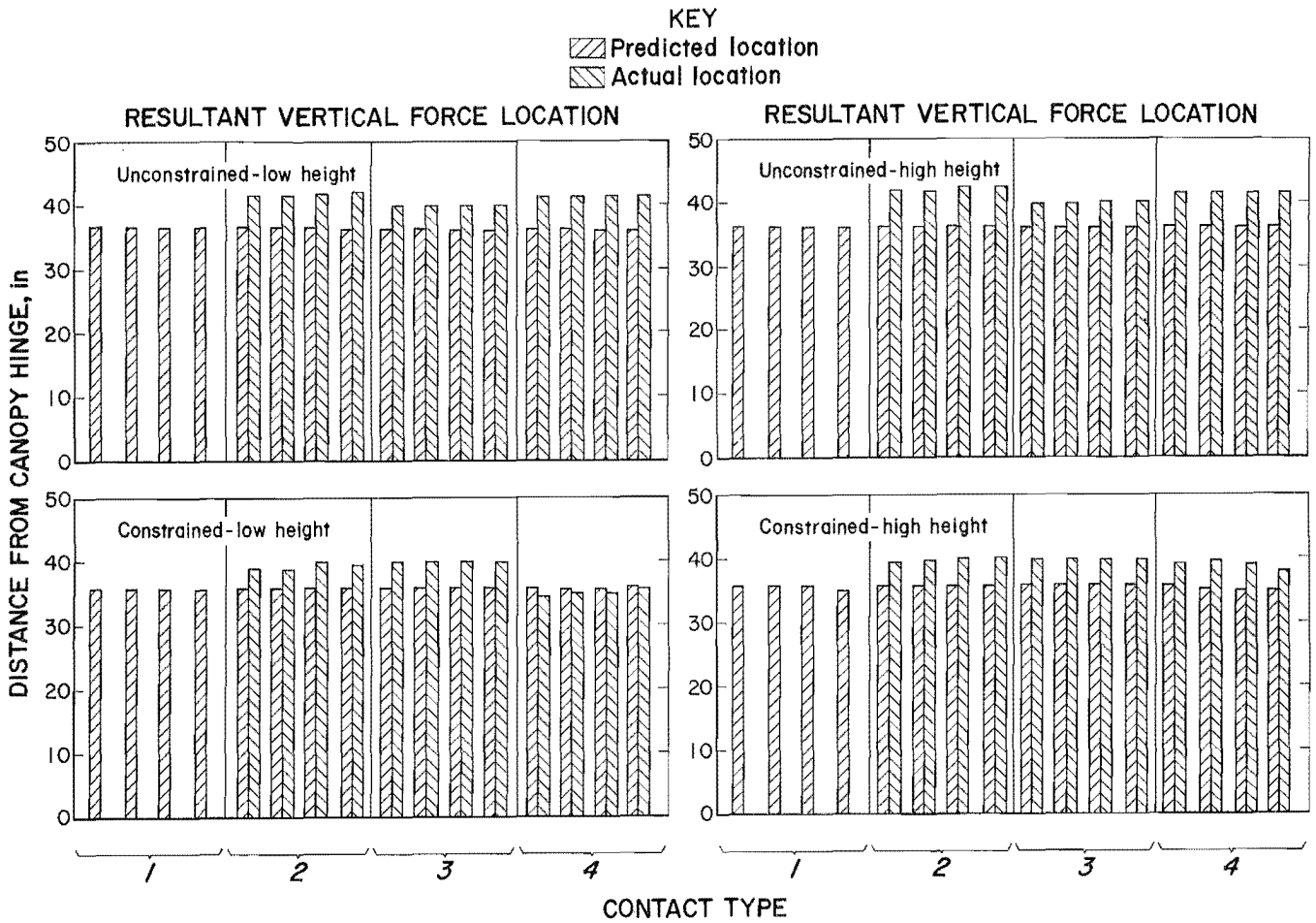

Figure 39.—Location predictions for leg-link (rigid-body) model. Type 1—full canopy and base contact, type 2—two-point canopy contact, type 3—one-point canopy contact, type 4—three-point canopy contact.

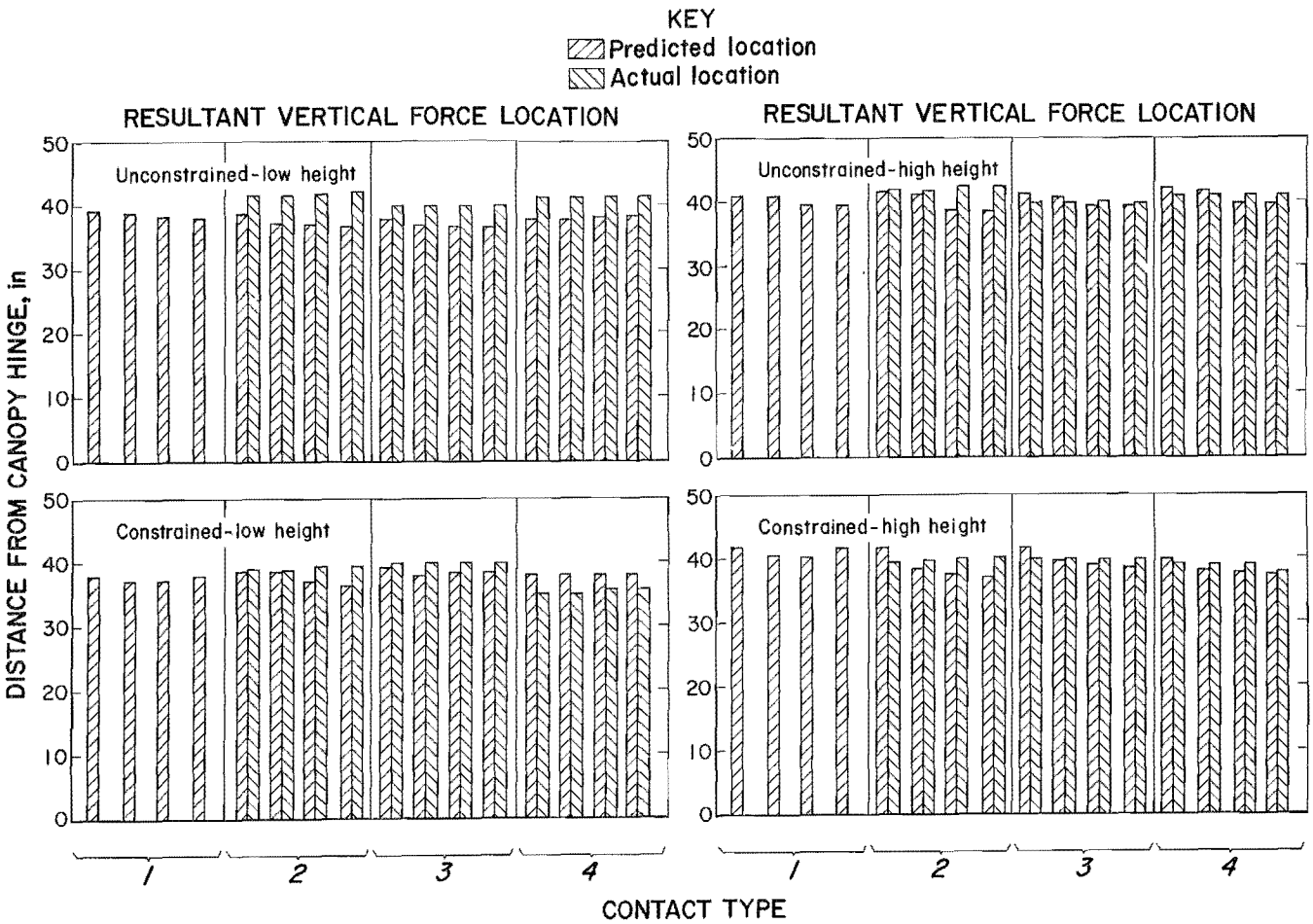

Figure 40.—Location predictions for elastic stiffness model. Type 1—full canopy and base contact, type 2—two-point canopy contact, type 3—one-point canopy contact, type 4—three-point canopy contact.

MODEL COMPARISONS

A comparison of the force prediction capabilities of the four models is illustrated in figures 41 through 43. These figures show average and maximum force prediction errors for each of the models for the same load condition. A general summary of model performance is also given in table 1.

Table 1.—Model comparison summary

Performance summary	Leg-pin	Leg-link	Elastic stiffness	Finite-element
Parameter sensitivity:				
Shield height	Yes	Yes	Yes	Yes
Constrainment	No	No	Yes	Yes
Displacement	Yes	Yes	Yes	Yes
Contact configuration	No	No	No	Yes
Error predictions, pct:				
Vertical force:				
Average	1.6 - 9.1	1.6 - 9.6	2.2 - 8.3	NAp
Maximum	4.2-36.0	3.4-35.7	6.3-26.8	5.0-11.0
Horizontal force:				
Average	3.1-12.4	3.2-20.3	2.4-18.0	NAp
Maximum	8.9-18.9	7.3-27.4	7.3-40.5	13.0-42.0
Location predictions . . in. .	[1]2-4	[1]2-4	±2	NE

NAp Not applicable.
NE Not evaluated.
[1]Overpredicted.

The following are observations of model force prediction capability comparisons.

1. In general, all models are able to predict vertical forces more accurately than horizontal forces.

2. Force predictions at the low shield height tend to be more accurate than force predictions at the high shield height for the rigid-body and elastic stiffness models. The same trend is observed for the finite-element model for horizontal forces, but the trend does not hold true for vertical force predictions.

3. For the cases shown, the least accurate model is the finite-element model. It is also the least versatile, presently being unable to accommodate horizontally unconstrained conditions and horizontal displacements. The two rigid-body models and the elastic stiffness model provided very similar predictions for most load conditions. The differences among the rigid-body models and the elastic stiffness model are not sufficient to recommend one model over another as a superior force predictor.

4. The rigid-body models do not demonstrate a preference to constrained or unconstrained load cases, but the elastic stiffness model seemed to perform better for constrained load cases. The elastic stiffness model predicted vertical forces to within 8.3 pct for unconstrained load cases and to within 4.2 pct for constrained load cases. Horizontal forces were predicted to within 18 pct for unconstrained load cases and to within 8.2 pct for constrained load cases.

5. The rigid-body models were slightly more accurate than the elastic stiffness model in predicting horizontal forces from horizontal displacement, while the elastic model was slightly more effective in predicting horizontal forces from vertical displacements. No discernible trend in vertical force predictions is noticeable.

6. A comparison of model performance for various canopy contact configurations (fig. 43) does not suggest a superior model for either vertical or horizontal force prediction. There is a trend that the leg-link rigid-body model on average is slightly less accurate than all other models in horizontal force predictions at the high shield height for each of the contact types, but the error differences among the models are sufficiently small to reserve suggestion of a superior model.

7. The rigid-body models exhibited nearly identical behavior in resultant vertical force location prediction. Both the leg-pin and leg-link model consistently overpredicted the location distance from the rear of the canopy by 2 to 4 in. The elastic stiffness model was less consistent, but generally predicted the resultant location slightly more accurately. None of the models demonstrated a preferred load condition; however, location predictions were least consistent for three-point canopy contact (type 4).

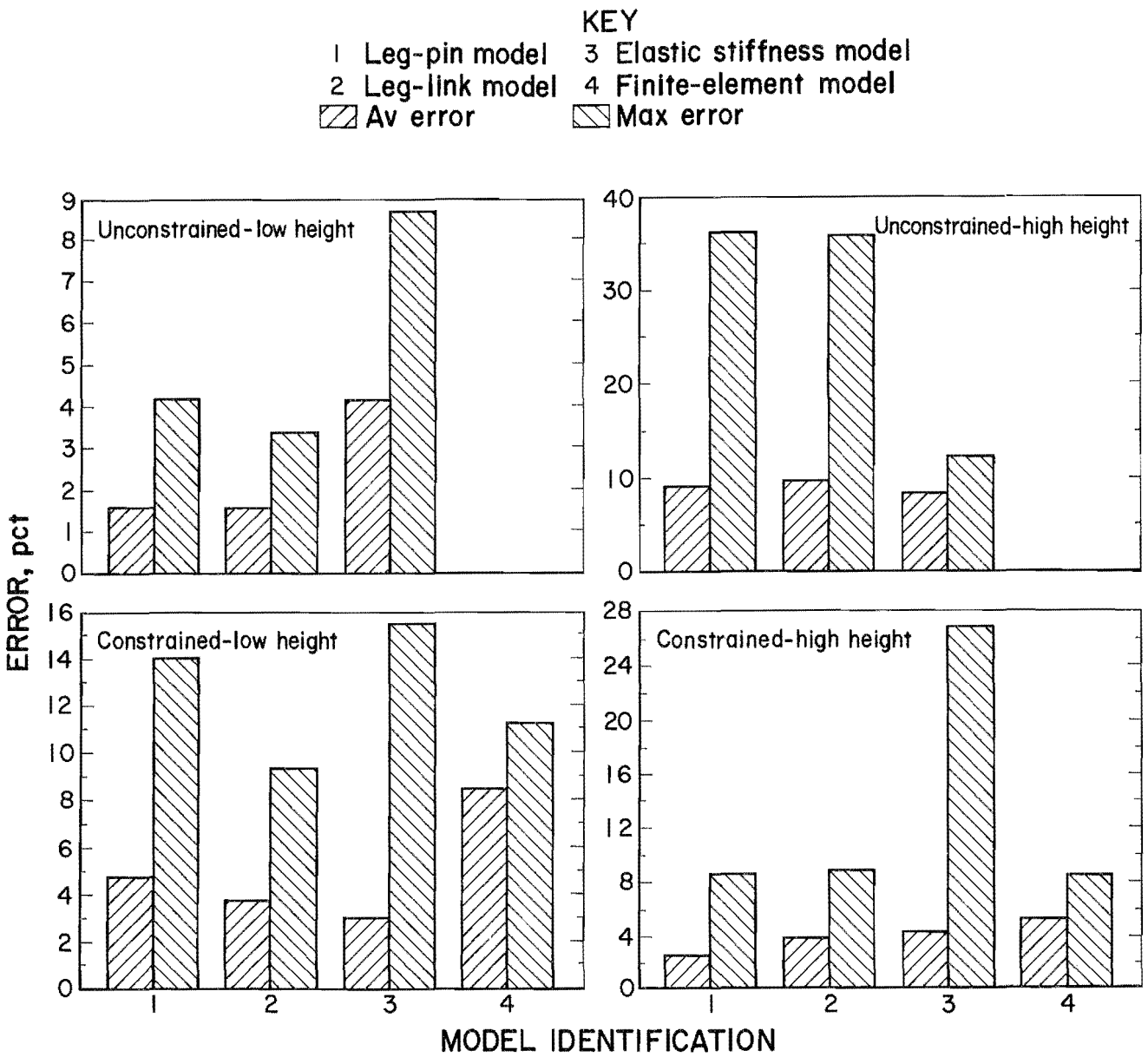

Figure 41.—Model comparisons of force predictions for horizontal constrainment parameter considerations. Vertical force predictions.

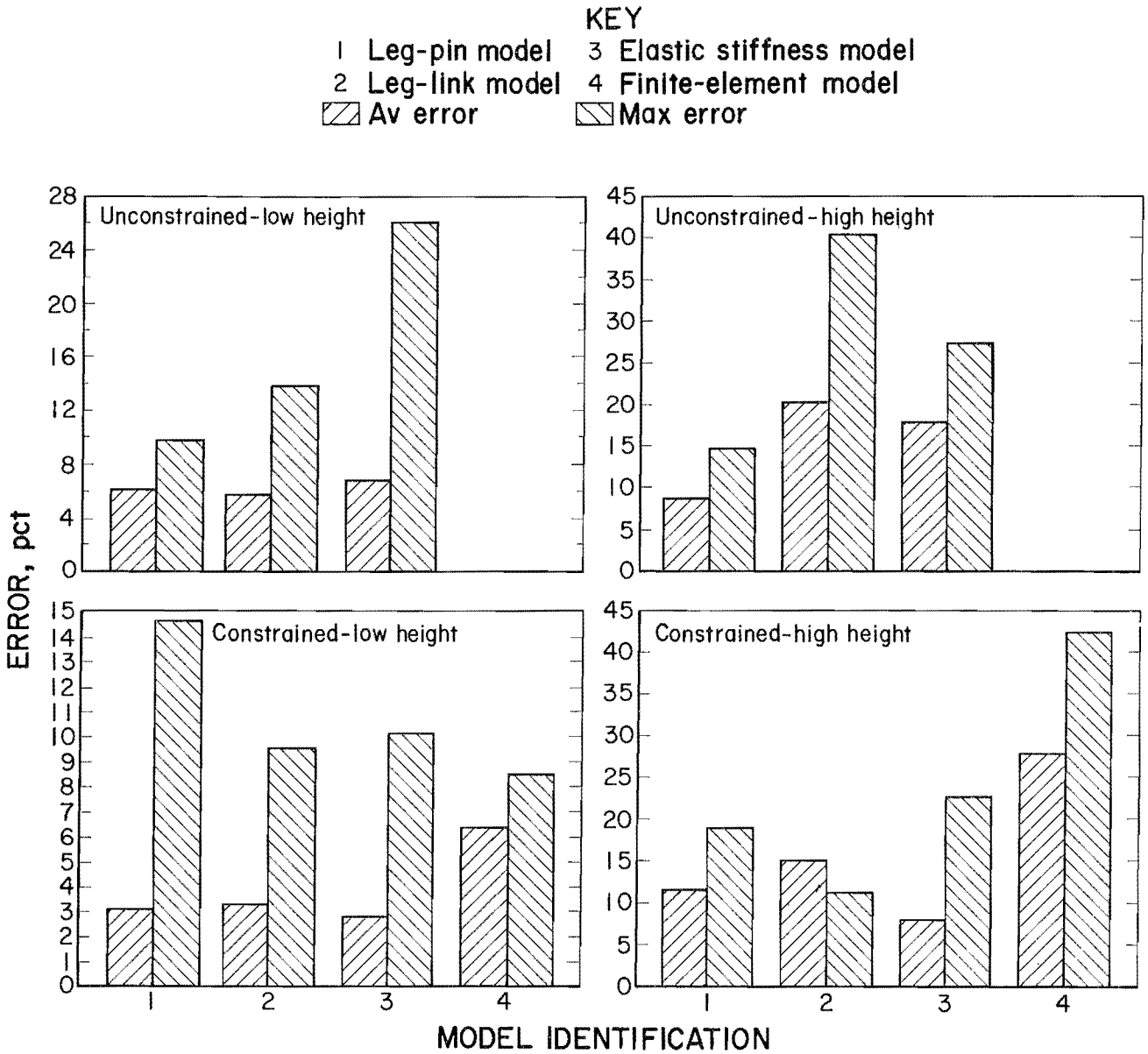

Figure 41.—Model comparisons of force predictions for horizontal constrainment parameter considerations—Continued. Horizontal force predictions.

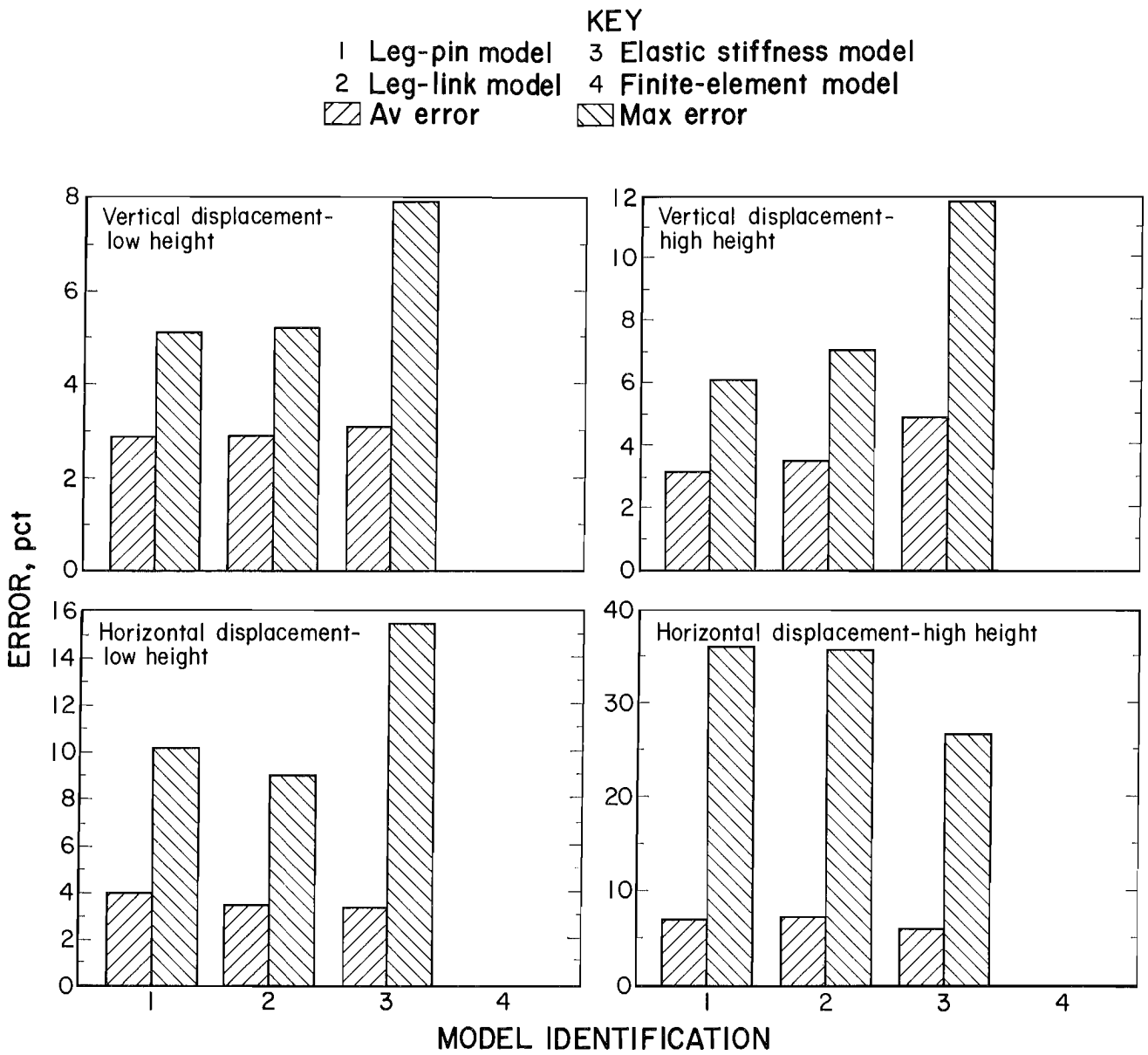

Figure 42.—Model comparisons of force predictions for displacement parameter considerations. Vertical force predictions.

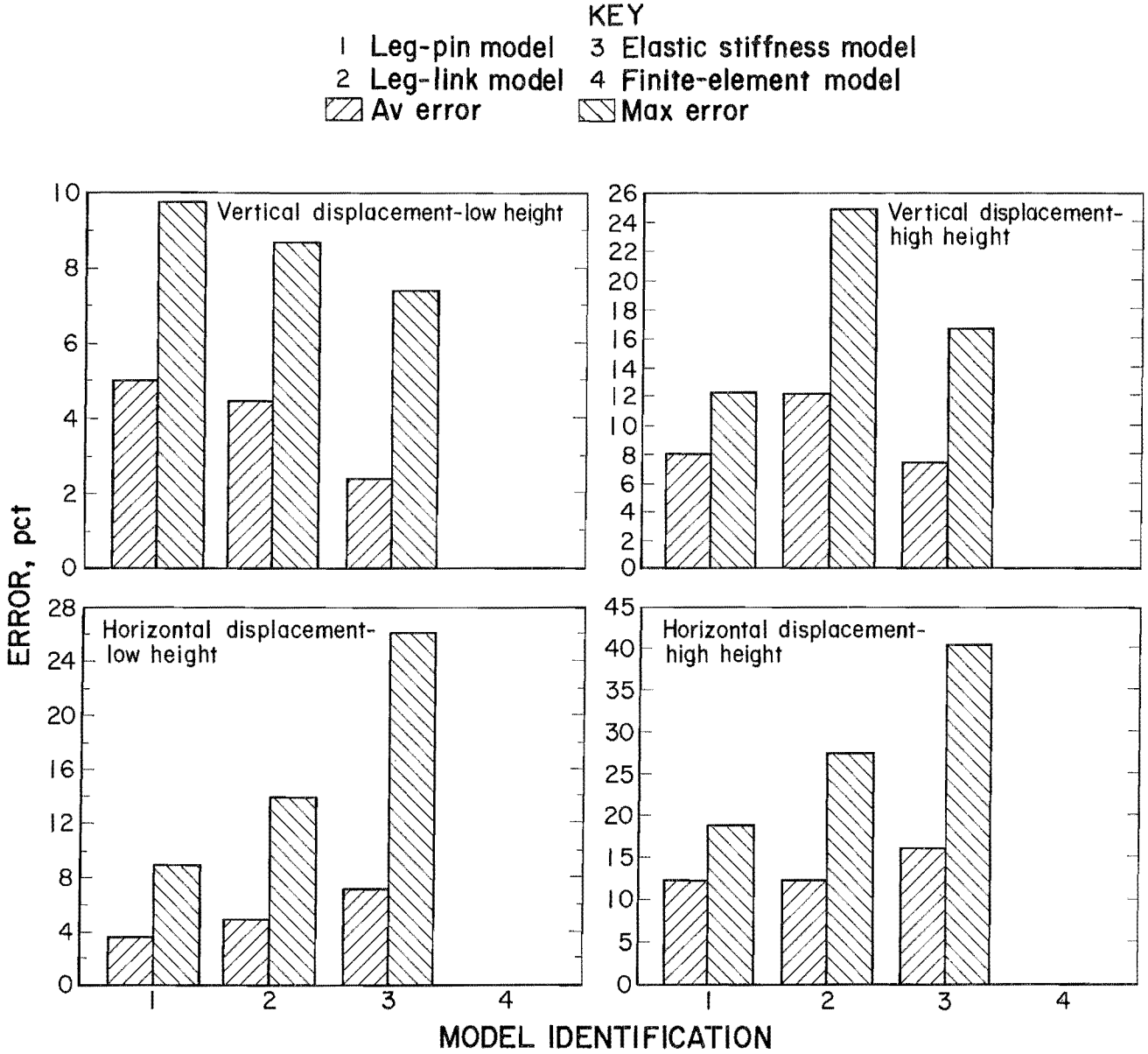

Figure 42.—Model comparisons of force predictions for displacement parameter considerations—Continued. Horizontal force predictions.

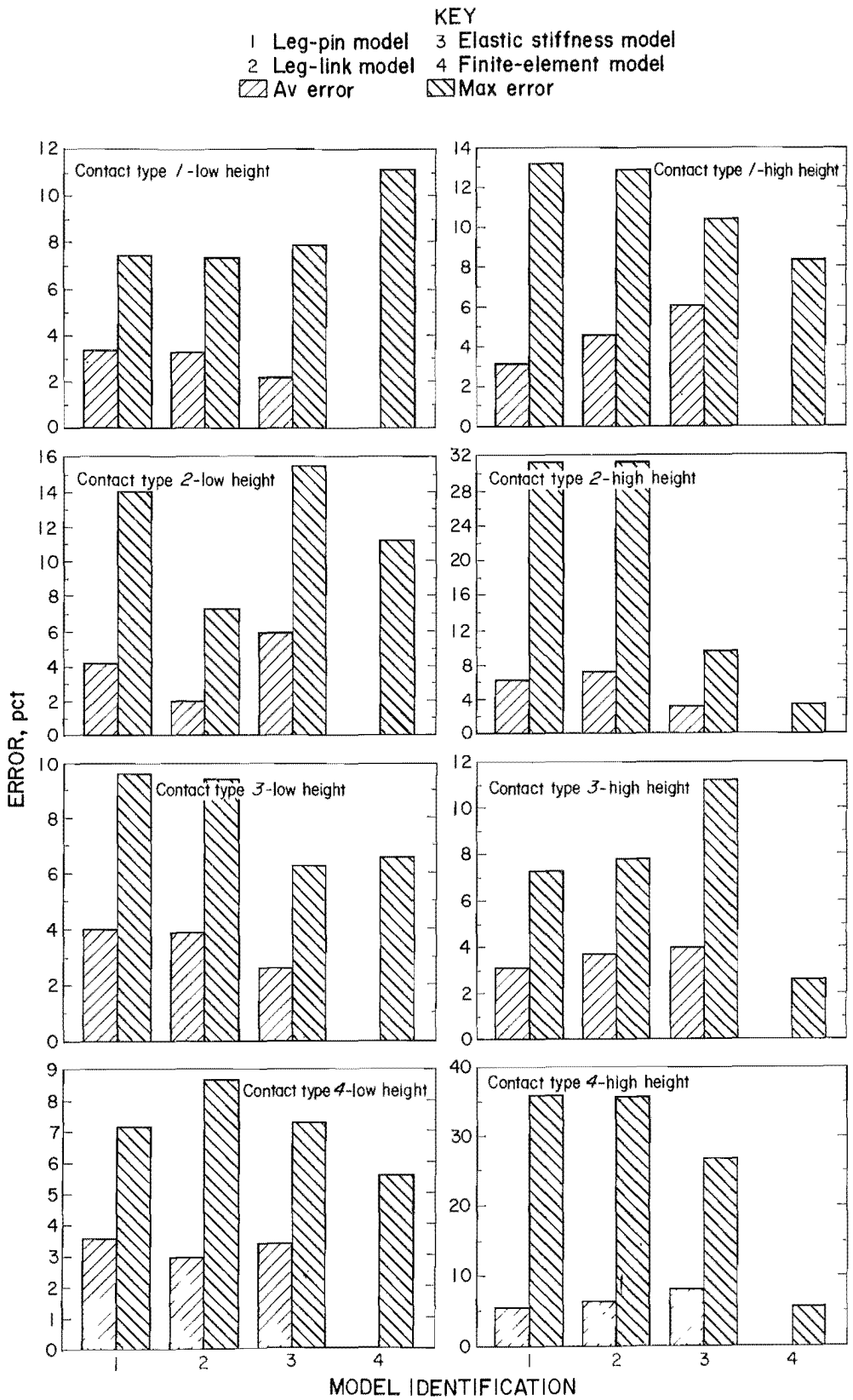

Figure 43.—Model comparisons of force predictions for canopy contact parameter considerations. Vertical force predictions. Type 1—full canopy and base contact, type 2—two-point canopy contact, type 3—one-point canopy contact, type 4—three-point canopy contact.

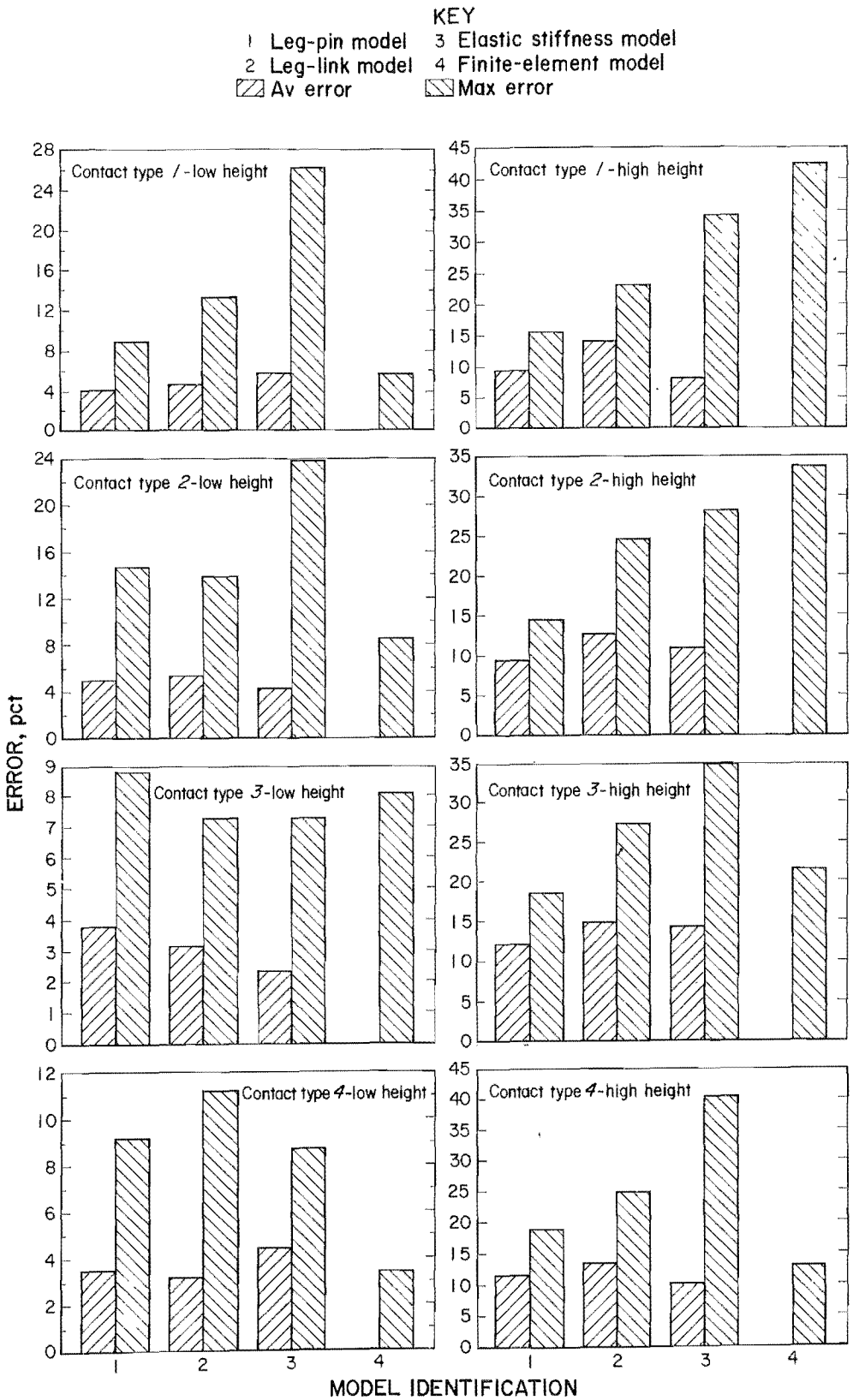

Figure 43.—Model comparisons of force predictions for canopy contact parameter considerations—Continued. Horizontal force predictions.

ERROR SOURCES AND APPLICATION LIMITATIONS

A discussion of error sources and application limitations for each of models is pursued. Explanations of model behavior are also explored.

LEG-PIN (RIGID-BODY) MODEL

The primary source of error in this rigid-body model is the conversion of leg pressure measurements into leg forces. Computation of leg forces from leg pressures requires knowledge of the effective leg area. The effective leg area for conditions of controlled vertical shield convergence was found to vary for changes in shield height as shown in figure 44. While the piston area of the leg remains constant for converging leg applications, friction between stages apparently can affect the leg force produced.

Effective leg areas, computed as the resultant mine roof simulator force acting along the leg angle divided by the measured leg pressure, were found to vary from approximately 55 to 72 in^2 for changes in shield height from 55 to 90 in. Variations in effective leg area were also found, depending on whether the shield was raised or lowered to the test height. An effective leg area of 70 in^2 was used for both test heights in this study since the leg mechanics were not found to be highly consistent. This is the likely reason why forces were generally overpredicted at the low height. It is anticipated that improvements in force prediction accuracy may be obtained by more accurate representations of leg area.

Leg mechanics become even more critical if this model is used to predict initial conditions created from setting the shield by active pressurization of the leg cylinders.

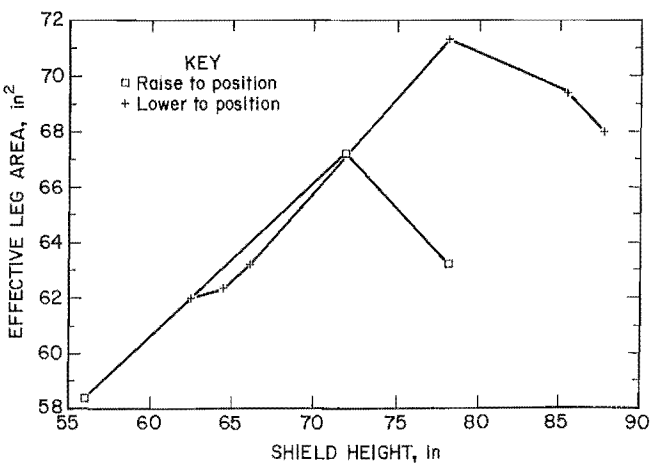

Figure 44.—Effective leg area variations with shield height.

Test results show that setting force is reduced by approximately 50 pct for high shield heights when the top stage of the leg cylinder is fully extended against the pressure chamber stops. The mechanics that produce this behavior are explained in detail in appendix D.

Another potential source of error in this model is the canopy pin force reactions as measured by the instrumented load-sensing pins. Assuming the pins are properly calibrated, force measurements should be fairly accurate. It is also necessary that the pins are properly oriented to assess vertical and horizontal forces consistent with the resultant force reference frame. Hence, any pin rotations should be monitored if the pins are not keyed to prevent rotation.

The analysis also assumes there is no moment reaction developed in the leg connection or canopy-caving shield joint. In reality, there is some friction developed in these joints, which produces some moment development that is ignored in the analysis. However, it is likely that the error resulting from these assumptions is small.

The primary limitation to the application of this model to the in situ measurement of shield loading is the installation of the load-sensing pins in the shield. It is very difficult to install these pins on an active longwall face. To provide access to the pin area at the canopy hinge, adjacent shields must be lowered, which would create a safety hazard. Even if access to the pins is attained, removal of the pins can be difficult. If access can be gained to the shield prior to its employment on the face, pin installation is more feasible.

LEG-LINK (RIGID-BODY) MODEL

The error sources associated with the leg mechanics and reaction moment development at the joints also apply to this rigid-body model.

The other source of error in this model is the computation of axial link force from measured link strain. Other publications have discussed in detail the computations for determining axial link force from link strain (*1, 5*). Assuming the strain gages are properly applied, these computations should produce accurate representations of link force. It is assumed that the links are primarily axially loaded members and a compatibility equation (equation 5) is generated by taking moments at the locus formed by extending the line of action of the front and rear links. It is assumed that the line of action of the axial link force is coincident with the pin centers. In reality, links also experience bending from pin eccentricity and moment development due to friction in the pin joints. In theory, the

bending produces link deflections that alter the line of action of the axial link forces, thereby creating a small error in the equilibrium analysis using the compatibility equation.

Unlike the leg-pin model, instrumentation required for the leg-link model can be readily installed underground on shields at the face. Weldable strain gages are recommended because of their ease of application. These gages are packaged with a metal tab to allow simple spot welding by a small, battery-powered welding unit. These gages also include bridge completion electronics within the gage package to simplify data acquisition requirements. The strain gages can easily be installed during a maintenance shift when the face is idle.

ELASTIC STIFFNESS MODEL

The primary error source in the elastic stiffness model is inaccurate representations of the stiffness coefficients (K_1, K_2, K_3, K_4) resulting from nonlinearity in the shield load-displacement characteristics and sensitivity of shield stiffness to pin freedom (horizontal constrainment). Stiffness characteristics of several shields are described in a Bureau report (*8*) and figures 10 and 11.

In general, coefficients K_2 and K_4, which are associated with horizontal displacements, tend to be the most inconsistent. Maximum variances are likely to occur because of differing degrees of pin freedom resulting from the degree of horizontal constrainment. This observation concurs with model responses illustrated in this report; the elastic model performed better for constrained load cases where the pin freedom was fully eliminated prior to load application.

Another source of error in using the elastic stiffness model is the measurement of displacements. The model requires accurate measurements of both vertical and horizontal displacements of the canopy relative to the base. Since the shield is a relatively stiff structure, maximum vertical and horizontal displacements are likely to be on the order of 0.5 in, with small changes in displacement producing large changes in shield loading. These displacements can be accurately measured with displacement measuring transducers, but care must be provided in maintaining a known frame of reference. This requires knowledge of shield geometry changes. The Bureau uses wire-pull displacement transducers and inclinometers mounted to the leg cylinder to obtain this information.

As indicated in equations 12 and 13, the elastic model also requires information of initial load conditions derived at shield setting to determine total support loading. Otherwise, the model will only identify changes in shield loading after the shield is initially set against the roof. Initial conditions can be determined from one of the rigid-body models, but these models are susceptible to errors involving leg mechanics.

The primary advantage of the elastic stiffness model over the rigid-body models is the elastic model provides a means to identify whether the horizontal forces are developed from vertical roof convergence or face-to-waste strata displacements, or whether forces are generated from active or passive horizontal loading. Active horizontal loading is defined as the horizontal force induced into the roof by the mechanics of the shield from roof-to-floor strata convergence; whereas passive horizontal loading is the resistance provided by the shield to face-to-waste strata movements. In principle, this information can be deduced from pin or link behavior in the rigid-body models, but these component responses are sensitive to initial load and subsequent boundary conditions that make interpretation of horizontal loading more difficult.

FINITE-ELEMENT MODEL

The finite-element model was found to be sensitive to its environment, in specific, boundary conditions describing how and where the shield is restrained during loading. Much of the boundary restraint in the actual operation of the shield is developed through friction, which is difficult to model. Fixtures that are used in the laboratory to horizontally restrain the canopy and base generally control one degree of freedom, but also develop frictional restraint in at least one other degree of freedom. The cable elements that act as stiff compression springs were found to be the most effective method to model boundary restraints, but they only model one degree of freedom.

Another major source of error is the inability to model pin-joint translational freedom, described as the degree of horizontal constrainment. This capability is necessary to account for the inactive and active periods of the caving shield-lemniscate assembly participation in the shield load transfer mechanics. Without this capability, the finite-element model tends to be too stiff horizontally, limiting its application to horizontal force predictions, particularly those developed from horizontal displacements of the canopy relative to the base. Other error sources include (1) utilization of a two-dimensional model, (2) computational errors of element geometric properties, and (3) less than optimum model division into elements.

As with the elastic stiffness model, the finite-element model requires accurate measurements of canopy displacements relative to the base. Like the elastic stiffness model, component force development is determined by the component stiffnesses and associated displacements. As a result, displacement errors can produce significant errors in

force predictions. In addition, canopy rotations need to be known to properly model nodal displacements and boundary conditions.

RESULTANT LOCATION PREDICTIONS

The resultant vertical force location predictions are derived from moment equilibrium using computed forces; hence, they are dependent upon the accuracy of the force predictions.

Another source of error in the resultant vertical force location predictions involves the determination of actual locations. Load cells (approximately 6 in wide) were used to measure contact load distribution. The assumed contact for moment equilibrium calculations was the center of the load cell. Because of asperities in the canopy surface, the actual load distribution through the load cell may not be at the cell center, and this assumption is a potential source of error. It is noted that force prediction errors were within the diameter of the load cell.

CONCLUSIONS

While the longwall shield may be a simple mechanical machine, the accuracy in determining stress states for various shield contact configurations and loading conditions is critical to research to improve shield selection and design. The measurement of in situ shield loading is complicated by the complex interaction of the shield with the strata and limitations imposed on data acquisition of shield behavior by the harsh mine environment. This report describes the development of four models to determine resultant vertical and horizontal shield forces and the location of the resultant vertical force on the canopy.

Models that are dependent upon initial conditions developed from setting the shield against the roof are subject to large possible errors because of the inability to accurately compute leg forces during setting operations. Of the four models investigated, the elastic stiffness model and the finite-element model were dependent upon initial setting load determinations for total load predictions. Further evaluations of leg mechanics for various amounts of leg extension is an issue that requires increased attention. Quantification of leg behavior would improve the performance of models that are dependent upon initial conditions, and would provide another piece of information for evaluating the interaction of the support with the strata. The inability to consistently compute leg forces from leg pressures with a high degree of accuracy for active leg pressurizations limits the use of shields as load-sensing monitors of setting conditions and limits the usefulness of the elastic stiffness and finite-element models.

The better shield models are those that are not dependent on determination of initial conditions and require only specific measurable information at the instance of interest, as displayed by the two rigid-body models. Additionally, from the point of view of someone monitoring shield behavior, evaluating instrument readings without having to first adjust them because of initial conditions would provide more immediate assessment of strata conditions and shield responses from which action could be taken to institute operational changes.

The elastic stiffness model provides reasonably accurate predictions of resultant shield forces in response to converging mine roof after the shield is set, but requires knowledge of the shield stiffness characteristics before interpretations of displacement measurements can be made. This can be a significant limitation in the application of this model to in situ measurements of shield loading, since the stiffness determinations require laboratory evaluations of the shield under controlled loading.

Numerical models are sensitive to boundary conditions that are only nominally known. More specific information is necessary as well as an accurate description of shield component asperities, an influential factor in the development of actual contacts. Also, the inclusion of an element to permit pin-joint horizontal freedom is necessary to account for the active and inactive periods of the caving shield-lemniscate assembly participation in the shield load transfer mechanics.

The resultant vertical force location on the canopy can be predicted rather well with any of the models. Hence, this is not a deciding factor in the selection of a best shield force predictor model. The advantages and disadvantages of specific model applications have been discussed in this report. Recommendations for the best force predictor model are narrowed to the two rigid-body models because of the dependence of the elastic stiffness model on leg mechanics to establish initial loading from shield setting and the sensitivity and lack of versatility of the finite-element model.

Both the leg-pin and the leg-link rigid-body models provide accurate representations of vertical and horizontal resultant shield forces. The leg-link model is the simplest to use because the leg-pin model requires the difficult task of installing instrumented pins underground on shields employed on an active longwall face. If pin installation is

no particular problem, then the leg-pin model is the most desirable because it also provides a direct evaluation of load transfer through the caving shield-lemniscate assembly. The state of horizontal constrainment can be deduced from this direct evaluation.

Recommendation of the rigid-body models is meant not to exclude the elastic stiffness model and finite-element model from other considerations or further development. The elastic stiffness model provides vital information on the interaction of the shield with the strata and the nature of the load development. The finite-element model at present is the least accurate, but numerical models possess the highest potential for shield optimization and should continue to be developed to their fullest potential.

REFERENCES

1. Barczak, T. M., and R. C. Garson. Shield Mechanics and Resultant Load Vector Studies. BuMines RI 9027, 1986, 43 pp.

2. Barczak, T. M., and S. J. Kravits. Shield-Loading Studies at an Eastern Appalachian Minesite. BuMines RI 9098, 1987, 81 pp.

3. Barczak, T. M., and D. E. Schwemmer. Horizontal and Vertical Load Transferring Mechanisms in Longwall Roof Supports. BuMines RI 9188, 1988, 24 pp.

4. ____. Two-Leg Longwall Shield Mechanics. BuMines RI 9220, 1989, 34 pp.

5. Barczak, T. M., and W. S. Burton. Three-Dimensional Shield Mechanics. BuMines 9091, 1987, 23 pp.

6. Barczak, T. M., and R. C. Garson. Technique To Measure Resultant Load Vector on Shield Supports. Paper in Proceedings of the 25th U.S. Symposium on Rock Mechanics, Evanston, IL, June 25-27, 1984. Soc. Min. Eng. AIME, pp. 667-680.

7. Barczak, T. M., and W. S. Burton. Assessment of Longwall Roof Behavior and Support Loading by Linear Elastic Modeling of the Support Structure. BuMines RI 9081, 1987, 7 pp.

8. Barczak, T. M., and D. E. Schwemmer. Stiffness Characteristics of Longwall Shields. BuMines RI 9154, 1988, 14 pp.

APPENDIX A.—DERIVATION OF STATIC EQUILIBRIUM EQUATIONS FOR RIGID-BODY SOLUTION OF RESULTANT SHIELD LOADING

The three equations of static equilibrium developed in the main text are

$$\sum M_A = -F_V * LOC + L * \sin\phi * (X_6 - X_3) = 0, \tag{A-1}$$

$$\sum M_B = -F_V * [LOC + (X_3 - X_0)] + F_H * (Y_3 - Y_0) + L * \sin\phi * (X_6 - X_0) - L * \cos\phi * (Y_3 - Y_0) = 0, \tag{A-2}$$

and

$$\sum M_C = -F_V * [LOC + (X_3 - X_1)] + F_H * (Y_3 - Y_1) + L * \sin\phi * (X_6 - X_1) - L * \cos\phi * (Y_3 - Y_1) - F * \cos\beta * (Y_2 - Y_1) - F * \sin\beta * (X_2 - X_1) = 0. \tag{A-3}$$

Using equation 2,[1] solving for F_H,

$$F_H = \frac{[F_V * LOC + F_V * (X_3 - X_0) - L * \sin\phi * (X_6 - X_0) + L * \cos\phi\ (Y_3 - Y_0)]}{(Y_3 - Y_0)}. \tag{A-4}$$

Using equation 1, solving for $F_V * LOC$,

$$F_V * LOC = L * \sin\phi * (X_6 - X_3). \tag{A-5}$$

Substituting equations 4 and 5 into equation 3, solving for F_V produces

$$F_V = L * V_L + F * V_F, \tag{A-6}$$

where $V_L = \sin\phi$,

$$V_F = \frac{[\cos\beta * (Y_2 - Y_1) + \sin\beta * (X_2 - X_1)] * (Y_3 - Y_0)}{X_1 * (Y_3 - Y_0) - Y_1 * (X_3 - X_0) + [(Y_0 * X_3) - (X_0 * Y_3)]},$$

and V_L, V_F = vertical leg and front link participation factors, respectively.

Continuing, from equation 4, substituting equation 6 and after rearrangement, one can write

$$F_H = L * H_L + F * H_F, \tag{A-7}$$

where $H_L = \cos\phi$,

$$H_F = \frac{[\cos\beta * (Y_2 - Y_1) + \sin\beta * (X_2 - X_1) * (X_3 - X_0)}{X_1 * (Y_3 - Y_0) - Y_1 * (X_3 - X_0) + [(Y_0 * X_3) - (X_0 * Y_3)]},$$

H_L, H_F = horizontal leg and front link participation factors, respectively.

The location of the vertical resultant (LOC) can be determined using equation 5 and substituting equation 6 as follows:

$$LOC = \frac{\sin\phi * (X_6 - X_3)}{\sin\phi + (F * V_F)/L}. \tag{A-8}$$

[1]Equation numbers without an A- prefix refer to equations in the main text.

APPENDIX B.—DETERMINATION OF SHIELD STIFFNESS COEFFICIENTS

The stiffness coefficients (K_1, K_2, K_3, K_4) were determined from controlled vertical and horizontal displacements of a shield in the mine roof simulator as illustrated in figure B-1. By commanding the mine roof simulator to maintain a fixed horizontal platen position (zero horizontal displacement) as shown in figure B-1 (top), the shield is subjected to vertical displacement only. Terms $K_2\delta_H$ and $K_4\delta_H$ then become zero since $\delta_H = 0$, leaving $F_V = K_1\delta_H$ and $F_H = K_3\delta_V$. Coefficients K_1 and K_3 are calculated as the ratio of vertical force to vertical displacement (K_1) and horizontal force to vertical displacement (K_3). Likewise, subjecting the shield to pure horizontal (face-to-waste) displacement (figure B-1, bottom) provides determination of stiffness coefficients K_2 and K_4.

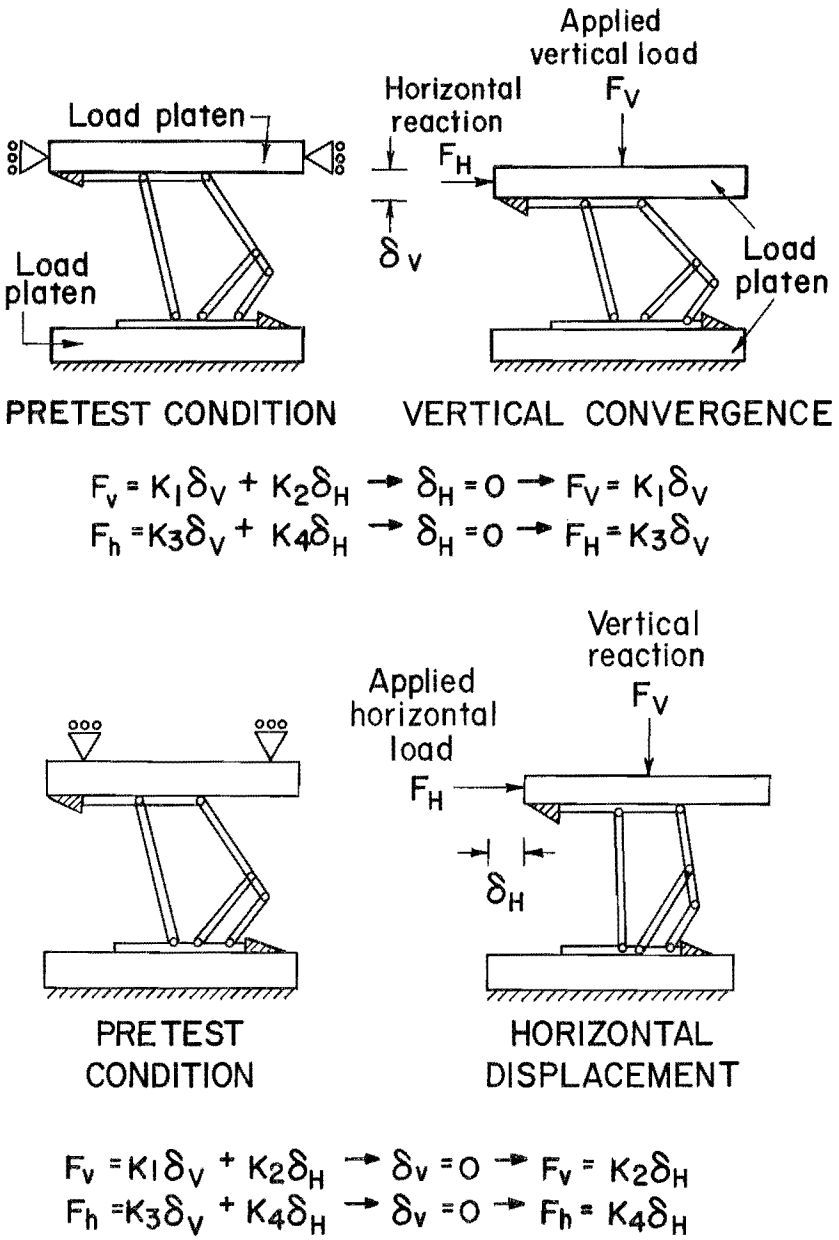

Figure B-1.—Shield stiffness test procedures.

APPENDIX C.—INPUT DATA FOR FINITE-ELEMENT SHIELD MODEL

ANALYSIS TYPE = 0
NUMBER OF ELEMENT TYPES = 3
  29 ELEMENTS CURRENTLY SELECTED. MAX ELEMENT NUMBER = 29
  40 NODES CURRENTLY SELECTED. MAX NODE NUMBER = 40
MAXIMUM LINEAR PROPERTY NUMBER = 2
MAXIMUM REAL CONSTANT SET NUMBER = 24
ACTIVE COORDINATE SET NUMBER = 0 (CARTESIAN)
MAXIMUM COUPLED D.O.F. SET NUMBER = 16

LIST ALL ELEMENT TYPES

NO.	STIF	KEYOPT VALUES									INOTPR	
1	54	0	0	0	0	0	1	0	0	0	0	TAPERED UNSYM. BEAM, 2-D
2	10	0	0	1	0	0	0	0	0	0	0	CABLE
3	1	0	0	0	0	0	0	0	0	0	0	SPAR, 2-D

LIST ALL MATERIALS PROPERTY= ALL

PROPERTY TABLE NUXY MAT= 1 NUM. POINTS= 2

TEMPERATURE	DATA	TEMPERATURE	DATA
0.00000E+00	0.30000	2300.0	0.30000

PROPERTY TABLE EX MAT= 2 NUM. POINTS= 2

TEMPERATURE	DATA	TEMPERATURE	DATA
0.00000E+00	0.29000E+08	2300.0	0.29000E+08

PROPERTY TABLE EX MAT= 3 NUM. POINTS= 2

TEMPERATURE	DATA	TEMPERATURE	DATA
0.00000E+00	0.29000E+12	2300.0	0.29000E+12

LIST ALL SELECTED NODE DSYS = 0

NODE	X	Y	Z	THXY	THYZ	THXZ
1	0.00000	4.5000	0.00000	0.00	0.00	0.00
2	12.000	2.8600	0.00000	0.00	0.00	0.00
3	24.000	3.5000	0.00000	0.00	0.00	0.00
4	37.000	6.7000	0.00000	0.00	0.00	0.00
5	50.250	6.0000	0.00000	0.00	0.00	0.00
6	64.500	17.500	0.00000	0.00	0.00	0.00
7	78.500	6.5000	0.00000	0.00	0.00	0.00
8	92.250	6.5000	0.00000	0.00	0.00	0.00
9	114.27	27.360	0.00000	0.00	0.00	0.00
10	97.340	31.110	0.00000	0.00	0.00	0.00
11	71.140	34.570	0.00000	0.00	0.00	0.00
12	59.750	49.000	0.00000	0.00	0.00	0.00
13	64.500	17.500	0.00000	0.00	0.00	0.00
14	92.250	6.5000	0.00000	0.00	0.00	0.00
15	114.27	27.360	0.00000	0.00	0.00	0.00
16	97.340	31.110	0.00000	0.00	0.00	0.00
17	0.00000	1.0000	0.00000	0.00	0.00	0.00
18	0.00000	4.5000	0.00000	0.00	0.00	0.00
19	-4.5000	4.5000	0.00000	0.00	0.00	0.00

NODE	X	Y	Z	THXY	THYZ	THXZ
20	92.250	2.0000	0.00000	0.00	0.00	0.00
21	96.250	6.5000	0.00000	0.00	0.00	0.00
22	92.250	6.5000	0.00000	0.00	0.00	0.00
23	92.250	6.5000	0.00000	0.00	0.00	0.00
24	0.00000	4.5000	0.00000	0.00	0.00	0.00
25	50.250	1.5000	0.00000	0.00	0.00	0.00
26	50.250	6.0000	0.00000	0.00	0.00	0.00
27	43.500	51.340	0.00000	0.00	0.00	0.00
28	30.500	43.500	0.00000	0.00	0.00	0.00
29	24.250	50.500	0.00000	0.00	0.00	0.00
30	19.500	52.100	0.00000	0.00	0.00	0.00
31	13.000	51.700	0.00000	0.00	0.00	0.00
32	6.0000	51.700	0.00000	0.00	0.00	0.00
33	-7.0000	51.700	0.00000	0.00	0.00	0.00
34	-20.000	52.940	0.00000	0.00	0.00	0.00
35	-34.500	53.640	0.00000	0.00	0.00	0.00
36	-51.000	54.400	0.00000	0.00	0.00	0.00
37	-68.000	55.150	0.00000	0.00	0.00	0.00
38	24.250	50.500	0.00000	0.00	0.00	0.00
39	50.250	6.0000	0.00000	0.00	0.00	0.00
40	59.750	49.000	0.00000	0.00	0.00	0.00

LIST ALL SELECTED ELEMENTS. (LIST NODES)

ELEM	MAT	TYP	REL	NODES	
1	1	1	1	1	2
2	1	1	2	2	3
3	1	1	3	3	4
4	1	1	4	4	5
5	1	1	5	5	6
6	1	1	6	6	7
7	1	1	7	7	8
8	1	1	8	14	15
9	1	1	8	13	16
10	1	1	9	11	12
11	1	1	10	10	11
12	1	1	11	9	10
13	2	2	12	17	18
14	2	2	12	19	24
15	2	2	12	20	23
16	2	2	12	21	22
17	2	2	12	25	26
18	1	1	13	37	36
19	1	1	14	36	35
20	1	1	15	35	34
21	1	1	16	34	41
22	1	1	17	33	32
23	1	1	18	32	31
24	1	1	19	31	30
25	1	1	20	30	29
26	1	1	21	29	28
27	1	1	22	28	27
28	1	1	23	27	40
29	1	3	24	38	39

LIST ALL REAL SETS

REAL CONSTANT SET 1		ITEMS 1 TO 12			
72.000	192.00	1.0000	1.0000	111.80	598.00
3.6400	2.8600	0.00000	0.00000	0.00000	0.00000
REAL CONSTANT SET 2		ITEMS 1 TO 12			
111.80	598.00	3.6400	2.8600	131.60	1146.0
4.5000	3.5000	0.00000	0.00000	0.00000	0.00000
REAL CONSTANT SET 3		ITEMS 1 TO 12			
131.60	1146.0	4.5000	3.5000	218.80	6234.0
11.300	6.7000	0.00000	0.00000	0.00000	0.00000
REAL CONSTANT SET 4		ITEMS 1 TO 12			
218.80	6234.0	11.300	6.7000	226.00	7228.0
12.030	6.9700	0.00000	0.00000	0.00000	12.030
REAL CONSTANT SET 5		ITEMS 1 TO 12			
226.00	7228.0	12.030	6.9700	200.00	8260.0
14.100	7.6500	0.00000	0.97000	0.00000	-9.8000
REAL CONSTANT SET 6		ITEMS 1 TO 12			
200.00	8260.0	14.100	7.6500	206.00	7386.0
8.0000	6.5000	0.00000	-9.8000	0.00000	0.00000
REAL CONSTANT SET 7		ITEMS 1 TO 12			
206.00	7386.0	8.0000	6.5000	163.00	2314.0
6.1000	4.9000	0.00000	0.00000	0.00000	-1.6000
REAL CONSTANT SET 8		ITEMS 1 TO 12			
88.600	660.00	4.2500	4.2500	88.600	660.00
4.2500	4.2500	0.00000	0.00000	0.00000	0.00000
REAL CONSTANT SET 9		ITEMS 1 TO 12			
70.000	583.00	5.0000	5.0000	29.800	564.00
4.5750	5.3000	0.00000	0.00000	-6.0000	9.5000
REAL CONSTANT SET 10		ITEMS 1 TO 12			
29.800	564.00	4.5750	5.3000	24.100	623.00
3.4900	8.7600	3.0000	10.500	1.4000	5.0000
REAL CONSTANT SET 11		ITEMS 1 TO 12			
24.100	623.00	3.4900	8.7600	24.100	349.00
2.7100	6.6650	1.4000	5.0000	0.00000	3.2500
REAL CONSTANT SET 12		ITEMS 1 TO 12			
1000.0	0.00000	0.00000	0.00000	0.00000	0.00000
0.00000	0.00000	0.00000	0.00000	0.00000	0.00000

REAL CONSTANT SET 13 ITEMS 1 TO 12

104.90	107.00	1.3500	2.6500	112.00	426.00
2.1000	3.5300	0.00000	0.00000	0.00000	0.00000

REAL CONSTANT SET 14 ITEMS 1 TO 12

112.00	426.00	2.1000	3.5300	119.00	712.00
2.8600	4.3900	0.00000	0.00000	0.00000	0.00000

REAL CONSTANT SET 15 ITEMS 1 TO 12

119.00	712.00	2.8600	4.3900	125.00	1372.0
3.5600	5.1900	0.00000	0.00000	0.00000	0.00000

REAL CONSTANT SET 16 ITEMS 1 TO 12

125.00	1372.0	3.5600	5.1900	137.00	1526.0
4.0600	5.9400	0.00000	0.00000	0.00000	0.00000

REAL CONSTANT SET 17 ITEMS 1 TO 12

157.00	1983.0	4.8100	5.1900	157.00	1983.0
4.8100	5.1900	0.00000	0.00000	0.00000	0.00000

REAL CONSTANT SET 18 ITEMS 1 TO 12

157.00	1983.0	4.8100	5.1900	157.00	1983.0
4.8100	5.1900	0.00000	0.00000	0.00000	0.00000

REAL CONSTANT SET 19 ITEMS 1 TO 12

157.00	1983.0	4.8100	5.1900	157.00	1610.0
4.3800	5.6200	0.00000	0.00000	0.00000	0.00000

REAL CONSTANT SET 20 ITEMS 1 TO 12

157.00	1610.0	4.3800	5.6200	192.00	2797.0
4.6900	10.310	0.00000	0.00000	0.00000	1.3100

REAL CONSTANT SET 21 ITEMS 1 TO 12

192.00	2797.0	4.6900	10.310	192.00	2797.0
4.6900	10.310	0.00000	1.3100	0.00000	8.3100

REAL CONSTANT SET 22 ITEMS 1 TO 12

192.00	2797.0	4.6900	10.310	242.00	3514.0
5.1600	6.8400	0.00000	8.3100	0.00000	0.00000

REAL CONSTANT SET 23 ITEMS 1 TO 12

242.00	3514.0	5.1600	6.8400	242.00	3514.0
5.1600	6.8400	0.00000	0.00000	0.00000	1.8400

REAL CONSTANT SET 24 ITEMS 1 TO 12

2.380	0.00000	0.00000	0.00000	0.00000	0.00000
0.00000	0.00000	0.00000	0.00000	0.00000	0.00000

LIST ALL COUPLED SETS

COUPLED SET = 1 DIRECTION = UX TOTAL NODES = 2
NODES = 6 13

COUPLED SET = 2 DIRECTION = UY TOTAL NODES = 2
NODES = 6 13

COUPLED SET = 3 DIRECTION = UY TOTAL NODES = 4
NODES = 8 14 22 23

COUPLED SET = 4 DIRECTION = UX TOTAL NODES = 4
NODES = 8 14 22 23

COUPLED SET = 5 DIRECTION = UX TOTAL NODES = 2
NODES = 9 15

COUPLED SET = 6 DIRECTION = UY TOTAL NODES = 2
NODES = 9 15

COUPLED SET = 7 DIRECTION = UX TOTAL NODES = 2
NODES = 10 16

COUPLED SET = 8 DIRECTION = UY TOTAL NODES = 2
NODES = 10 16

COUPLED SET = 9 DIRECTION = UX TOTAL NODES = 3
NODES = 1 18 24

COUPLED SET = 10 DIRECTION = UY TOTAL NODES = 3
NODES = 1 18 24

COUPLED SET = 11 DIRECTION = UX TOTAL NODES = 3
NODES = 5 26 39

COUPLED SET = 12 DIRECTION = UY TOTAL NODES = 3
NODES = 5 26 39

COUPLED SET = 13 DIRECTION = UX TOTAL NODES = 2
NODES = 29 38

COUPLED SET = 14 DIRECTION = UY TOTAL NODES = 2
NODES = 29 38

COUPLED SET = 15 DIRECTION = UX TOTAL NODES = 2
NODES = 12 40

COUPLED SET = 16 DIRECTION = UY TOTAL NODES = 2
NODES = 12 40

MAXIMUM COUPLED SET NUMBER = 16

APPENDIX D.—DISCUSSION OF LEG MECHANICS

Figure D-1 depicts a double telescoping leg cross section in its four possible configurations. Figure D-2 presents an analysis of leg forces in these four configurations. Anomalous shield behavior at setting conditions (active leg pressurization) is investigated with these diagrams.

When the shield leg is pressurized to a predetermined set pressure, σ_{IN}, the vertical force developed on the bottom stage becomes $\sigma_1 A_1$, where A_1 is the area of the bottom stage. This force is equilibrated by the vertical force developed in the bottom stage $\sigma_2 A_2$, where A_2 is the area of the bottom of the top stage or the top of the bottom stage. Note that A_1 is approximately twice as large as A_2. A check valve operates to permit the bottom stage cavity to pressurize and not bleed off into the supply chamber.

When the bottom stage is fully extended, the vertical force developed is equilibrated by the sum of that force produced in the bottom stage, which is about one-half that developed in the supply pressure chamber outside walls. This latter force is developed as the bottom stage flange contacts the pressure chamber stops. Therefore, the leg capacity is computed as $\sigma_2 A_2$.

In configurations when the bottom stage is not fully extended (figs. D-1*C* and D-1*D*), the vertical force developed is equilibrated only by the force produced in the bottom stage. This is accomplished because of the check valve, which allows the internal pressure in the bottom stage to increase appropriately to provide the balancing force. Thus the bottom stage will move in relation to the supply chamber and the top stage, which is fixed at an overall height (that is the shield height). This requires that the bottom stage walls be designed to withstand a pressure approximately twice as large as the supply, based on the ratio of the bottom stage and the top stage horizonal sections. The results of these mechanics is a leg force capacity approximately twice that found when the bottom stage is fully extended. Thus, depending on the extension of the lower stage, initial shield conditions can vary by a factor of 2.

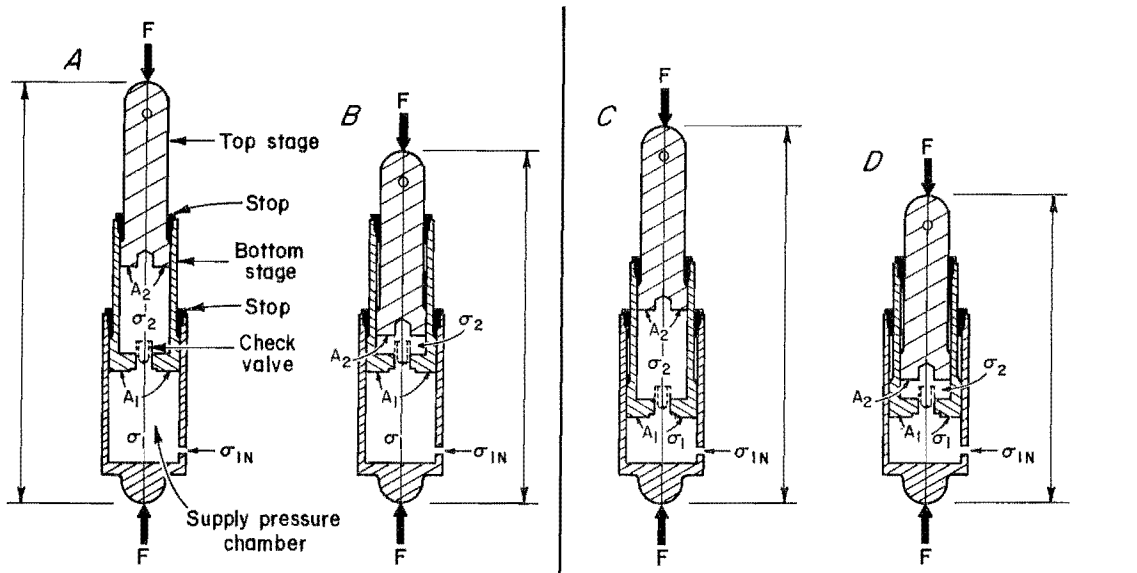

Figure D-1.—Illustration of leg configurations. *A*, Top and bottom stages fully extended: *B*, bottom stage fully extended, top stage partially extended; *C*, top stage fully extended, bottom stage partially extended; *D*, top and bottom stages partially extended.

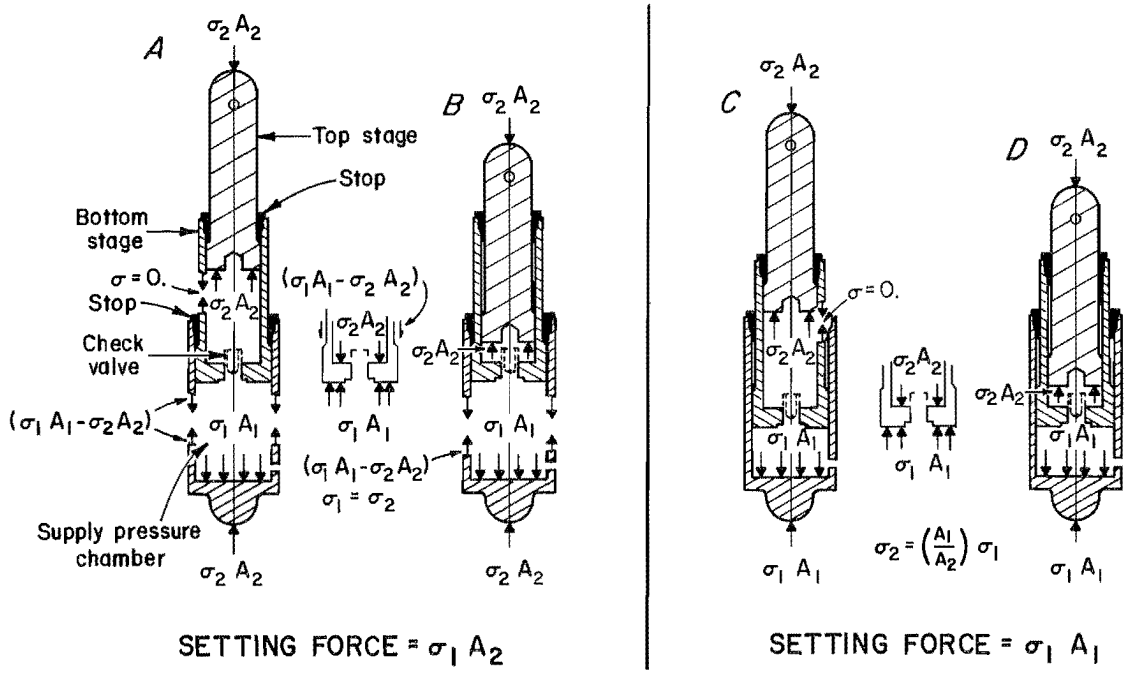

Figure D-2.—Analysis of leg forces. *A*, **Top and bottom stages fully extended;** *B*, **bottom stage fully extended, top stage partially extended;** *C*, **top stage fully extended, bottom stage partially extended;** *D*, **top and bottom stages partially extended.**

☆U.S. Government Printing Office: 1990-511-010/40001